SHORT ECHO TIME SINGLE VOXEL MAGNETIC RESONANCE SPECTROSCOPY IN THE CHARACTERISATION OF CHILDHOOD BRAIN TUMOURS

by

LISA MARIA HARRIS

A thesis submitted to
The University of Birmingham
for the degree of
DOCTOR OF PHILOSOPHY

Institute of Child Health
Medical School
The University of Birmingham
June 2009

UNIVERSITY OF
BIRMINGHAM

University of Birmingham Research Archive

e-theses repository

This unpublished thesis/dissertation is copyright of the author and/or third parties. The intellectual property rights of the author or third parties in respect of this work are as defined by The Copyright Designs and Patents Act 1988 or as modified by any successor legislation.

Any use made of information contained in this thesis/dissertation must be in accordance with that legislation and must be properly acknowledged. Further distribution or reproduction in any format is prohibited without the permission of the copyright holder.

ABSTRACT

INTRODUCTION
Brain tumours are the most common solid tumour in childhood, while Magnetic Resonance Spectroscopy (MRS) studies have been performed on brain tumours previously, the majority have been performed on the adult patient population and at long echo times. The work presented in this thesis outlines work performed in the usage of short echo time MRS in the characterisation of childhood brain tumours.

METHODS
Short echo time MRS was performed on children with brain tumours at the time of diagnostic imaging. In addition, follow up data was accrued for some patients. Resulting spectra were assessed for characteristics either of diagnosis, prognosis or treatment response.

RESULTS
Spectra collected were used in assessing characteristics of an array of childhood brain tumours. Initially the technique was tested on a well understood dataset of cerebellar tumours, and was later expanded to provide diagnostic aids for both brain stem tumours and pineal region tumours. A group of pilocytic astrocytomas were assessed for differences by location within the brain, for prognosis and for response to treatment.

CONCLUSIONS
The additional information given by short echo time MRS was useful in the characterisation of childhood brain tumours.

Dedication

This thesis is dedicated to my parents, who offered me unconditional love and support all the way since the beginning of my studies.

ACKNOWLEDGEMENTS

There are a large number of people I would like to thank, and without whom this thesis is unlikely to have been written.

I would like to thank all my former colleagues from the Institute of Child Health and Electrical, Electronic and Computer Engineering. I would especially like to thank both of my supervisors, Dr Andrew Peet and Dr Theodoros Arvanitis, whose assistance, enthusiasm and encouragement helped me in all stages of my PhD. I would also like to thank Nigel Davies, Martin Wilson and Greg Reynolds for vast amounts of patience with helping me to learn computer programming. Additional thanks goes to Yu Sun, Kal Natarajan and Alex Gibb. Additional thanks goes out to everyone who made the department run smoothly.

I would like to thank the radiology team at BCH, especially Dr Lesley MacPherson and Shaheen Lateff. Thanks also goes out to all those involved in this study at the Royal Marsden Hospital (Sutton), Great Ormond Street Hospital and Queen's Medical Centre.

I offer warm thanks to both Martin Wilson and John Easton for offering a sounding board for ideas, listening to me complain when some of them didn't work and providing a near endless supply of coffee!

I would like to thank Alan Wright and Richard Harrison for proof reading my thesis, and correcting numerous grammatical errors.

I would like to thank all of my family for their unconditional love and support throughout both my research and the writing up of this thesis. I cannot state how much I would like to thank my parents for their support and encouragement at all stages of my education. They supported me both emotionally and financially for so long and without them I cannot see that this PhD would have been possible. I would like to thank my grandparents for their limitless encouragement and for believing in me when even I didn't! I would like to thank all my extended family, especially my cousins, Amanda and Carolyn, for always being there to listen when I needed them to.

I offer heartfelt thanks to all my housemates over the duration of my PhD. Massive amounts of gratitude goes out to Helen and Nicole, for always knowing when chocolate/wine/DVD night was required.

I would like to thank all of my friends, for listening, encouraging and for always making me laugh when things were going less than well. I would like to warmly thank Martina, Ben, Seema, Mischa, Alan, Nic, 'len, Daf and Ellen.

I would like to offer huge thanks to Sean, for giving me so much love and support, and providing me with sanity, chocolate and dancing!

Finally I would like to thank all of my new colleagues at the University of Surrey for their support in the final stages of writing up.

DECLARATION

I confirm that this work is my own and that I have been involved in the design and conduct of these studies, analysis of data and preparation of this thesis. The following aspects of these studies were undertaken as part of collaboration.

Data was collected from four hospitals: Birmingham Children's Hospital; The Royal Marsden Hospital (Sutton); Queen's Medical Centre (Nottingham); and Great Ormond Street Hospital (London). The staff of the radiology departments in these hospitals were responsible for collecting magnetic resonance imaging and spectroscopy data. Histopathology was undertaken by the pathology department within each hospital.

Data analysis was performed by the author, with some additional programming assistance given by Dr Nigel Davies, Dr Martin Wilson and Dr Gregory Reynolds.

High resolution in vitro MRS was performed and analysed by Dr Martin Wilson.

The multi-centre radiology review of brain stem tumours was performed by Dr Lesley MacPherson, Dr Dawn Saunders and Dr Tim Jaspan.

CONTENTS

CHAPTER 1: INTRODUCTION
- 1.1 Brain Tumours in Children
- 1.2 Methods for Diagnosing Childhood Brain Tumours
  - 1.2.1 Histopathology
  - 1.2.3 Blood Markers for Diagnosis
  - 1.2.2 Magnetic Resonance Imaging (MRI)
  - 1.2.3 New Imaging Techniques
- 1.3 Tumour Types
  - 1.3.1 Glial Tumours
  - 1.3.2 Primitive Neuroectodermal Tumours (PNETs)
  - 1.3.3 Germ Cell Tumours (GCTs)
  - 1.3.4 Other Tumours
- 1.4 Tumour locations
  - 1.4.1 Distribution
  - 1.4.2 Cerebellar Tumours
  - 1.4.3 Brain Stem Tumours
  - 1.4.4 Pineal Region Tumours
  - 1.4.5 Optic Pathway Tumours and NF1
- 1.5 Current State of MRS
- 1.6 Current uses of MRS in Brain Tumour Research

CHAPTER 2: MAGNETIC RESONANCE SPECTROSCOPY
- 2.1 Theory of the NMR Phenomenon
- 2.2 Magnetic Resonance Spectroscopy (MRS)
- 2.3 Clinical MRS
  - 2.3.1 Pulse Sequences
  - 2.3.2 Water Suppression
  - 2.3.3 MRS Signal Pre-processing
  - 2.3.4 Types of MRS Localisation
  - 2.3.5 Echo Times
  - 2.3.6 Functions of Different Metabolites
- 2.4 Analysis Tools
- 2.5 Extensions
- 2.6 Challenges of 1H MRS
- 2.7 Summary

AIMS AND OBJECTIVES

OVERVIEW OF RESULTS

CHAPTER 3: METHODS
- 3.1 EXPERIMENTAL PROTOCOLS
- 3.2 ANALYSIS METHODS
  - 3.2.1 Pre-Processing and Processing
  - 3.2.2 Quality Control
  - 3.2.3 Analysis Using Spectra Produced by Scanner Software
  - 3.2.4 Analysis Using Metabolite Concentrations

3.3 STATISTICAL METHODS FOR THE INTERPRETATION OF RESULTS

CHAPTER 4: CEREBELLAR TUMOURS
4.1 INTRODUCTION
4.2 A DIAGNOSTIC SCHEME BASED ON MRS PEAK HEIGHTS
4.2.1 A Diagnostic Scheme based on MRS Peak Heights from Retrospective Analysis
4.2.2 Prospective Evaluation of Peak Height Classifier
4.2.3 Updating and Extending the Peak Height Classifier
4.2.4 Summary
4.3 A DIAGNOSTIC SCHEME BASED ON LCMODEL™ METABOLITE CONCENTRATIONS
4.3.1 An enhanced diagnostic scheme based on metabolite concentrations determined from retrospective analysis
4.3.2 An enhanced diagnostic scheme based on metabolite concentrations determined from retrospective analysis using a full set of metabolite concentrations
4.3.3 Prospective Evaluation – diagnostic scheme based on metabolite concentrations
4.7 SUMMARY OF MAIN FINDINGS AND CONCLUDING REMARKS

CHAPTER 5: PINEAL REGION TUMOURS
5.1 INTRODUCTION
5.2 METHODS AND PATIENTS
5.3 RESULTS
5.4 DISCUSSION
5.5 CONCLUSION

CHAPTER 6 BRAIN STEM TUMOURS
6.1 INTRODUCTION
6.2 METHODS AND PATIENTS
6.3 RESULTS
6.4 DISCUSSION
6.5 CONCLUSION

CHAPTER 7: PILOCYTIC ASTROCYTOMAS: SPECTRAL VARIATION WITH LOCATION AND PROGRESSION
7.1 INTRODUCTION
7.2 METHODS
7.3 RESULTS
7.3.1 Differences in MRS metabolite Profiles between Cerebellar and Supratentorial Tumours
7.3.2 Pre-Treatment MRs as a Prognositic Indicator in Supratentorial Tumours
7.3.3 Supratentorial Tumours: Treatment Monitoring and Early Predictors of Progression
7.4 DISCUSSION
7.5 CONCLUSION

CHAPTER 8: CONCLUSIONS

REFERENCES

LIST OF ILLUSTRATIONS

Figure 1: Pie chart depicting the cause of death in children under the age of 15 years, in the year 2007

Figure 2: Pie Chart depicting the distribution of deaths from cancers in children under the age of 15 years, in the year 2007

Figure 3: Labelled side view of the brain

Figure 4: Synthesised in vivo ^{1}H-MR spectrum

Figure 5: Lactate
a) Molecular structure
b) 1H MR spectrum

Figure 6: PRESS sequence

Figure 7: Examples of 1H-MR spectra at different echo times:
a) TE = 135ms
b) TE = 30ms

Figure 8: Synthesised spectra for individual metabolites
a) N-Acetyl Aspartate and N-Acetyl Aspartyl-glutamate
b) Glycerophosphocholine and Phosphocholine
c) Creatine
d) Myo-Inositol
e) Scyllo-Inositol
f) Glycine
g) Lactate
h) Taurine

Figure 9: Voxel placement for a cerebellar tumour
a) Axial plane
b) Sagittal plane

Figure 10: Example of a 1H-MR spectrum processed by the Siemens' Symphony NUM4 software

Figure 11: Examples of poor quality 1H-MR spectra
a) An example with broad lines
b) An example with very low SNR.

Figure 12: 2 step classification scheme for cerebellar tumours based on peak height ratio measurement – retrospective study of cerebellar tumours using peak height ratios

Figure 13: Peak height classification scheme measurement – retrospective study

Figure 14: Flow diagram showing the analysis of multicentre data

Figure 15: Average spectra for the three main cerebellar tumours

Figure 16: Prospective evaluation of the peak height classification scheme – new cases on the original classification axes

Figure 17: 2 step classification scheme for cerebellar tumours based on peak height ratio measurement – using the full, multicentre data set

Figure 18: Peak height classification scheme measurement – using the full, multicentre data set

Figure 19: Plot showing cerebellar tumour separation on the axes tNAA/Cr Vs mIns/tCho – using LCModel™ generated metabolite concentrations

Figure 20: Principal Component Analysis of cerebellar tumours – using LCModel™ generated metabolite concentrations

Figure 21: Plot showing cerebellar tumour separation on the axes tCho Vs mIns – using LCModel™ generated metabolite concentrations

Figure 22: Bar charts showing the average (a) metabolite and (b) LMM concentrations for each of the 3 major tumour types of the cerebellum, as determined from LCModel™

Figure 23: Prospective evaluation of the metabolite classification scheme – the full, multicentre data set on the axes tCho Vs mIns

Figure 24: Bar charts showing metabolite (a) and LMM (b) concentrations of rare tumours of the cerebellum compared with those found in the 3 major tumour groups of the cerebellum

Figure 25: Average spectra for pineal region tumours

Figure 26: Germ Cell Tumours and other pineal region tumours plotted on axes for LMM regions at 0.9ppm and 1,3ppm

Figure 27: Germ cell tumours plotted on axes tCho Vs Cr

Figure 28: Average spectra for brain stem tumours

Figure 29: Principal Component Analysis of brain stem tumours

Figure 30: Brain stem tumours plotted on axes mIns/tCho Vs Cr/tCho

Figure 31: Diffuse gliomas within and extending beyond the pons plotted on axes for the LMM regions (relative to tCho) at 0.9ppm and 1.3ppm

Figure 32: Bar charts showing (a) metabolite and (b) LMM concentrations (relative to total Cho) for brain stem tumour

Figure 33: Pie chart depicting pilocytic astrocytoma distribution within the brain

Figure 34: Mean spectra for pilocytic astrocytoma by location

Figure 35: Principal Component Analysis of pilocytic astrocytoma by location

Figure 36: Pilocytic astrocytoma, separated by location, plotted on the axes mIns Vs Glx

LIST OF TABLES

Table 1: Patient information for retrospective study of scanner produced spectra of cerebellar tumours

Table 2: AUC values for retrospective study of scanner produced spectra of cerebellar tumours

Table 3: Classification Rates for prospective evaluation of classification scheme for cerebellar tumours, based on peak height measurement from spectra produced by MR scanner software

Table 4: T-Test results for re-optimising the classification scheme for cerebellar tumours based on spectra from the scanner software

Table 5: AUC values for prospective study of scanner produced spectra of the three main cerebellar tumour types

Table 6: Classification of cerebellar tumours using a multicentre dataset, using peak height measurement

Table 7: Peak height ratios of rare cerebellar tumours

Table 8: Classification of rare tumours of the cerebellum using the revised peak height classifier

Table 9: ANOVA and AUC results for using ratios of LCModel™ derived metabolite concentrations, in the classification of cerebellar tumours

Table 10: Average metabolite values for each cerebellar tumour type and ANOVA results using a full LCModel™ basis set

Table 11: T-test results and AUC values for building a 2-step classification scheme using metabolite concentrations.

Table 12: Comparison of classification rates of the different schemes for classifying cerebellar tumours

Table 13: Average metabolite and LMM concentrations for pineal region tumours

Table 14: T-test results for comparison between germ cell tumours of the pineal region and pineal parenchymal tumours

Table 15: P-values for the comparison of germinoma metabolite concentrations with other germ cell tumours of the pineal region

Table 16: Diagnosis summary for patients in the brain stem tumour study

Table 17: T-Test results for comparison of brain stem tumours

Table 18: Average metabolite values for each brain stem tumour type and ANOVA results using a full LCModel™ basis set

Table 19: P-values and averages for comparison between cerebellar and supratentorial pilocytic astrocytoma

Table 20: P-Value and average metabolite values for determination of progression of supratentorial pilocytic astrocytoma from pre-treatment MRS

LIST OF ABBREVIATIONS

Ala – alanine
Asp – aspartate
ATRT – Atypical Teratoid/Rhabdoid Tumour
BCH – Birmingham Children's Hospital
CCLG – Children's Cancer and Leukaemia Group
Cho - choline
CNS – central nervous system
Cr – creatine
CRLB – cramer-rao lower bound
CSF – cerebrospinal fluid
CSI – chemical shift imaging
CT – computed tomography
DG – diffuse glioma
DPG – diffuse pontine glioma
DTI – diffusion tensor imaging
DWI – diffusion weighted imaging
FID – free induction decay
FWHM – full width at half maximum
GCT – germ cell tumours
Glc – glucose
Gln – glutamine
Glu – glutamate
Glx – glutamine + glutamate
Gly – glycine
GM – grey matter
GOSH – Great Ormond Street Hospital
GPC – glycerophosphocholine
Gua - guanadinoacetate
HCG – human chorionic gonadotropin
HGG – high grade glioma
Lac – lactate
LGG – low grade glioma
LMM – lipids + macromolecules
mIns – myo-inositol
MMP-2 - matrix metallopeptidase 2
MR – magnetic resonance
MRI – magnetic resonance imaging
MRS – magnetic resonance spectroscopy
MRSI – magnetic resonance spectroscopic imaging
NAA – n-acetyl-aspartate
NAAG – n-acetyl-aspartyl-glutamate
NF1 – neurofibromatosis type 1
PA – pilocytic astrocytoma
PC – principal component
PCA – principal component analysis
PCh – phosphocholine
PCr - phosphocreatine
ppm – parts per million

PPT – pineal parenchymal tumour
QMC – Queen's Medical Centre (Nottingham)
RMH – Royal Marsden Hosptial
sIns – scyllo-inositol
SNR – signal-to-noise ratio
SVS – single voxel spectroscopy
Tau – taurine
tCho – total choline
TE – echo time
tNAA – NAA + NAAG
TPG – tectal plate glioma
TR – repetition time
VOI – volume of interest
WHO – World Health Organisation
WM – white matter

CHAPTER 1: INTRODUCTION

1.1 BRAIN TUMOURS IN CHILDREN

Although cancer is very rare in childhood, with less than 1% of all cancers registered in 2005 being from children [1], it is the most common cause of death from disease in children over one year of age (figure 1).

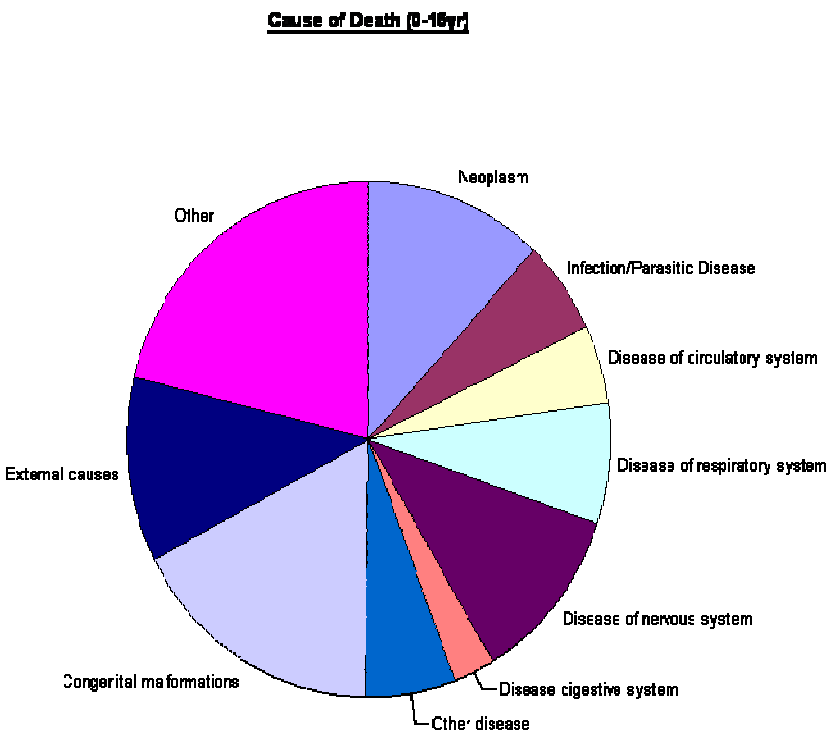

Figure 1: Pie chart depicting cause of death in children under the age of 15 years in the year 2007 [1]

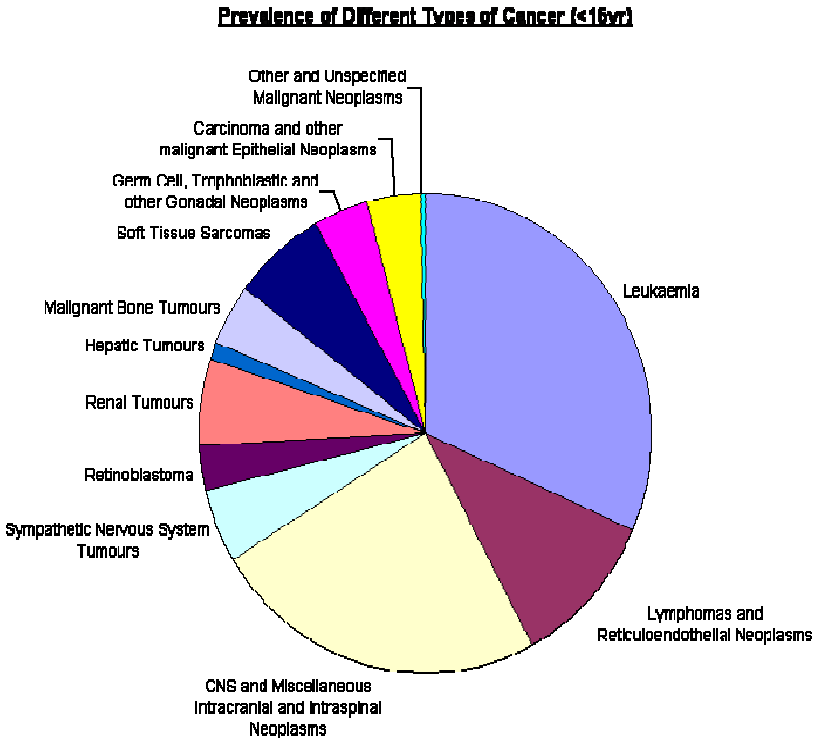

Figure 2: Pie Chart depicting the distribution of deaths from cancers in children under the age of 15 years, in the year 2007 [1]

Of all cancers that can occur in childhood, brain tumours are the commonest type of solid tumour (figure 2), with 24% of registered cancer being in the CNS [2]. The only cancer more prevalent in childhood is leukaemia, with a reported 31% of registered cancers being attributed to this in 2000. In the year 2000, 340 new CNS tumours were diagnosed in the UK [2], out of an overall 1426 reported. Survival rates of childhood cancer in the UK have improved overall over time, with an overall survival of 33% in the period 1962-1971 increasing to 73% in the period 1992-1996 [2]. The survival in CNS tumours has increased from 38% to 66% in the same period. Improved and earlier diagnosis and characterisation is vital in the continuation of this trend.

1.2 METHODS FOR DIAGNOSING CHILDHOOD BRAIN TUMOURS

When a child has a suspected brain tumour, one of the first and most important procedures performed is either a CT or MRI scan. This then confirms the presence, or absence, of a tumour. A CT examination is quicker and cheaper to perform and many types of brain tumours will appear on these images. MRI is often preferred as it has much more detail present and most brain tumours will be apparent on these scans. It can essentially be used to confirm or remove the likelihood of a brain tumour being present in a child exhibiting symptoms indicating the presence. Conventional MRI can be used to detect the presence of abnormalities in the brain, but it is usually not enough to determine the type of tumour present. This is achieved by performing a biopsy and histopathology.

1.2.1 HISTOPATHOLOGY

Histopathology is a microscopic examination of a biopsy sample in order to assess the presence and type of disease. It is the current 'gold standard' for the diagnosis of brain tumour type and grade.

Once the tissue has been removed, it needs to be stabilised by fixing it in formalin. It is then embedded into paraffin, which allows for very thin slices to be cut and these can then be processed and assessed through staining. To assess the tissue sample, the slices are stained with a variety of stains, which reveal cellular components and allow contrast. A combination of hematoxylin

and eosin is used to stain the nuclei blue and the cytoplasm pink, which allows the cellular structure to be assessed [3].

There are many other stains, which allow highlighting of different features and categories of cells under the microscope using the technique of immunohistochemistry. Immunohistochemistry allows for the staining of proteins and lipids using antibodies of specific types. One example of this is the presence of glial fibrillary acidic protein (GFAP); this is found in glial cells such as astrocytes. A common stain used is for the Ki-67 protein, this is a marker of cell proliferation. As such, this is highly elevated in cells which have a fast turnover, and thus elevated in tumour tissue. This is one of the methods used to grade tumours, and in the assessment for aggressiveness and invasion. The stain MIB-1 is most commonly used to stain for this protein and is used to determine the Ki-67 labelling index of a sample, which is higher in more aggressive tumours [4].

The use of histopathology and immunohistochemistry allows for a definitive diagnosis of the tumour. This is not always achievable in cases of small specimens that may be lacking in viable tumour tissue [5], but we can normally obtain a diagnosis using this method. This is further complicated when there is not complete concordance between histopathologists, and in some cases an agreement between histopathologists is difficult.

There are risks associated with the surgery necessary for obtaining the tumour tissue sample [5-7]. This is not always required as part of a treatment

plan for a patient. Some of these tumours do not require surgical intervention because of their benign nature, meaning that watching these tumours would be preferable. Other tumours are less amenable to surgery, but do respond to other treatments available. An example of the latter would be a germinoma; these grow back rapidly post-operatively, but are exquisitely sensitive to radiotherapy [8, 9]. These tumours are located in the midline of the brain, for example in the pineal region, which is a highly delicate area to biopsy, and would therefore benefit from surgery not being performed unnecessarily.

Characterising tumours, which are within a set group, creates further limitations concerning histopathological diagnosis. Two particular tumours may be given an identical diagnosis due to an identical histopathological appearance, but each may respond differently to certain treatments or, alternatively, one may be significantly more aggressive that the other. It may not be possible to detect these subtle differences using standard histopathology and immunohistochemistry [10]. Much interest have been generated into the discovery of novel biomarkers which have the ability to give additional information about the tumour's behaviour and, in particular, prognosis

In addition, to obtain the best resection, it would benefit the surgeon to know a diagnosis prior to surgery. This information could be used to plan the resection extent.

1.2.2 BLOOD MARKERS OF DIAGNOSIS

There are a small number of tumours which secrete substances into the blood which, if detected, can be used for diagnosis. The main example of tumours where this is present is germ cell tumours, which may secrete alpha-fetoprotein and Beta HCG.

1.2.3 MRI

MRI has been used in the assessment of brain tumours for many years. It is often the first imaging procedure performed when a brain tumour is suspected. It is non-invasive and may offer a means to determine a diagnosis pre-surgically. In tumours where surgery is very high risk, for example those located within the brain stem, it forms a major part of the final diagnosis [11].

Diagnosis using MRI is achieved using certain features such as the location of the tumour with a high accuracy [12, 13], whether it has metastasised and whether there is a cyst present. Other features such as being iso-dense or hypo-dense are also considered, as is the apparent invasion of surrounding tissue [14].

1.2.4 NEW IMAGING TECHNIQUES

Newer imaging techniques often used in the assessment of a suspected brain tumour include diffusion weighted imaging (DWI), diffusion tensor imaging (DTI) AND magnetic resonance spectroscopy (MRS).

DIFFUSION WEIGHTED IMAGING

DWI is a modification of standard MRI techniques, and allows for the measurement of random motion of molecules. From this, images can be weighted with characteristics of water diffusion. This has been shown to be useful for the differentiation between brain abscesses, cystic and non-cystic tumours [15-17].

DIFFUSION TENSOR IMAGING

DTI is an MR technique that enables the measurement of the restricted diffusion of water in tissues. This allows for the imaging of neural tracts. DTI can be used to perform tractography within white matter, where fibres can be tracked along their entire length [18-26]. This is a useful tool for measuring deficits in the white matter, and has been used in the assessment of white matter lesions, such as those caused by trauma ([19, 21, 23]. DTI has also been used in the assessment of tumours [18, 20, 22, 24-26], including in surgical planning [18, 22, 25, 26] and determining recurrence [20, 24].

MAGNETIC RESONANCE SPECTROSCOPY

MRS is a technique that allows for the non-invasive assessment of the metabolites present in a given volume of tissue using an MR scanner. A region of interest is selected either in the tumour or in a region of suspicion. A cubic region is selected, called a voxel, and this is the region which the spectrum is depicting. This can either be performed using one region of interest (single voxel spectroscopy – SVS) or a grid of many voxels (magnetic resonance spectroscopic imaging – MRSI or chemical shift imaging – CSI).

This has been shown to be useful in the assessment of a variety of conditions, including brain tumours [27-30], brain injury [31-34], and a variety of neurological conditions [35].

1.3 TUMOUR TYPES

Tumours that occur in children are mainly different to those occurring in the adult population, with some tumour types being unique to the paediatric population. These are usually classified by the WHO classification system of 2007 [36].

1.3.1 GLIAL TUMOURS

The glial group of tumours is a diverse group, derived from astrocytes, oligodendroglial cells, and ependyma [37]: astrocytomas, ependymomas and, in rare instances, oligodendrogliomas. Each of these has a very different prognosis and requires different treatment plans.

ASTROCYTOMAS

Astrocytomas are one of the subgroups of gliomas, unbiopsied astrocytomas are usually referred to as gliomas. Astrocytomas can vary in aggression and prognosis, ranging from slow growing (WHO grade 1; pilocytic astrocytoma (PA)) to very fast growing, highly invasive (WHO grade 4; glioblastoma multiforme (GBM)).

In the adult patient population higher grade astrocytomas are common, but these are rare in children. The majority of astrocytomas diagnosed in children

are PAs [38], which have a Ki67 usually <5% [39, 40], with a 10 year survival rate greater than 85% [41].

Diffuse gliomas do not carry such a good outlook; these are common in the brain stem. Diffuse intrinsic brainstem gliomas comprise 15-20% of all CNS tumours in children [42]. These are one of the main causes of death in children with brain tumours, with more than 90% of those diagnosed dying within 2 years of diagnosis [42]. Since biopsy carries a significant risk they are commonly diagnosed on clinical and imaging grounds alone, restricting the opportunity for biological studies.

Higher grade gliomas can also occur in children, but these are less common, comprising approximately 5% of childhood brain tumours. These are more common in the adult population, where they carry an extremely poor prognosis. However, in children, although the prognosis is still poor, even patients with grade IV lesions can become long term survivors implying that these lesions are different biologically than those found in adults.

EPENDYMOMA

Ependymomas are the third most common brain tumour in children [41, 43], and are especially common in younger children, with the average age of diagnosis being less than 6 years [43, 44]. As with astrocytomas, these tumours can have a spectrum of grades from WHO grade 1 to 3 [45, 46]. Grade 1 ependymomas occur predominantly in the spine. Grades 2 and 3 can occur both infratentorially and supratentorially, these form a continuum

and the distinction between these is controversial. However, they are more common in the posterior fossa [45] and this percentage is increased in childhood ependymomas.

1.3.2 PRIMITIVE NEUROECTODERMAL TUMOURS (PNET)

PNETs are aggressive tumours, corresponding to WHO grade 4; these tumours have a tendency towards metastasising. They can occur both infra- and supra-tentorially, those occurring supratentorially are referred to as supratentorial PNETs (SPNETs), or pineoblastomas when located in the pineal region. Those occurring infratentorially are referred to as medulloblastomas. PNETs in the posterior fossa are the most common, with medulloblastomas comprising 20-25% of all childhood brain tumours reported [47]. SPNETs are much less common, comprising <3% [47].

These tumours have similar appearances on histology, but SPNETs have been shown to carry a worse prognosis than medulloblastomas [47, 48], with a markedly lower 5 year recurrence free survival [47]. Another important prognostic factor with these tumours is the presence of metastases. These have a huge impact on the 5 year overall free survival rates, with 1 study quoting a drop from 87.2% to 25.0% in the presence of metastatic spread [47].

1.3.3 GERM CELL TUMOURS (GCTs)

These tumours are thought to arise from primordial germ cells and account for about 3% of cancers in children. They most commonly occur in the testes or

ovaries, but can occur intracrainially. Intracranial GCTs are more common in children than in adults [49]. They occur in the midline, mainly in the pineal or suprasellar regions of the brain. Intracranial GCTs comprise <5% of all brain tumours [9], although this is higher in Japan and the Far east. They are a highly diverse group, ranging from the benign to the highly malignant. There are 3 main subgroups of GCT: germinomas; secretory GCTs (SGCTs); and teratomas. Germinomas are the most common [9], despite being highly aggressive tumours they are highly radiosensitive [9, 50] and, hence, carry a good prognosis with quoted 5 year progression free survival rates often in excess of 90% [8, 9, 51-53]. Around 25% of intracranial GCTs are secretory [8, 9, 49, 50, 52]; these are diagnosed on the basis of serum markers [9, 49]. These are highly malignant and less sensitive to radiotherapy than germinomas [9, 52]. This leads to a worse prognosis, with an event free survival of 5-years being approximately 50% [9, 52, 53]. The remaining 10% of intracranial GCTs are variants of teratoma. These can be either benign (mature teratoma) or malignant (immature teratoma) [54]. There is a good prognostic outcome for patients with a mature teratoma, with a 5 year survival of around 86% [53]. This is worse for a patient with an immature teratoma, with a survival rate of about 50-70% [9, 53]. There is a benefit from aggressive resection in these tumours [53, 54].

1.3.4 OTHER TUMOURS

In addition to the tumours listed, there are many other histological types. The list provided above covers all the major tumour types. Rare tumours provide a particular challenge in both diagnosis and management.

1.4 TUMOUR LOCATIONS

Different tumours can occur in different regions of the brain, and this affects diagnosis and prognosis.

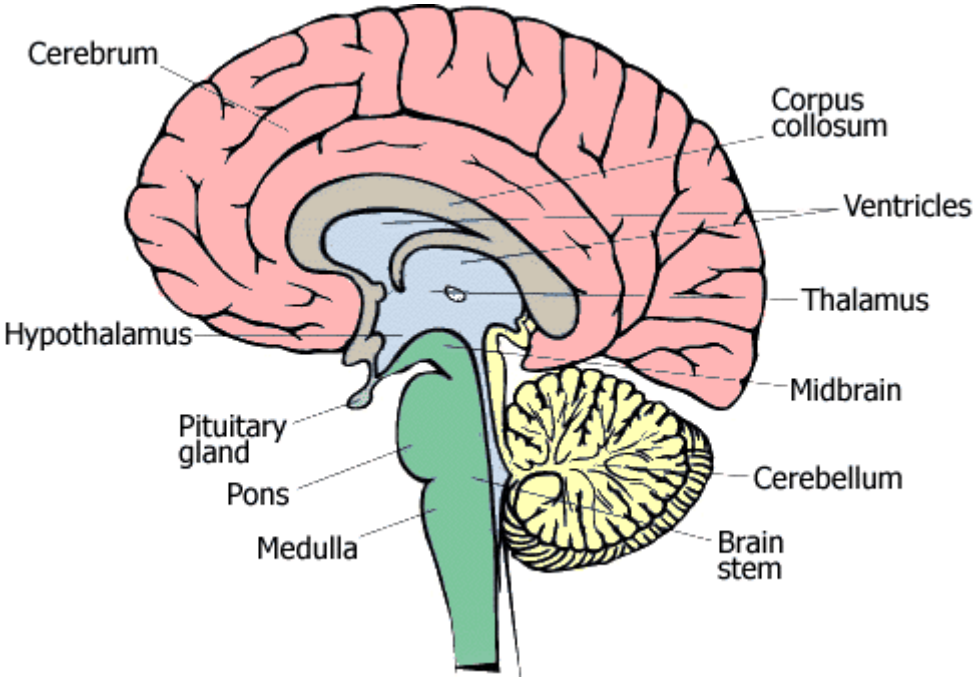

Figure 3: Brain diagram showing all major regions [55]

The following is a list and description of the major regions of the brain, relevant to this thesis:

- Supratentorial regions:
    - The cerebrum – this is the largest area of the brain and is made up of 2 hemispheres. Each hemisphere is subdivided into lobes: frontal, temporal, occipital and parietal. The cerebrum is largely concerned with mental functions such as thinking and memory, along with motor function and sensation.
    - Pineal gland – this is a small endocrine gland that produces melatonin, which affects the sleep/wake cycle.

- Pituitary gland – this is a small endocrine gland that secretes hormones that regulate homeostasis.
- Thalamus – amongst other functions, the thalamus plays an important part in the regulation of the sleep/wake cycle and is involved in level of awareness.
- Hypothalamus – this acts as a link between the nervous system and the endocrine systems. This is performed via the pituitary gland.
- Optic pathway – information about an image is transmitted via the optic nerves, these meet and cross at the optic chiasm. The chiasm is at the base of the hypothalamus; at this point the information coming from each eye is combined, split and, later, processed.

- Infratentorial:
  - The cerebellum - this is concerned with coordination and with balance.
  - The brain stem – this is at the base of the brain and connects it to the spine. It controls the functions that are essential for maintaining life: blood pressure, breathing and heart beat.

1.4.1 DISTRIBUTION

The location of a lesion affects the type of tumour considered in diagnosis. In the adult population most brain tumours occur in the cerebral hemispheres. This, however, is not the case in the paediatric population. Tumours in

children commonly occur infratentorially, in the brain stem or cerebellum, with around 50% of reported brain tumours being reported in these locations. Around 20% are in the suprasellar/sellar region; this refers to tumours above the sella turcica (a saddle shaped decompression in the sphenoid bone). The remaining 30% occur in other supratentorial locations.

1.4.2 CEREBELLAR TUMOURS

Tumours that occur in the cerebellum are usually confined to 1 of 3 types:

- Pilocytic Astrocytoma
- Medulloblastoma
- Ependymoma

Although, other tumours, such as ATRTs [56] and high grade gliomas, can also occurs here, amongst other rarer tumours.

1.4.3 BRAIN STEM TUMOURS

Most commonly types of astrocytoma occur in this region of the brain. There are either high or low grade:

- Diffuse Pontine Glioma (DPG)
- Tectal Plate Glioma (TPG) – assumed to be focal low grade glioma
- Focal astrocytoma of various grades

1.4.4 PINEAL REGION TUMOURS

3-8% of childhood brain tumours occur in the pineal region. This is a complex area to biopsy, with surgery carrying a risk of morbidity and mortality. This diverse group of tumours varies from the benign to the highly malignant, with highly different treatment requirements.

The most common pineal region tumours are germ cell tumours (GCTs):

- Germinoma
- Teratoma (mature and immature)
- SGCT

The other major group of pineal tumours arise from pineocytes:

- Pineoblastoma
- Pineal parenchymal tumour of intermediate differentiation (PPTID)
- Pineocytoma

Astrocytomas can also occur around the pineal gland.

1.4.5 OPTIC PATHWAY TUMOURS and NEUROFIBROMATOSIS TYPE 1

3-5% of childhood brain tumours are optic pathway gliomas [57]. Of these, approximately 25% are confined to the optic disc and nerve and 40-75% involved the chiasm. These are most common in the first decade of life, with approximately 75% being diagnosed at this age [58].

Neurofibromatosis Type 1 (NF1) is a familial condition which predisposes the carrier to developing low grade gliomas. These tend to be present in the optic pathways or chiasm and are more indolent than other low grade gliomas occurring in these locations [59-63]. If a diagnosis has been made using general diagnostic criteria for NF1 [59-61, 63] and a slow growing lesion is seen in the optic pathways/chiasm a biopsy is not usually performed as this is enough for a diagnosis [62, 64]. These tumours tend to be observed rather than treated aggressively [62].

1.5 CURRENT STATE OF MRS

To date there have been several studies published relating to the use of MRS in the assessment of brain tumours, and these have shown the promise of this technique in this area [29, 65]. MRS has been used to improve diagnostic accuracy [27, 65], grading tumours [66-68], assessing for the presence of prognostic markers [69], and offer guidance for surgical intervention [70].

A much more limited number of studies have been performed in the paediatric population, which have also shown the benefit of using MRS to aid in the characterisation of tumours [71-73]. The number of studies achievable in the paediatric population has been hindered by small numbers of cases. Brain tumours are not common in children and thus only small groups are available for study. Much of the work published is in the form of case reports or a small series of cases. This leads to the need for larger multicentre studies, which introduces new problems. Multicentre studies need to be subject to strict protocols that are followed rigorously in order to allow for the data between institutions to be analysed together.

Much of the published data is also from MRS collected at a longer echo time (chapter 2.5); this leads to a loss of information from certain metabolites, lipids and macromolecules. The signals lost at longer echo times have been shown to be useful in the characterisation of tumours in studies collected at shorter echo times [66, 67, 71, 72, 74-76] .

1.6 CURRENT USES OF MRS IN BRAIN TUMOUR RESEARCH

When a patient has a suspected brain tumour they traditionally have an imaging evaluation. This is performed either by CT or MRI scan. Contrast-enhanced MRI has been shown to offer a higher diagnostic accuracy than CT [77-79]. However, while MRI is very good at detecting the presence of lesions, it does not have a high diagnostic accuracy, with problems in the diagnosis of many tumours [80]. An improvement in accuracy has been shown to be possible by the addition of MRS to the standard MRI study [81]. One study using a mixed age group quotes an increase in diagnostic accuracy of indeterminate brain lesions from 55% to 71% when comparing MRS with MRI [27]. In another study, 104 out of 105 spectra were correctly identified by using 'leave-one-out' discriminant analysis on MRS data. This can be compared with conventional preoperative diagnosis methods, which misclassified 20 out 91 tumours that were analysed [69]. In addition to this, conventional MRI offers us little information on the prognosis of tumours [82], little information about the grade of the tumour [74] and no information with regards to the biology of the tumour [83]. Conventionally, this is achieved by taking a biopsy sample and processing it using histopathology. This can lead to a sampling error in heterogeneous tumours, which may be reduced by using techniques such as MRS to target active tumour tissue [29, 70, 84]. Also, since all tumours do not require surgery as part of their curative treatment [9, 85], it would be better to remove unnecessary risks associated with surgery for these patients.

To date, many studies have been performed to assess the utility of MRS in adult patients in the diagnosis of both tumours and neurological disorders [27, 29, 30, 65-68, 84, 86-97]. There are a more limited number in the paediatric population [28, 71, 73, 75, 76, 86, 98-107]. Adult studies have shown the considerable promise of MRS as a method to diagnose and characterise tumours and also as an aid to assist in the understanding of the biology of these tumours.

Most studies using MRS use ratios between NAA, Cr and Cho as their major discriminating factors, as these appear to be the metabolites that alter by the greatest measureable amount in tumours compared with 'normal' brain, and these also vary strongly between tumour types. A common finding described is an elevated signal arising from Cho, either relative to water [87, 90, 94, 108-111] or in ratio to Cr or NAA [66, 70, 84, 87, 97].

Cho is a marker of cell turnover and is therefore elevated in tumour tissue. It has frequently been used to differentiate between tumour types that look similar using conventional MRI [90]. Cho/Cr is elevated in nearly all tumours [84]. This has also been used to grade tumours, with higher levels being reported in more aggressive tumours [68, 87, 97]. The ratio between Cho/Cr is such a strong indicator of cancerous tissue, that it has been used in one study to guide biopsies, leading to a success rate of 100% in obtaining tissue useful for histopathological processing [70]. NAA/Cho is also altered in glioma tissue [84, 87], and this can also be used to differentiate between high and low grade gliomas [66, 84]. Cho ratios have also been used in monitoring

treatment response [108, 110, 111] and in determining the difference between recurrence and radiation changes post radiotherapy [109].

NAA is another metabolite closely linked with tumour characterisation. It is a marker of neurons and is, therefore, usually higher in healthy brain tissue when compared with tumour tissue [87, 90, 94, 96, 97, 112]. This is lower in high grade tumours compared with low grade tumours, and this can be used to differentiate these either referenced to internal water [90, 94, 96] or in ratio to Cr [84, 97]. NAA and Cho can be used in combination as a ratio to target areas of active tumours tissue, the area where this is highest has been shown to be the densest area of infiltration of tumour cells [84], this ratio has also been shown to alter prior to progression [110].

Creatine is often used as an internal concentration reference as it is usually present in brain tissue. This is not always the case in glioma tissue though [94], where it is decreased. It is often absent entirely in high grade gliomas [94], and can therefore be used as a method of grading these tumours. This can mean that it is more useful to use Cho or internal water as a reference rather than Cr.

Signals arising from Lipids and Macromolecules are not usually seen in healthy brain tissue, but are elevated in tumour tissue [66, 68, 84, 94, 110, 113]. These are higher in aggressive tumours than benign and are often linked with malignancy [66, 68, 84, 94], and have also been shown to increase before progression [110]. LMM have also been confirmed using ex vivo sampling as a method to grade tumours [113].

One of the most prominent peaks associated with LMM signals is at 1.3/1.4ppm and 0.9ppm. This peak often overlaps with the doublet assigned to Lac, leading to some mis-assignment and inaccurate quantitation. This can be resolved by using an intermediate echo time of ~135ms, at this point Lac is inverted and the LMM signals have decayed. This inversion has been seen in glioma tissue [68]. Lac has been repeatedly seen in glioma tissue [68, 84, 89, 93, 94, 110]. As with LMM concentrations, Lac has been used in the grading of tumours, in particular in the grading of gliomas [68, 84, 93, 94]. One study saw only Lac in LGGs, whereas LMM signals were strong in higher grade tumours [94]. When performed on the cysts that are associated with a tumour, it has been shown that Lac is of use in the grading of tumours. Higher levels of lactate within a cyst pertain to higher level of aggression of the lesion [89].

Another metabolite present at short echo times, but not long, is mIns. This has been shown to be very important in the analysis of glioma tissue [67, 87, 90]. Lower grade gliomas show an elevated mIns signal [67, 90], whereas this is decreased in higher grade gliomas [67].

Other smaller metabolites not seen at long echo times include Glu, Gln, sIns and Tau. These have all been seen in tumour tissue [66, 87, 108], and have been useful in determining prognosis [108] and in grading tumours [66, 87].

PAEDIATRIC STUDIES

These findings have been echoed in studies performed on a paediatric cohort. Cho is repeatedly elevated in higher grade tumours and is useful for grading purposes [74]. NAA can also be used for grading, being higher in controls [72, 105] and in lower grade tumours [98] compared with more malignant lesions. Both of these metabolites have also been used to predict response to treatment [101, 114]. Percentage change in Cho concentration can be used to predict progression [101, 114], as can the maximum Cho/NAA ratio at diagnosis to predict survival time [107]. Creatine has again been shown to be significantly lower in tumour tissue when compared with normal surrounding brain tissue [86], this is especially low in glioma tissue [71, 98].

Again, LMM signals have been shown to be elevated in tumour tissue [72, 74, 75, 115, 116] and have been used in both diagnosis [72, 74, 115] and monitoring treatment response and progression [75, 116]. A conjunction with the signal arising from Cho, the best diagnostic accuracy [74] and independent predictor of survival [75] was achieved.

Not all tumours arising in adults occur in children and vice versa, and as such there are some findings that can only be detected in a paediatric cohort. Approximately one half of childhood brain tumours occur in the posterior fossa [41]. The three most common histopathological tumour types in the cerebellum are PA, medulloblastoma and ependymoma.

Cr concentration is especially low [71] in PAs and they usually have a prominent NAA peaks present at 2.0ppm and a high Cho concentration [73] .

The NAA peak is decreased in ependymoma and medulloblastoma spectra compared with PA spectra [71, 73, 100]. The presence of a large concentration of Cho in medulloblastoma spectra leads to the ratio NAA/Cho being able to be used to distinguish medulloblastoma from other posterior fossa tumours [73, 100].

Ependymoma spectra exhibit a very strong peak assigned to mIns [98, 99]. This can be used as a major distinguishing feature of the spectra associated with these tumours. The ratios mIns/Cho and mIns/NAA are lowest in medulloblastoma spectra [72, 99].

The presence of Tau in the medulloblastoma spectra is another distinctive characteristic of these tumours [71, 96, 98, 100]. This resonance is not seen in a large concentration of any other posterior fossa tumour, although it has been seen in germinoma spectra [71].

Other features seen in these 3 tumour types include PAs having a higher Lac/Cho ratio compared with the other 2 tumours types [73]. This echoes observations made with gliomas showing a high Lac concentration [68, 84, 89, 93, 94, 110]. Glx has also been reported as being elevated in PAs compared with other tumour types [72].

Another, less studied tumour type, more common in children, is the diffuse pontine glioma. This is a tumour with a particularly dismal prognosis [42] and little is understood about their biology due to lack of biopsy tissue. MRS has shown a strong resonance due to mIns and less pronounced increase in Cho compared with other tumours, leading to an elevated ratio mIns/Cho [72]. They also show a low ratio for Glx/Cho [72]. It is tumours such as these, where biopsy carries too large a risk that MRS can be of the most use.

AIM AND OBJECTIVES

AIM

The aim of this body of work is to improve the non-invasive characterisation of childhood brain tumours

OBJECTIVES

1. To assess short echo time (TE=30ms) MRS for the characterisation of childhood brain tumours, in particular the metabolites not easily quantitated in long echo time (TE=135ms) MRS
2. To compare MRS peak height ratios with metabolite concentrations for the diagnosis and characterisation of childhood cerebellar tumours
3. To apply these analysis methods to brain tumours of the pineal gland and brain stem, for which non-invasive diagnosis would be particularly useful
4. To explore the ability of MRS to predict the clinical and biological behaviour of pilocytic astrocytomas

MAJOR CONTRIBUTIONS

1. A simple classifier for childhood cerebellar tumours based on differences between peak height ratios [99] (chapters 4.2)
2. A comparison of methods between a simple peak height classifier and a more sophisticated method based upon metabolite and LMM concentrations as given by LCModel™ (chapters 4.3 and 4.4)

3. An analysis of the differences in spectra between childhood germ cell tumours of the pineal region and other tumours occurring in this area [117] (chapter 5)
4. An analysis of childhood brain stem tumours with an emphasis on diffuse tumours of the pons [118] (chapter 6)
5. An analysis of the variation between spectra of pilocytic astrocytoma occurring supratentorially and infratentorially [119] (chapter 7)
6. Determining preliminary prognostic markers for supratentorial pilocytic astrocytomas [119] (chapter 7).

OVERVIEW OF RESULTS

In chapters 5, 6 and 7, short echo time MRS is studied in a series of important clinical scenarios involving children with brain tumours. The ability of the technique to aid non-invasive diagnosis, provide prognostic biomarkers and improve treatment monitoring of childhood brain tumours is investigated. In particular, the role of metabolites which are not well quantified at long echo times is determined. The emphasis of the work is on providing guidance to clinicians in the use of MRS.

The strategy starts with the development and evaluation of simple classification schemes for cerebellar tumours at diagnosis, chapter 4. The aim of this chapter is to determine the ability of short echo time MRS to characterise a specified set of childhood brain tumours and determine the feasibility of providing a diagnostic scheme for clinicians. Cerebellar tumours were selected as the test-bed for this part of the work, since they have a

relatively high incidence and surgery usually forms part of the treatment making a definitive histopathological diagnosis available. Previous MRS studies have also been reported for this tumour group allowing important comparisons to be made.

Two approaches to MRS analysis are used in chapter 4. The first approach was designed to be used entirely in a clinical setting, where sophisticated MRS processing and analysis tools are not readily available (chapter 4.2). The method relies on measuring MRS peak heights of major metabolites from spectra produced by software available on the MR scanner. This scheme was developed using data collected using a single MR scanner (chapter 4.2.1) then evaluated prospectively using data collected from more that one centre (chapter 4.2.2). The classification scheme was also re-optimised using the entire data available (chapter 4.2.3). The second approach used a more sophisticated MRS analysis in which a commercially available software package (LCModel™ [120]) was used to quantify the concentrations of a larger number of metabolites and these were used to provide a simple classifier for diagnosis (chapter 4.3.1). This scheme was also evaluated prospectively on the same dataset that was used to evaluate the classifier based on peak heights (chapters 4.3.2).

Having investigated short echo time MRS on a group of tumours with a histopathological diagnosis, the technique was applied to brain tumours in the pineal gland (chapter 5) and brain stem (chapter 6). Developing non-invasive diagnostic techniques for tumours in these locations is of particular

importance, since surgery poses significant risks. Furthermore, the lack of tumour tissue for research makes non-invasive techniques for providing information on the biology of these tumours particularly valuable. This is illustrated in chapter 6 where the ability of two distinct types of diffuse pontine glioma a particularly poor prognosis and poorly understood tumour, is investigated and two distinct types may be defined by their MRS profiles.

The final clinical study of the thesis concentrates on one specific diagnostic type, pilocytic astrocytomas (chapter 7). A number of important biological and clinical problems exist for this tumour group beyond non-invasive diagnosis for which MRS could be an important tool. The non-invasive detection of variations between tumours in different locations of the brain; the measurement of prognostic biomarkers and the detection of early markers of treatment failure are investigated.

CHAPTER 2: MAGNETIC RESONANCE SPECTROSCOPY

The NMR phenomenon was first described in 1946 by both Felix Bloch [121] and Edward Mills Purcell [122], who later shared the Nobel prize in physics in 1952 for the discovery. Since then, NMR techniques have been increasingly used in both research and clinical settings.

Two important applications of the NMR phenomenon are now in both clinical and research use: Magnetic Resonance Imaging (MRI) and Magnetic Resonance Spectroscopy (MRS). In MRI, the protons present in tissue water are detected and these are used to generate a structural image. In MRS, it is the protons present in metabolites and macro-molecules other than water that are of particular importance.

A basic understanding of the fundamental principles of magnetic resonance (MR) is vital for understanding the role of MRS in a clinical setting. The following section outlines the basic principles of MR, equipment used and how it is applied in a clinical and research setting [123]. A full account of NMR physics and instrumentation is beyond the scope of this thesis, there are many standard texts which cover this in more detail [123, 124].

2.1 THEORY OF THE NMR PHENOMENON

Cells in the human body contain up to 90% water, this leads to a large prevalence of hydrogen atoms in the human body. The hydrogen nucleus is a

single proton, which has a positive charge and possesses a magnetic quality called nuclear spin. Other atomic nuclei, including carbon-13 and phosphorus also possess nuclear spin and can be used in an MR experiment, but hydrogen is usually the preferred choice. Hydrogen is the most abundant nuclei in the human body that possess a nuclear spin.

In the absence of an external magnetic field, the directions of nuclear spin vectors, usually known as magnetic dipole moments, are oriented randomly. However, when a body is exposed to a strong static external magnetic field (B_0), the magnetic dipole moments will align with this external field and they will begin to precess about the main direction of the field. An oscillating magnetic field is generated by the precessing net magnetisation. The frequency of this precession, the Larmor frequency, can be calculated via the Larmor equation:

$$\omega_0 = \gamma B_0$$

Equation 1: The Larmor Equations

ω = frequency; γ = gyromagnetic ratio; B = magnetic field strength

Under these conditions, known as the ground or equilibrium state, there exist marginally more spins aligned parallel to the field, in a low-energy state, than anti-parallel, in a high-energy state.

This excess number of magnetic dipole moments aligning parallel with the field produces a potentially observable bulk magnetization for a sample of spins when placed in an external magnetic field and it is known as the

macroscopic or equilibrium magnetization. Using a second electromagnetic field, oscillating at radiofrequencies perpendicular to the main field, these nuclei are pushed out of alignment, moving the net magnetization to a different angle. As these nuclei drift back to align with the main field they emit a detectable radiofrequency. Protons in different environments, i.e. in different tissue types, will realign at different speeds, and thus they will have a differing T1 relaxation time. When the spins precess in the transverse plane they induce an oscillating current that can be detected by the receiver coil. This signal corresponds to an exponentially decaying sinusoid in the time domain, and is called the Free Induction Decay (FID).

The energy difference between the two spin states is proportional to the frequency. This frequency is proportional to both B_0 and the gyromagnetic ratio, equation 1. The gyromagnetic ratio is characteristic of a given nuclei, and is relatively high for hydrogen. Thus, a nuclei with a high gyromagnetic ratio will lead to a larger energy difference between spin states. Hydrogen has a relatively large gyromagnetic ratio, leading to a larger energy difference and therefore improving the sensitivity of the technique. This, in addition to the relatively high abundance in the human body, is why 1H-MRS is the most commonly used for of MRS.

One factor affecting the strength of this signal is the number of nuclei that give rise to it, in order to increase the signal-to-noise ratio (SNR) several data acquisitions are recorded and the resulting signal is averaged over all of these.

The relaxation rate can be characterised by two time constants known as T1 and T2.

T1 (longitudinal) relaxation time describes the recovery of the z-component on the net magnetisation vector, while the T2 (transverse) relaxation time describes the decay of the xy component.

T1 (longitudinal) relaxation time is the time it takes to recover 63% of the equilibrium magnetisation [123]. It is related to the transfer of energy from a nuclear spin to the surrounding environment, this is usually referred to as a lattice and hence this can sometimes be referred to as spin-lattice interactions. At equilibrium point, all the magnetisation is aligned with the external field.

The T2 relaxation time is related to the effect that nuclear spins have on each other; these are often referred to as spin-spin interactions. This refers to the loss of phase coherence of the spins as they interact via their oscillating magnetic fields. The slight change in B experienced by the proton cause its Larmor frequency to change (Equation 1). The result of this is that the precession of spins moves out of phase and this loss of phase coherence results in a reduction in the transverse magnetisation. In general, T2 is greater than or equal to T1.

In an ideal model, the FID will decay exponentially with T2. Spins will dephase due to molecular interactions as well as an inhomogeneous magnetic field. These inhomogeneities in the external field cause the field to

have slightly different strengths at different locations in a sample. This causes the Larmor frequency to vary across the body, which leads to destructive interference. This interference, in turn, shortens the FID. The observed decay of the FID is described by a time constant known as T2*. T2* is always shorter than T2. Additional coils can be used to compensate for these inhomogeneities. These are referred to as shim coils and the current in these coils can be altered to improve the magnetic field distribution. This process is known as shimming.

2.2 MAGNETIC RESONANCE SPECTROSCOPY (MRS)

Metabolites, and other resonances, can be distinguished in a spectrum due to a feature known as chemical shift. The chemical environment of a given nucleus will effect the resonance frequency, the chemical shift is a measure of this dependence [123].

A synthesised proton MR spectrum is shown Figure 4, this spectrum was produced using software that uses the density matrix formulation of NMR [125]. Each of these peaks is 'fixed' at a given frequency [123]. This is shown as a fixed position on the x-axis, which shows the chemical shift. The chemical shift on this axis is parts per million (ppm) of B_0. Some of the signal is seen as being inverted, this is due to not all of the signal being refocused at an echo time of 30ms.

This can be explained using an example, such as lactate which has a J-coupling of 14Hz. To fully refocus something with a J-coupling of 14Hz you

need an echo time of 1/14. For lactate this will be a TE = 0.270s or 270ms or multiples of this, i.e. TE = 0, 270, 540ms etc. If a TE of half of this is use, i.e. 135ms for lactate, then the peak/s will be inverted. TE of 30ms is close to 0ms, thus a majority of the signal from lactate will be refocused, but a small component will appear inverted about the x-axis.

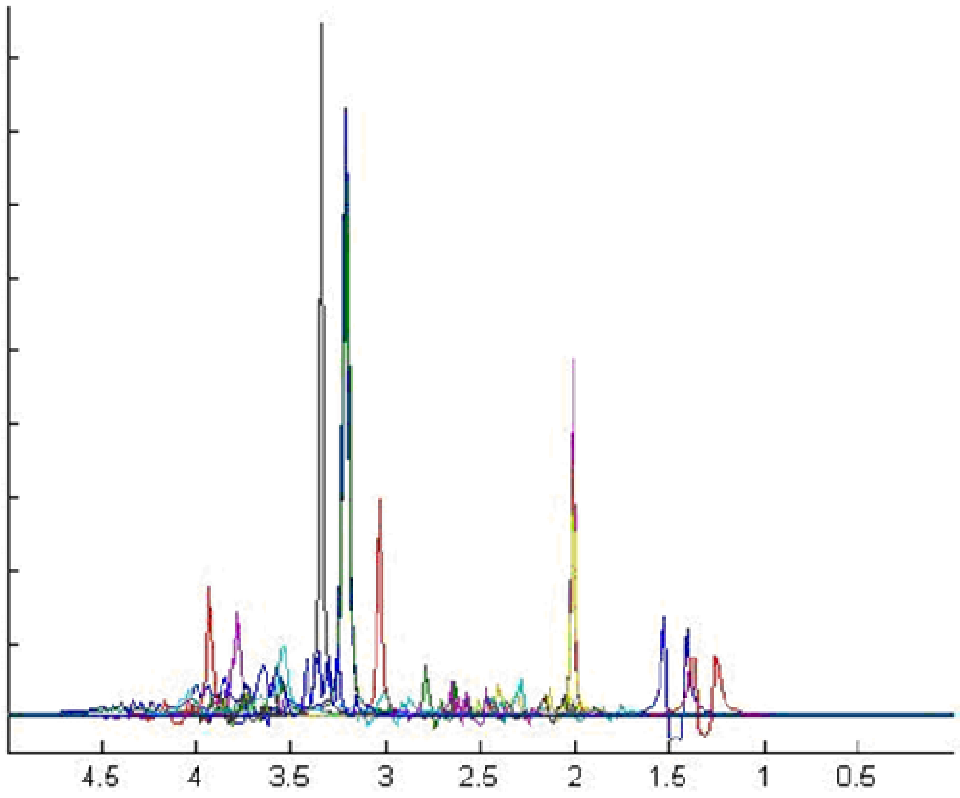

Figure 4: Synthesised in vivo 1H-MRS spectrum, the region is limited to 0ppm – 5ppm. Each metabolite's individual spectrum is shown in a different colour.

Simple metabolites may just give a single peak. Other metabolites lead to a combination of singlets and multiplets.

Nuclei that are connected with covalent bonds will experience some effect from each other's effective magnetic field. This effect can be detected in the MR spectrum between non-equivalent nuclei. This effect is known as J-

coupling, or spin-spin coupling, and is seen in the MR spectrum as a splitting of peaks [123]. An example of this effect can be depicted by the doublet shown by lactate (Figure 5)

Lactate has three magnetically equivalent methyl protons coupled to a single methine proton. Since the methyl protons are magnetically equivalent they do not produce any splitting between themselves, but they do experience an effect from the methine proton, this results in the doublet seen at 1.31ppm. The methine proton experiences three spins, all of which have the same coupling constant. The result of this is the line at 4.10ppm splitting into four (a quartet), with a ratio of 1:3:3:1 (figure 5b).

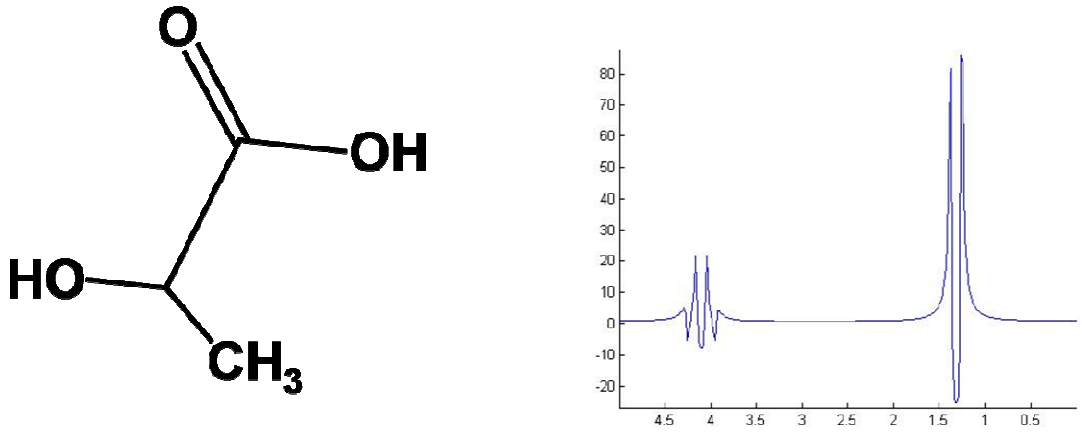

(a) (b)

Figure 5: (a) molecular structure of lactate; (b) 1H spectrum of lactate

From the pattern of the resulting peaks we can determine which metabolites are being seen in a spectrum. This can be achieved by using a combination of the known spectra of specific individual metabolites (Figure 4). These known spectra can then be used to 'fit' to the experimental spectrum, and this can give information regarding which metabolites are present and in what

abundance. All metabolite concentrations have to be calculated in reference to a known peak; usually water.

MRS can be performed both in vivo and in vitro. Spectra taken in vitro can be used to aid in the interpretation of those taken in vivo. In the case of in vitro, or ex vivo, NMR, the tissue is frozen at the time of surgery using liquid nitrogen. This tissue can then be transported to the spectrometer for analysis. The field strength used to obtain in vitro spectra can be as high as 21T compared to the usual 1.5T used clinical practice. A higher magnetic field strength will lead to better signal-to-noise, resulting in a clearer spectrum with greater peak resolution. In addition to this, leading to a spectrum with sharper peaks, that can be more easily assigned to metabolites.

2.3 CLINICAL MRS

2.3.1 PULSE SEQUENCES

A spin-echo is the reappearance of the MR signal after the initial FID has decayed. To generate a spin-echo signal, a 180° pulse is applied after the 90° pulse. Local variations in the field cause some spins to precess faster than others, this leads to a spread of phases at the 180° pulse. This refocusing pulse reverses the order, but not the direction, of the precession. Thus, those spins that were precessing faster are now behind, in the sense of phase, the lower frequency spins. After a period of time, equal to that between the 90° and 180° pulses, the spins realign to form an echo. This process can be repeated by applying subsequent 180° pulses, creating an ‘echo train’ of signal. The 180° pulse does not cause all of the protons to fully

rephase, due to the inhomogeneous magnetic field; therefore the full transverse magnetisation is not fully recovered. The pulse does cause a proportion of the original phasing to be recovered. Therefore, the maximum intensity at each pulse is limited by an exponential decay curve, this has the decay constant T2. This value is always greater than T2*, since T2* has components from both fluctuations in the magnetic field within the body and also non-uniformities in the magnet itself.

This can be used to obtain localised MRS data, by only exciting and refocusing signal within a desired volume. The two most common methods, used in single-voxel spectroscopy (SVS), are stimulated echo acquisition mode (STEAM) [126] and point-resolved spectroscopy (PRESS) [127]. For all the work published here, the PRESS sequence is used.

The PRESS sequence [127]:

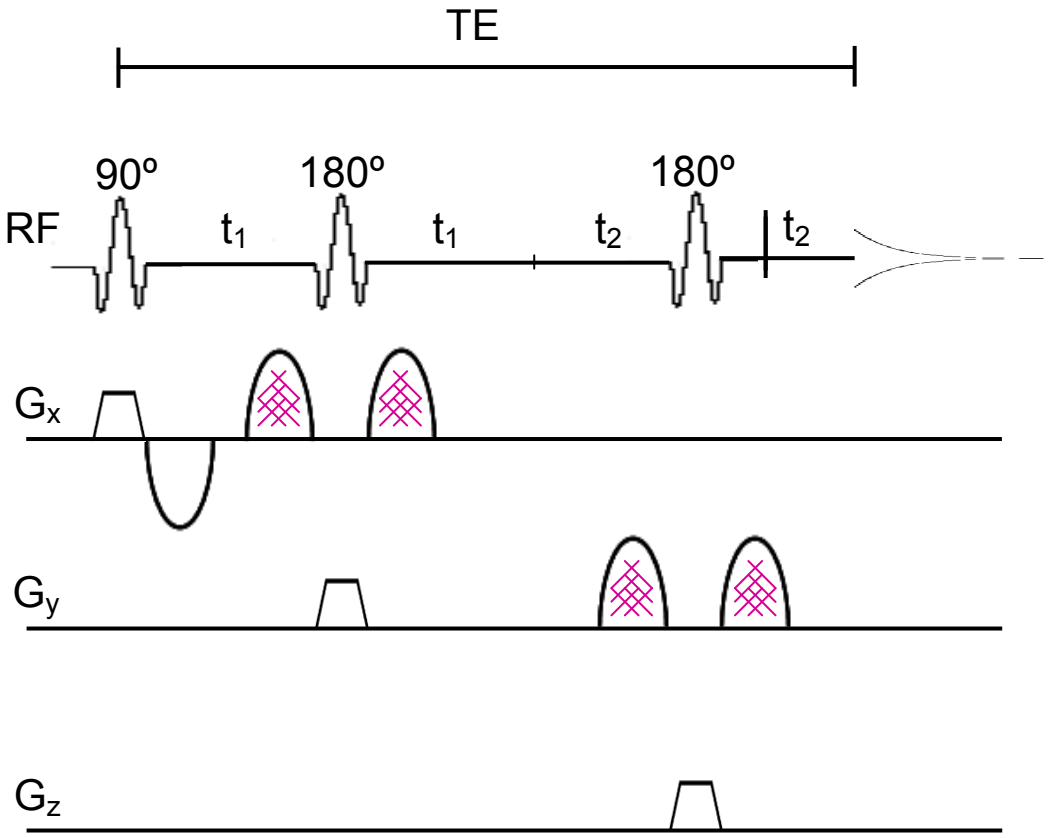

Figure 6: The PRESS Sequence
The use of crusher gradients (highlighted in pink) to flank the 180º refocusing pulses will ensure that there is selection of the desired coherences, while destroying all others.

PRESS is a double spin-echo method, where slice-selective excitation is used in combination with two slice-selective refocusing pulses (figure 6). The initial 90º pulse is followed after a time period t_1 by a 180º pulse. This is followed by a spin-echo at 2 t_1. The second 180º pulse is applied to refocus this spin-echo at a delay time $2t_2$. This leads to a final spin-echo appearing at a time $2t_1 + 2t_2$, this is equal to the echo time of PRESS ($TE = 2t_1 + 2t_2$). The first spin echo only contains signal from the column that is the intersection between the two orthogonal slices selected by the 90º pulse and the first of the 180º pulses. The second spin-echo only contain signal from the intersection of the

three planes selected by the three pulses, this results in the selection of the desired volume. Signal outside of the volume of interest is either not excited or not refocused; this leads to rapid dephasing of the signal by the “TE crusher” magnetic field gradients. This block of three pulses (90°-180°-180°) is successively repeated. The repetition time (TR) refers to the time interval between 90° pulses and the time between the 90° pulse and signal sampling is referred to as the echo time (TE).

2.3.2 WATER SUPPRESSION

The metabolites of interest have much lower concentrations (mmol/l) than that of tissue water (1-10mmol/l). This leads to a signal at 4.7ppm dominating the ^{1}H-MR spectrum. In order to detect the metabolite signal, it is necessary to suppress the large signal from water [123].

One method in which to achieve this is by applying sequences of short, high amplitude RF pulses with delays between. This allows for frequency selective excitation. These sequences are designed to allow the metabolite resonances to rotate into the transverse plane, thus allowing for signal detection, while the water is returned to the longitudinal axis, rendering it unobservable. While this method is imperfect, it does perform well and allows for the majority of the signal from the water molecules to be removed [123].

2.3.3 MRS SIGNAL PRE-PROCESSING

The FID consists of signal from a variety of sources, including those from all metabolites, LMM and macromolecules. In addition to this, there will be components from noise and, potentially, a signal due to residual water. Several steps can be undertaken in order to maximize data quality and remove any irrelevant information.

FREQUENCY ALIGNMENT

Spectra are referenced by assigning a known chemical shift to a metabolite. In scanner processed spectra the spectra will be aligned to the water peak at 4.8ppm. This is generally stable at 4.8ppm; however it does have a sensitivity to temperature and pH. The molecular location of the water can vary between intercellular and extracellular water, which can also lead to some line broadening of the water peak.

In spectra processed by LCModel™ [120] there are two options on processing, dependent on whether the region of interest is healthy brain or tumour. In the case of healthy brain, the spectrum is aligned to the NAA peak at 2.0ppm, which is generally stable and the largest peak in health brain in the region 0-4ppm. In tumour spectra, the spectrum is aligned with a combination of peaks and shifted accordingly to allow for the variation seen in tumour spectra.

PHASE AND LINESHAPE CORRECTION

A water unsuppressed spectrum can be used to correct the phase of a spectrum, by dividing the water suppressed signal by the phase term of the water unsuppressed signal. This step corrects for eddy currents, which are caused by imperfections in the instruments.

Most quantification tools model the spectrum as a sum of lorentzian lineshapes. In practice, this is not achieved in vivo due to the effects from eddy currents and inhomogeneities in the magnetic field. Eddy currents cause a time varying magnetic field, this distorts the MR resonances. Time varying magnetic fields are the same for all resonances, thus the unsuppressed water spectrum can be used to correct for these contributions. Contributions due to inhomogeneities can be removed by dividing the water suppressed FID by the unsuppressed envelope.

RESIDUAL WATER

In the region 1-4.2ppm residual water is not generally a problem; this is the region of interest for the scope of this thesis. In regions closer to the water peak, there are several automated post acquisition methods, most of which use a single value decomposition of the FID signal [123].

BASELINE CORRECTION

Most spectra will exhibit sharp metabolite peaks superimposed upon a baseline of broader components, mainly arising due to contributions from

macromolecules. Many analysis tools use prior knowledge of these macromolecules to account for this signal.

2.3.4 TYPES OF MRS LOCALISATION: SVS Vs MULTIVOXEL

The 2 main approaches of collecting MRS data: SVS and multivoxel (also known as chemical shift imaging (CSI) or magnetic resonance spectroscopic imaging (MRSI)). SVS is performed by selecting a region of interest and placing 1 voxel (volume of interest) in this region. CSI is performed by placing a grid of voxels over the region of interest; this can be performed in 2D or 3D.

In a CSI examination, a grid of voxels is placed on the area of interest. This can then either be viewed as a matrix of spectra or as a colour map, with areas of high concentration of a selected metabolite (or ratio of metabolites) being graded.

CSI is particularly useful in detecting spread of disease beyond the obvious foci; this is of particular use in diffuse tumours [112, 128]. MRS can be used in surgical planning to guide biopsy [70], by targeting areas of active tumour in adults. It is also very useful post operatively, in the assessment of irregular shaped or large, heterogeneous lesions, to determine response to treatment and areas of recurrence [109, 110]. However, it is challenging to perform CSI at shorter echo times and thus the amount of information contained is limited. Also, long acquisition times are needed to obtain a good quality spectrum.

2.3.5 ECHO TIMES

In a spin-echo experiment a second RF pulse is applied after the initial 90° pulse, with a precession angle of 180° after a given delay time. A spin-echo can then be detected, this information can be collected at different echo times (TEs). In principle both the spin-echo time domain signal and the FID contain the same information about frequencies and intensities. However, the delay time between the 2 RF pulses used in the spin-echo experiment allows nuclear magnetisation to be manipulated and this can be used to create spatial localisation.

The timing of the different RF pulses used is determined by both TE and TR. TE is defined as being the time between the initial application of a 90° RF pulse and the peak of the echo. This results in a differing amount of metabolite information being present in the resulting spectrum. TR is defined as being the time between pulse sequences as applied to a single slice. SNR will be greatly improved by the collection of repeated measurements, thus TR results from the compromise between the desired SNR and the time for the taken for the experiment.

Signals from different metabolites have different rates of decay; this is due to the T2 value being dependent on the environment protons is found in. By collecting data at different echo times we obtain information from a different number of metabolites. At short echo times less metabolite signals have decayed, leading to more information being present in the spectrum.

However, this can be problematic due to overlapping peaks and the presence of signals from lipids and macromolecules.

Longer echo times (TE>135ms) allow for a more signal intensity to decay, resulting in fewer peaks and, thus, a clearer spectrum (figure 7a). However, this leads to the loss of potentially interesting metabolite information.

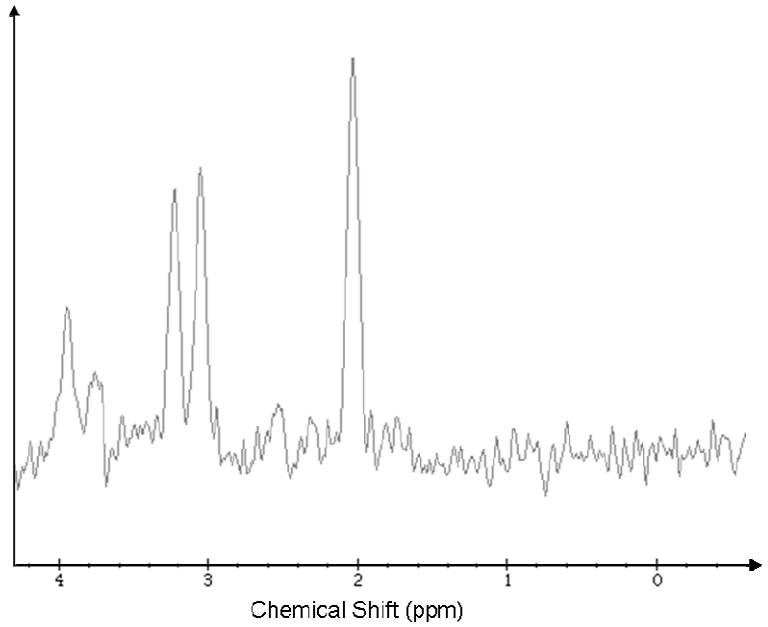

Figure 7a: Example of a 1H spectrum taken at TE = 135ms

Signal due to small metabolites with strong J coupling decay at longer echo times, due to destructive interactions between resonances with *J*-coupled induced phasing. These include signals from Glutamate, Glutamine and myo-inositol (mIns). Lipids and Macromolecules can often dominate a short echo time spectrum, however these have short T2 decay times and are, therefore, not present in a long echo time spectrum.

Spectroscopy at a long echo time is particularly beneficial in certain regions, such as, between 2 and 2.6ppm. This region contains signals from NAA, Glu,

Gln, LMMs, as well as smaller metabolites such as GABA. Despite this benefit, problems can occur in the determination of NAA in a spectrum [129], usually, with concentrations often being overestimated. By using a longer echo time Glu, Gln, much of the LMM signals and those from smaller metabolites have decayed and, so, this peak is clear and the concentration is more easily determined. In addition to this, lactate is inverted at longer echo times (TE~135ms), and this can be more easily assigned.

However, this benefit of easy peak assignment and quantitation is offset by the lack of information present in a long echo time spectrum. Those metabolites which decay quickly are often of a lot of importance when it comes to analysing a tumour, and a short echo time spectrum could be beneficial. An example of a short echo time spectrum is shown in figure 7b, this spectrum was taken at the same time as that in figure 7a. Both spectra were of the same voxel and were taken using identical parameters with only the echo time varying between them.

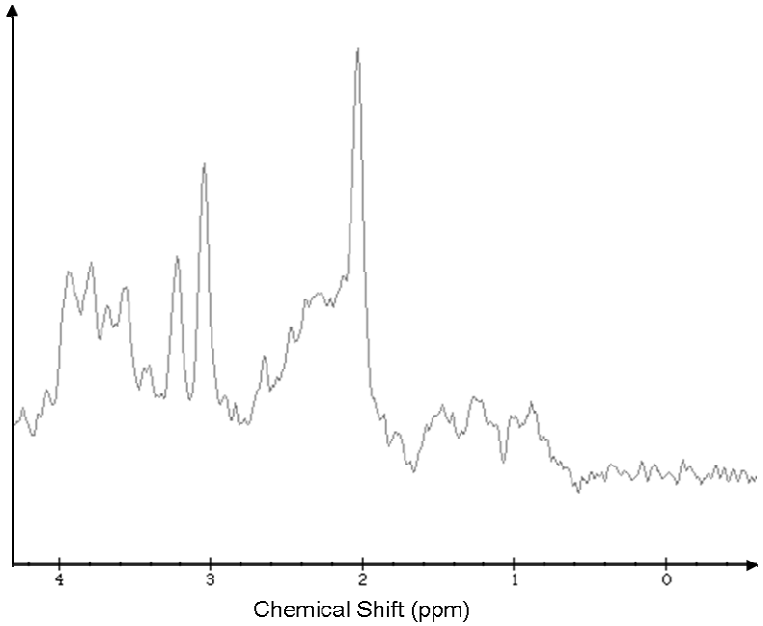

Figure 7b: Example of a 1H spectrum taken at TE = 30ms

For example, the signals from the LMM regions have been shown to be important in the analysis of tumours [65, 66, 68, 72-75, 94, 110, 115]; these are no longer present in long echo time spectra. In short echo time MRS, signals from small, strongly coupled metabolites and LMM regions can be detected and quantified.

In some cases, using 2 echo times in the same investigation is beneficial, to obtain the maximum information. For example, mIns has decayed at longer echo times, and this has been shown to be useful in many studies investigating neurological problems [35, 88, 91, 130-132] and brain tumours [67, 68, 71, 72, 87, 98, 102, 112, 128, 133]. However, there is some argument as to whether the peak at 3.6ppm is due to mIns or whether it is due to glycine (Gly) [128, 134]. Gly is a singlet whereas mIns is a multiplet, and this leads to a different appearance, that may be possible to distinguish

between at higher field strengths due to an improvement in SNR. This is not easily achievable at 1.5T, but by using 2 echo times the information about both metabolites can be determined and also the peak assignment can be verified. However, this is often not possible in a clinical scenario, due to time constraints.

2.3.6 FUNCTIONS OF DIFFERENT METABOLITES [123]

NOTE: All spectra are simulated as if acquired with PRESS and a 30ms echo time

N-Acetyl-Aspartate (NAA) (prominent peak from methyl group at 2.01ppm + smaller resonances arising from the CH_2 and CH groups corresponding to doublet of doublets at 2.49, 2.67, 4.38ppm; plus amide proton broad temp sensitive resonance at 7.82ppm) is exclusively localised to the central and peripheral nervous system and is a marker of neuronal density.

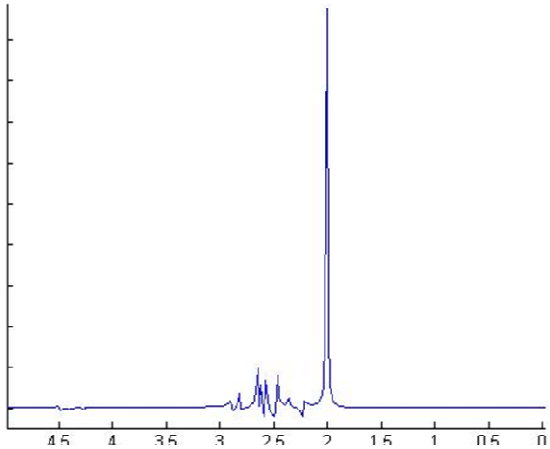

Figure 8a: Spectra of NAA

It is the largest peak seen in a spectrum of healthy brain. It has been shown to vary in neurological conditions [131, 135] and be decreased in brain tumours [72, 73, 87, 90, 96, 97, 99, 105, 107, 110, 114].

In addition to this there is some overlap NAA peaks with those arising from ***N-Acetyl-Aspartyl-Glutamate (NAAG)***, a prevalent neurotransmitter.

Choline containing metabolites (most prominent in vivo at 3.2ppm, with secondary peaks between 3.5 and 4.0ppm)) include ***GPC***, ***PCH*** and free choline. It is often not possible to clearly distinguish between the singlets around 3.2ppm at 1.5T, although some studies claim that this may be possible [98].

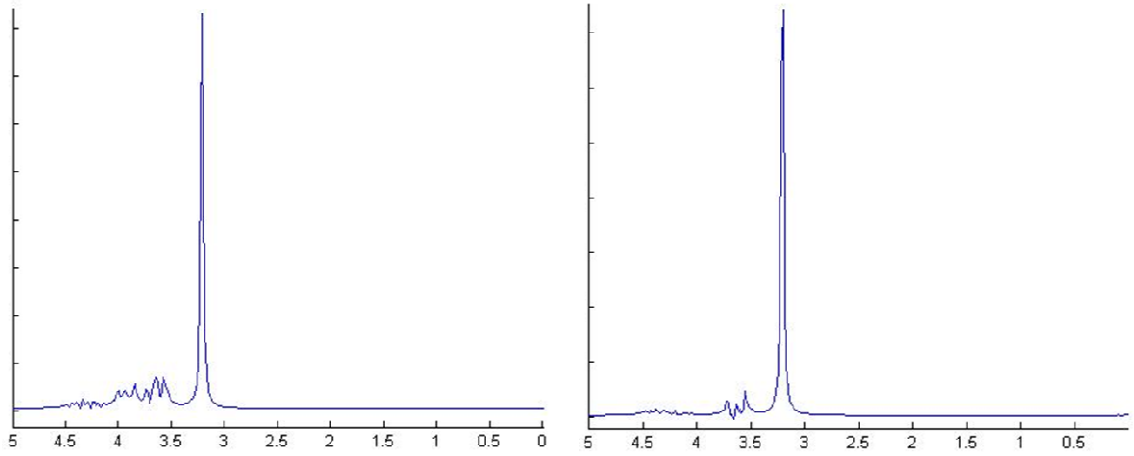

(i) (ii)

Figure 8b: Spectra of (i) GPC and (ii) PCh

These metabolites are more easily distinguished by using 31PMRS [86]. An analysis of the combined peak (***tCho***) has been correlated with cell proliferation and is usually elevated in tumours [66, 70-72, 74, 75, 84, 87, 90, 93, 98-101, 128, 136].

Creatine (Cr) and ***Phosphocreatine (PCr)*** (3.03ppm and 3.93ppm) are usually combined in spectral analysis to become total Cr (Cr henceforth), due to the close proximity of their peaks at 1.5T.

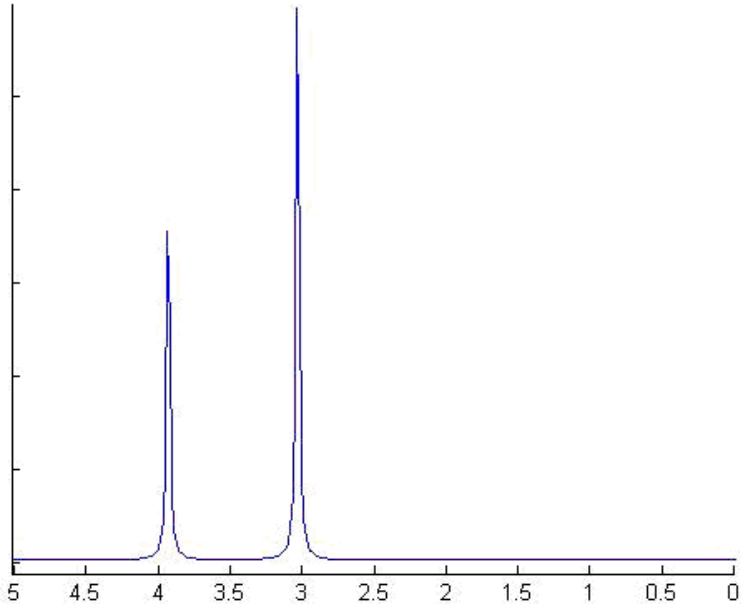

Figure 8c: Spectrum of Cr

This is present in neuronal and glial cells and is involved in energy metabolism. It has been shown to be decreased in gliomas [71, 96, 98, 137].

Myo-inositol (mIns) (multiplets between 3.27-3.61ppm) has a doublet of doublets at 3.52ppm and 2 triplets (1 at 3.61 and 1 at 3.27ppm – which are close enough together to form a single multiplet at 1.5T). It has a function that is, as yet, unknown. It has been shown to be altered in many tumours [27, 29, 35, 67, 68, 71, 72, 87, 90, 98, 99, 112, 128].

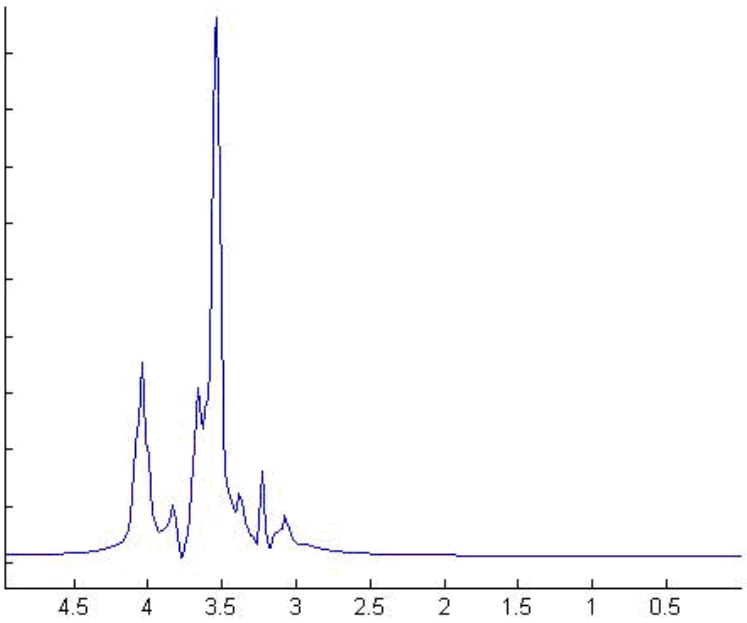

Figure 8d: Spectrum of mIns

It has been used as a glial marker [87], and there is evidence of an association with gliosis. It is elevated in gliomatosis [90, 112], has been used in grading astrocytomas [67, 68], has been shown to be high in ependymomas when compared with other cerebellar tumours [98, 99], and it is high in diffuse pontine gliomas [72]. In addition to mIns, ***scyllo-inositol (sIns)*** can occasionally be distinguished (singlet at 3.34ppm); this also varies in neurological problems and tumours [35, 108, 130, 132, 134].

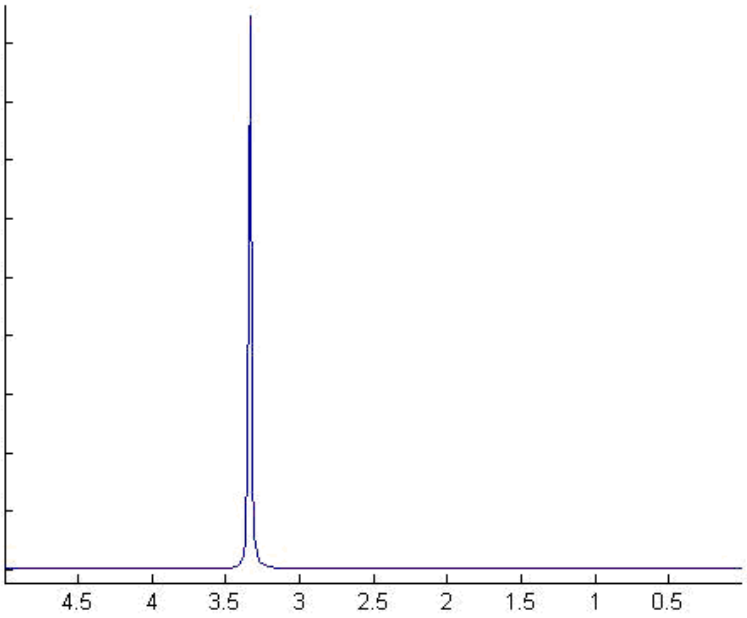

Figure 8e: Spectrum of sIns

Glycine (Gly) is an amino acid and resonates as a single peak at 3.55ppm. This peak is often indistinguishable from mIns at low field strength.

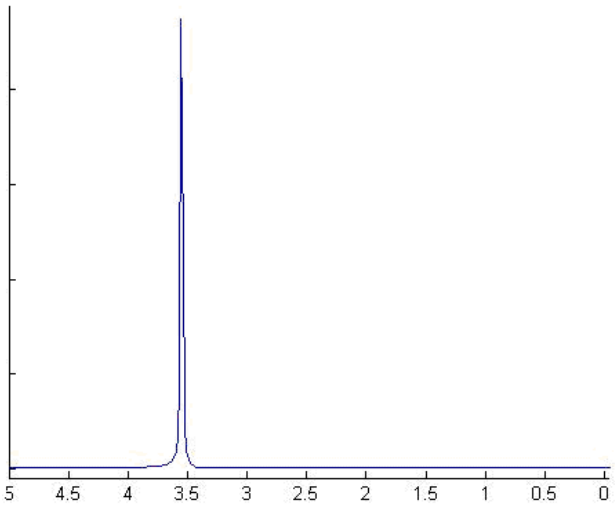

Figure 8f: Spectrum of Gly

Lactate (Lac) is an end product of anaerobic glycolysis with doublet at 1.31ppm (these peaks become inverted at an echo time of 135ms, this allows for clarification of assignment).

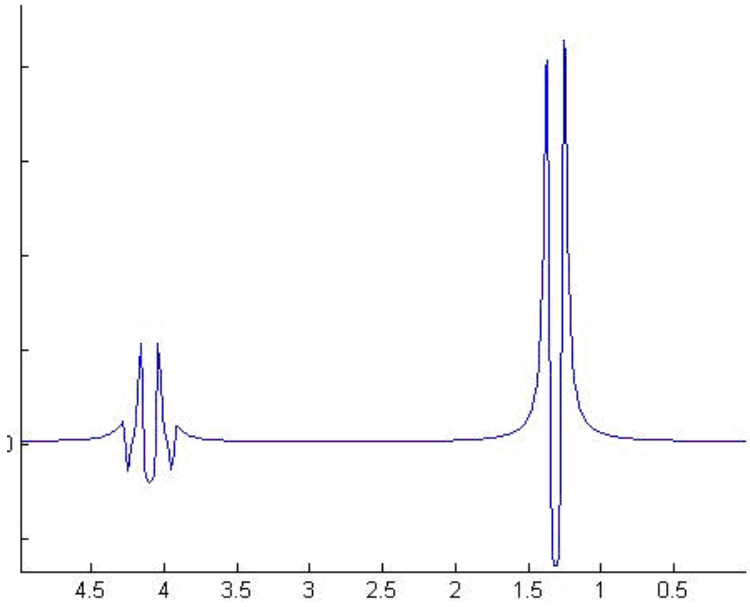

Figure 8g: Spectrum of Lac

There can often be some confusion over the assignment of Lac when signals from lipid and macromolecular signals are present at short TE [75]. Lac is high in cysts and cystic masses [89, 94]. It has been used in the grading of gliomas [68, 93] and for distinguishing between pilocytic astrocytomas and other cerebellar tumours [73].

The peaks attributed to ***taurine (Tau)*** (2 triplets at 3.25ppm and 3.42ppm – the two triplets are close enough together to form a single multiplet at 1.5T) often merge with tCho at low field strengths, and can only be reliably assessed in good quality spectra.

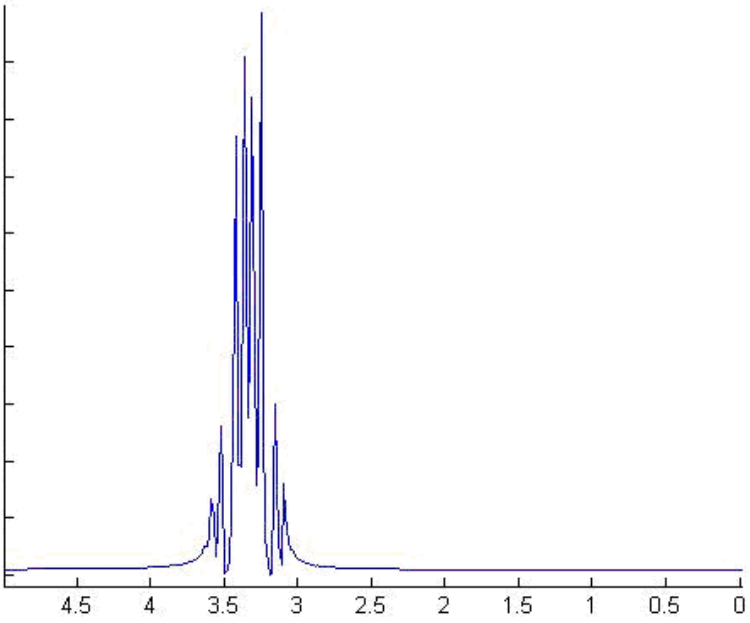

Figure 8h: Spectrum of Tau

Tau has been shown to be high in medulloblastomas [71, 96, 98, 100] and is also seen in pineal germinomas [71].

Lipid and macromolecular (LMM) resonances occur at various regions in a 1H MR spectrum. Particular areas of interest are the regions around 0.9ppm, 1.3-1.4ppm and 2.0-2.6ppm. These can be very large and dwarf metabolite signals. The signals are not always due to the tumour being analysed, they can be due to lipid in surrounding tissue, especially the scalp if the tumour is close to the skull. Saturation bands can be placed to remove signals being observed from outside the voxel. These should be used where possible to remove the chance of external contamination of the spectrum. LMM resonances can be due to necrosis, and therefore are high in high grade tumours [66, 72, 74, 75, 94, 110] and one study showed them to increase before progression [110].

2.4 ANALYSIS TOOLS

There have been numerous analysis tools published for MRS pre- and post-processing. These are generally automated with some user input dependent on the desired output. Two of the most commonly used analysis tools are LCModel™ [120] and jMRUI [138].

LCMODEL™[120]

The Linear Combination Model (LCModel™) is a robust tool frequently used in the analysis of MRS due to its flexibility and relative user-independence. It comprises automated pre-processing and uses a basis set of experimental single metabolite and LMM spectra. This also enables it to potentially discern partially overlapping spectra, such as PCh and GPC, under good conditions. The basis set can be either obtained on site or imported from a library of those from a wide range of scanners.

LCModel™ gives a 'fit' to the spectrum of a combination of the peaks in the basis set; in addition to this it gives a list of the known metabolites, lipids and macromolecules in the spectrum.

JMRUI

The Java-based MR User Interface for the processing of in vivo MR spectra (jMRUI) offers considerably more user input. This offers a broad range of pre-processing options available for implementation by the user. Peak-picking can be used to select peaks for quantitating, using tools such as AMARES [139].

2.5 EXTENSIONS

It is possible to perform MRS using any nucleus with a magnetic moment. The second most commonly used is 31PMRS. 31PMRS has many applications in vivo, including observing phospholipid metabolism. This has been used to predict the rejection of liver transplants [140] and in assessing the livers of diabetic patients [141]. Other uses include the assessment of muscle metabolism [142] and heart disease [38]. In addition to this, it has been used in the oncology setting both extracranially [143, 144] and intracranially [30, 86, 103, 113, 145-148]. It is especially useful to better visualise the choline region [30, 86, 103, 145, 147]. ^{31}P is also found in other neurometabolites such as PMEs, PDEs and PCr.

2.6 CHALLENGES OF MRS

Despite the information that MRS can provide, there are technical challenges that restrict and hinder the use of MRS. The first of these can be attributed to the signal arising from water. Due to its abundance in mammalian tissue, the water signal (resonance at circa 4.7ppm) is several orders of magnitude stronger than any of the metabolite signals. This leads to much difficulty in the detection and quantitation of metabolite signals.

An important limitation is the limited chemical shift range visible using in vivo MRS, this is approximately 10ppm. Limited resolution leads to a large number of resonances overlapping and makes quantification difficult. Only 15-20 metabolites can be detected at a short TE.

Correct voxel placement is vital in obtaining a valid spectrum, classification rates have been shown to vary depending on where the voxel was placed within the tumour [149]. Where the edge of the tumour was included in the voxel the classification rate was significantly higher.

Contaminants in the spectrum can also pose a serious problem. When a voxel is placed close to the edge of the brain, scalp lipid can affect the spectrum, giving peaks at 0.9pmm and 1.3ppm. If unaccounted for these could dominate the spectrum or be mistaken for lipid signals from within the tumour itself. Voxel placement near vessels and CSF also affect the spectra, often increasing the noise significantly and making a spectrum largely unreadable. Mannitol is sometimes given to reduce intracranial pressure, which is common at presentation with a brain tumour. This has a peak around 3.8ppm, which can be mis-assigned as a metabolite within the tumour [150], although if this is known this issue can be avoided.

At short echo times there is the lack of distinction between peaks, due to spectral congestion [129-131, 133, 151-157]. Small metabolites with a weak signal can often become difficult to quantify in a spectrum. These metabolites can potentially be of much use in assessment of tumour and other neurometabolic disorders, such as sIns and Tau [66, 71, 96, 98, 100, 108, 130, 132]. These can be either mis-assigned or incorrectly quantified. There are 2 regions that are of particular challenge: the region between 2 and 2.6ppm and the tCho region around 3.2ppm.

The region between 2 and 2.6ppm contains Glu, Gln, NAA and numerous smaller metabolites such as GABA and NAAG. These all overlap and can be mis-assigned [129]. NAA is more easy to quantify at long echo times [158], but this is not the preferable solution as much information will be lost regarding the smaller metabolites. Some sequences can be used to better quantitate these metabolites [154, 157] or a higher field strength can be used to ensure a better resolution and SNR.

Although the tCho peak occurring at ~3.2ppm varies between tumours, this is not one metabolite alone. The tCho peak seen at 1.5T at 3.2ppm is made up from contributions of PCh, GPC, choline and phosphotidylcholine. These peaks can be difficult to distinguish at 1.5T, although this can potentially be achieved, for data obtained under good conditions, using fitting tools such as LCModel™ [98]. One study of posterior fossa tumours in children showed that GPC and PCh varied between tumours and could be used to distinguish between medulloblastoma and ependymoma spectra, with higher concentrations of PCh being reported in medulloblastomas and higher concentrations of GPC in ependymomas [98]. These findings were confirmed by ex vivo high resolution NMR. The observation of elevated PCh in medulloblastoma would be in agreement with observations made using high resolution NMR of neuroblastoma tissue [159], these tumours are of the same origin, so it would be expected for them to show similar metabolite profiles.

Further problems can be caused by normal alterations in metabolite concentrations. As the brain matures, metabolite concentrations will vary [130, 134, 160, 161]. In addition to this, metabolite concentrations can vary with the region of the brain being studied [134, 160, 161]. Both of these can potentially interfere with the interpretation of a spectrum, and can also impact on whether finding we see in adult tumours can be used in the assessment of paediatric tumours.

Some metabolite changes occur very early in life (within the first year) and then remain approximately stable, including PCr, Cho, mIns and Glu [161]. In this time NAA increase in grey matter, but remains stable in white matter [161]. There is a high concentration of Tau in the cerebellum and in grey matter in infancy, which then decreases and stabilise [161]. In the basal ganglia, both Tau and NAA remain constant with age [161]. There is an increase in NAAG in the thalamus and in white matter and a decrease in Gln in white matter [161].

Some variation has been reported later in life [130, 160]. A significant increase in total metabolite concentration was reported between the ages of 25 and 31 in the orbital frontal cortex and sensor-motor cortex [160]. Both of these regions also exhibited a gender dependence, with women showing increased concentrations [160]. Other metabolites have been shown to alter in the normal ageing brain [130].

2.7 SUMMARY

MR sequences can be manipulated in many ways in order to achieve different information from MRS. Features such at echo time and field strength impact upon both the quality of the data obtained and also the information it is possible to extract from the resulting spectrum.

It is more challenging to both collect and analyse data at shorter echo times, however these can be partially resolved by using tools such as LCModel™, or moving to higher field strength to ensure a higher SNR and better resolution.

The additional information available in a short echo time spectrum could be potentially of much importance in the better understanding of childhood brain tumours; as such these are the spectra that will be analysed in this thesis.

CHAPTER 3: METHODS

3.1 EXPERIMENTAL PROTOCOLS

At BCH the majority of data was collected using a 1.5T Siemens' Symphony, although some spectra are acquired using a 1.5T GE Signa Excite. Single voxel MRS was acquired using a PRESS sequence [127] at either short (TE = 30ms) or long (TE = 135ms) echo time. Studies all used a relaxation time of 1500ms. If the voxel had a 2cm side, then data was collected at both short and long echo times. If the voxel had a 1.5cm side, only short echo time data was collected. This was done primarily to verify the quantitation of certain metabolites, such as NAA. Dual echo time data was also used to verify the assignment of certain metabolites with different decay rates which may lie very close to each other, an example of this is mIns and glycine (Gly).

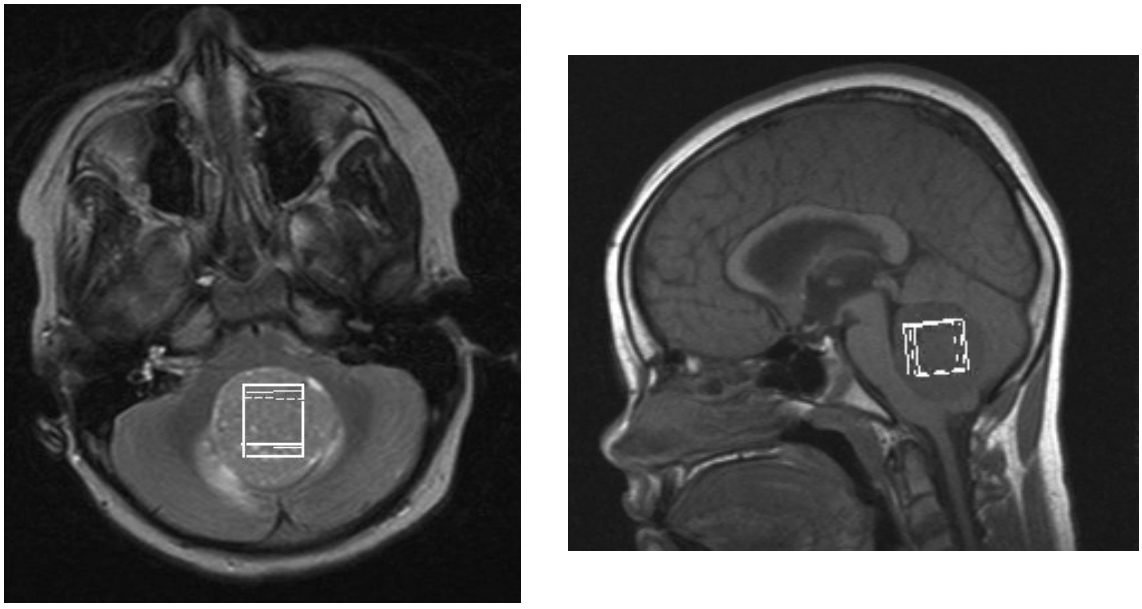

(a) (b)

Figure 9: Voxel placement for a cerebellar tumour (a) in the axial plane and (b) in the sagittal plane

A cubic voxel was placed by the radiologist or an experienced radiographer. This was ideally to be placed entirely within the tumour, maximally over the

solid tumour component. This criteria was not always possible, as some tumours were smaller than the 1.5cm sided voxel, in these cases it was required that the tumour filled over 50% of the voxel and special consideration was taken over these cases when using the spectra in analysis, and it was usually removed from formal analysis. Voxel placement was confirmed by storing MR images with the voxel location recorded (figure 9). For a 1.5cm cubic voxel, 256 repetitions were used and for a 2.0cm cubic voxel, 128 repetitions were used. For patients who had tumours which were large enough to accept a 2cm sided voxel, an additional MRS acquisition was performed using an echo time of 135ms. All other parameters remained unchanged including shimming, gain and water suppression. In all cases, a water MRS acquired at the same time as the water suppressed MRS was used to correct for eddy currents and as a reference for metabolite concentrations.

For studies involving data from other centres within the Childhood Cancer and Leukaemia Group (CCLG), MRS was performed on children from one of four centres: Birmingham Children's Hospital (BCH); the Royal Marsden Hospital – Sutton (RMH); Queen's Medical Centre – Nottingham (QMC); and Great Ormond Street Hospital (GOSH). At GOSH data was collected using a 1.5T Siemens' scanner, at QMC data was either collected on either a GE or Phillips scanner, both 1.5T and at RMH data was collected using a 1.5T Phillips scanner.

The acquisition protocol remained the same between centres, with parameters remaining largely constant. Data was collected following the protocol laid out by the CCLG, although there were some marginal discrepancies in the echo time. This was not a large enough variation for any difference to be seen within the spectrum.

3.2 ANALYSIS METHODS

3.2.1 PRE-PROCESSING AND PROCESSING

Regardless of the analysis method employed, voxel location needed to be checked before an examination could be included in a study. At the time of MRS being performed the voxel location was saved in 3 planes if possible, this was not always achieved for studies performed on the GE Signa Excite at BCH where only 1 plane could be stored. The placement of the voxel was checked. Ideally, the voxel had to be placed entirely within tumour, maximally over the solid component. In some incidences, where the tumour was of a small volume, this was not achievable. In these cases, the spectrum was still assessed for interesting features and how well it corresponded with tumours of the same type, but not included in the formal analysis due to the contribution from 'normal' brain.

The method used for analysing data chosen was heavily dependent on the intended user and the software available to them. Spectra were processed in one of 2 ways: either using the software on the scanner or using tools such as LCModel™[120], which uses a linear combination of empirically obtained metabolite spectra to 'fit' to the experimentally obtained spectra. LCModel™

has a choice of basis sets acquired at different echo times on a variety of scanners, thus allowing for a close match with the data to be made. The metabolite concentrations are then referenced to the internal water concentration.

When the classifier was designed for use by clinicians, the application of the method needed to be fast and simple to use, despite the underlying analysis being complex. In these studies, spectra produced by the scanner software were selected as these were readily available without any need for additional software. For studies that required a more in depth analysis of the metabolic differences between tumours, spectra produced by tools such as LCModel™ were used. These were assessed along with the metabolite concentration tables produced and the quality control measurements. In the case of mulitcentre data, all the raw data was sent to BCH and was processed with the onsite version of LCModel™, to reduce the risk of variability between centres.

3.2.2 QUALITY CONTROL

Before a spectrum could be included in a study some basic quality control measures needed to be met.

SIGNAL TO NOISE RATIO (SNR)

SNR is a measure of how high the strength of the signal under analysis in relation to that of the background noise. The higher this value, the less obtrusive this background noise is. This was kept in the region of an acceptable spectrum have an SNR of at least 5 to be able to reasonably

analyse the metabolite peaks. This was reduced in the analysis of peaks due to LMM resonance; this was seen as being reasonable due to the high signal strength of these peaks, relative to the metabolite peaks.

FULL WIDTH HALF MAXIMUM (FWHM)

FWHM is a measure of how broad the peaks are. If a spectrum is dominated by broad peaks, peaks can merge into one. In cases with broad peaks, metabolite concentrations determined are not done so with high confidence. FWHM has to be low, and in the region of 0.015ppm, in order for a spectrum to be included in a study.

OTHER FACTORS

Both SNR and FWHM are quantifiable, but there are other factors that can deem a spectrum not fit for analysis. If the water suppression is not sufficient, the region greater than 3 ppm can be difficult to interpret. Phasing can sometimes be inadequate, which can lead to a spectrum that is not easily analyzable. Issue such as these, and the determination of artefacts within the spectrum, are only determined by visual inspection of the spectrum. This should be done to ensure the results from the analysis of metabolite concentrations are valid.

3.2.3 ANALYSIS USING SPECTRA PRODUCED BY SCANNER SOFTWARE

For MRS to be used in a clinical setting, the application of the tool developed needs to be simple to use, fast and robust. A radiologist or clinician is most likely to need a classifier at the time an imaging investigation being performed. In this case, it is most convenient to use the software provided on the scanners. Since a majority of the MRS investigations at BCH are performed on the Siemens' Symphony, initially tools were developed using NUM4 processed spectra (figure 10).

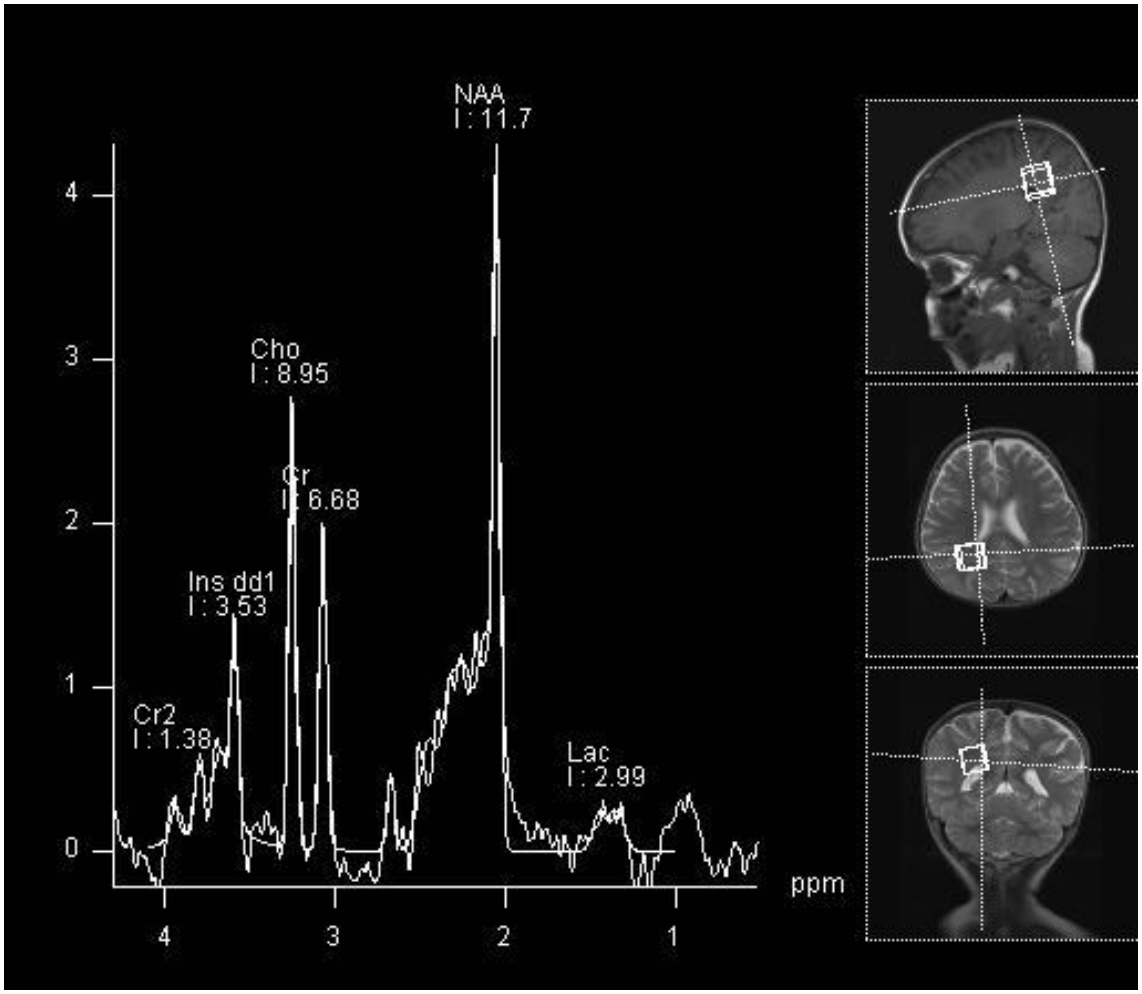

Figure 10: Example of a 1H-spectrum processed by the Siemens' Symphony NUM4 software, with voxel placement images on the right hand side in all 3 planes. Peaks marked, and intensities (I) given, for myo-inositol – Ins; creatine – Cr (and Cr2 for the secondary peak due to Cr); total choline – Cho; total NAA + NAAG – NAA; and lactate – Lac

Prospective studies included data from both the Siemens' Symphony and the GE Signa Excite at BCH, in addition to data from other centres in the CCLG. Data in prospective studies included spectra produced by software from all 3 major scanner manufacturers. This allowed me to assess whether tools were robust to new data from the same scanner, but also whether the tool was robust to data from other sources. This is an important part of the assessment to determine the usage of the tool in a clinical scenario.

The spectra produced by the NUM4 software, used in this study, have an arbitrary y-axis. This means that peaks within a spectrum can be compared with one another, but a comparison between different spectra is not possible using absolutes, since absolute values are not available. To overcome this, ratios were generated between peak heights/areas to allow for comparisons to be made.

QUALITY CONTROL

No values for SNR or FWHM were produced by the scanner software; visual measures had to be established. These factors were determined by visually assessing a group of spectra, and from these determining at what point little or no information could be reliably extracted.

Firstly the MRS peaks have to be sufficiently narrow for the Cr (3.0ppm) and tCho (3.2ppm) peaks to be visually well separated. Figure 12a shows an example where poor shimming has led to broad peaks, which do not therefore meet this criterion.

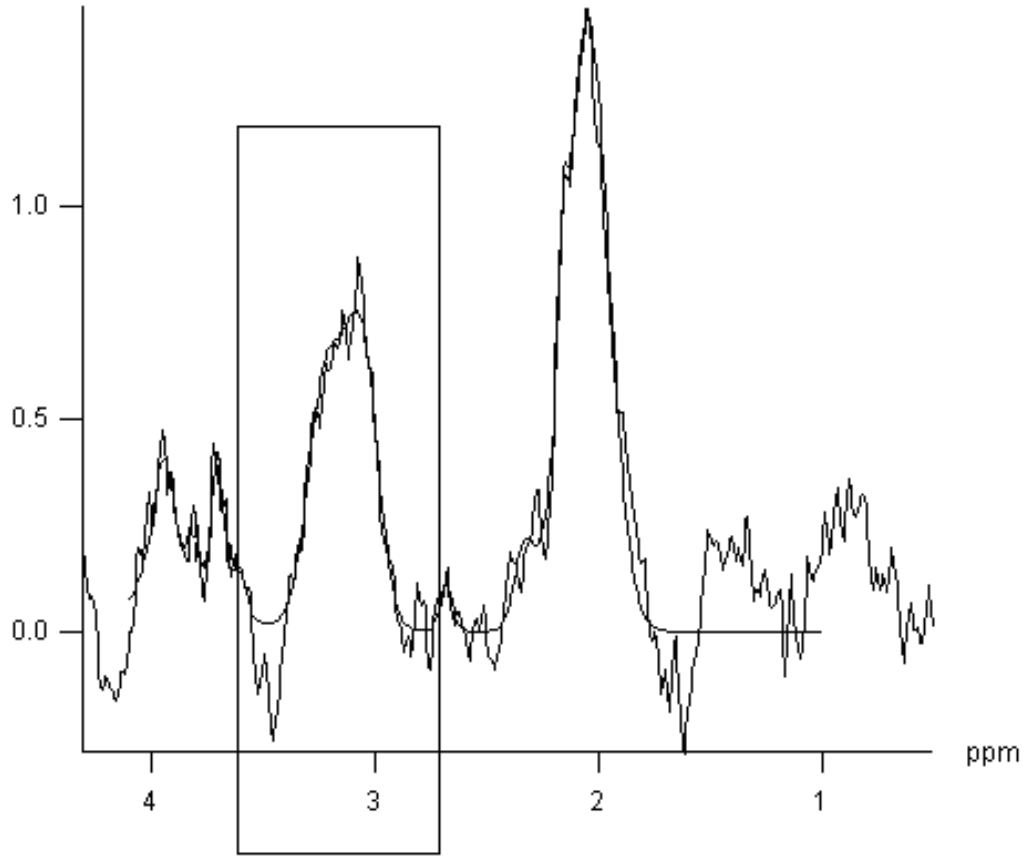

Figure 11a: An example of a 1H-spectrum with broad lines. The highlighted region shows the peaks arising from Cr and Cho merging into one broad peak, making it highly difficult to estimate the contribution from each metabolite

Secondly, the tCho peak height must be at least 5 times greater than the level of the noise. The noise level was taken as half the height spanned by the noise on the spectral intensity axis. The noise was measured in the region of the spectrum between 0.0ppm and 0.5ppm, which is outside the range where metabolite peaks are seen. An example of a spectrum with unacceptably poor SNR is shown in figure 11b.

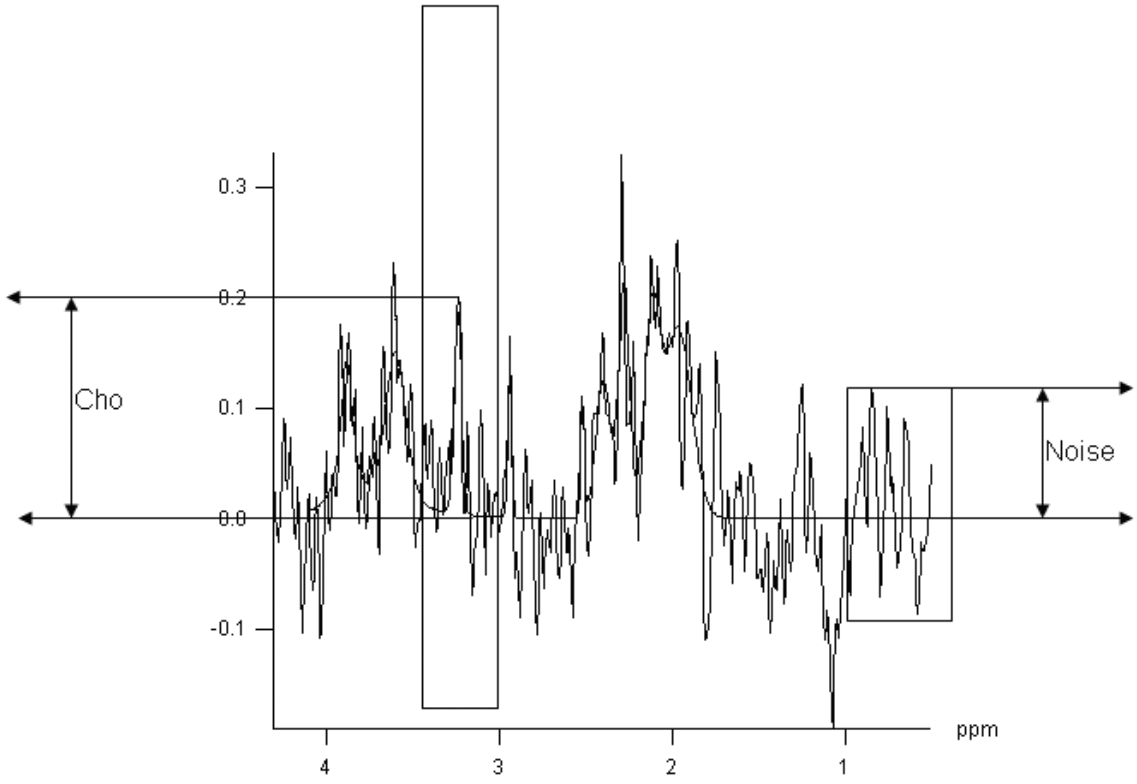

Figure 11b: An example of a 1H-spectrum with very low SNR. The highlighted noise region is shown to be far less than the acceptable 5xCho peak, metabolite peaks are difficult to distinguish from background noise in the spectrum

Although scanner software can give values for shimming and SNR, there is no generally agreed definition for these parameters and an ability to assess them from the processed spectrum is an important part of analyzing any MRS investigation. Whilst the measure used for determining adequate SNR and FWHM are not precise, experience in their implementation should allow a clinician to assess the reliability of the data collected.

PEAK AREAS

The NUM4 software routinely assigns the peaks for mIns, tCho, Cr and tNAA; this enables a less experienced observer to easily assess a spectrum. In addition to labelling these peaks, the software also determines the area under each of these peaks by fitting them to standard curves. The areas under the

peaks are proportional to the metabolite concentrations. The peaks shown in a NUM4 produced spectrum do not have a concentration reference and as such ratios needed to be generated to allow for comparison. Ratios could then be compared between spectra for the same, and different tumour types. However, the determination of peak areas is subject to large inaccuracies when peaks overlap and the estimation of the errors involved in this is difficult. This problem is a particular challenge in short echo time MRS, where more peaks are present. The most complex region, with the most difficulties was the region around tNAA (2.0-2.6ppm). This region contains resonances from Glx, LMMs and other smaller metabolites. In addition to this problem, the NUM4 software is designed in a way that it assumes tNAA will be the strongest signal. The tNAA resonance is largely decreased in tumour tissue and therefore is no longer the strongest resonance. To compensate for this the NUM4 software tended to over fit the tNAA resonance, by including contributions from the surrounding combined peak, thus giving a larger signal for tNAA than actually given. This meant that the intensity given for tNAA was no longer valid.

PEAK HEIGHTS

An alternative method was investigated by measuring the heights of various peaks in the spectrum. This is simple and fast to implement in a clinical setting and ratios between peak heights are easy to visualise. This method also allowed for additional peaks to be included in the analysis, such at Lac (doublet at 1.31ppm) and LMM resonances at both 0.9ppm and 1.3ppm. Peak

heights were measured directly from the Siemens processed spectra using imageJ™, a standard DICOM viewer (available at http://rsb.info.nih.gov/ij/).

For spectra with a flat baseline, peak heights were measured from the baseline to the peak tip. For spectra with an irregular baseline, a midpoint for the base of the peak was calculated and the peak height was taken to be from this point to the peak tip. Measurements were repeated 3 times to reduce error.

3.2.4 METABOLITE CONCENTRATIONS

LCModel™ was the preferred tool for determination of metabolite concentrations. This is a tool which uses a linear combination of an empirically derived basis set, of metabolites and LMM resonances expected in the brain, in order to determine the concentration of each metabolite seen in a spectrum. LCModel™ is an accurate, automatic and robust method that uses the frequency-domain to generate a list of metabolite concentrations (relative to water) along with confidence estimates.

Another method assessed for analysis using metabolite concentrations was JMRUI. JMRUI allows for processing of MRS in either the time- or frequency-domain. This method also allows for the determination of metabolite concentrations relative to water and allows for considerably more user-input. This means that this method is more time-consuming and more vulnerable to user-error. Hence, LCModel™ was used for the analysis presented here, where the method refers to schemes derived from metabolite concentrations.

LCModel™ gives values for both the SNR and FWHM of a spectrum; these values can be used to determine quantitative cut-off values for the assessment of data quality. These cut-offs, however, were allowed to vary between studies, depending on the signals under consideration. There is a large difference between the strength of a signal from an LMM region and that of a resonance due to a metabolite in weak concentration. In studies where LMM resonances were the main interest, the SNR cut-off value was decreased and the FWHM increased. This served to allow for more data to be included in these studies. This was seen as acceptable, due to the clarity of the LMM resonances. To ensure that the QC criteria being implemented were reasonable, spectra were also checked visually by an expert spectroscopist. This also allowed the assessment of quality issues not quantifiable, including satisfactory phasing, spectral artefacts and to ensure that residual water signal was not excessive.

A value for the Cramer-Rao lower bounds [120] is also given for each metabolite concentration calculated. This is an estimate of how well this value is determined. Any signal with consistently high Cramer-Rao lower bounds (>50%) was removed from further analysis, since these would be very poorly determined.

LCModel™ can be used to obtain a more complete list of metabolite concentrations, including those due to smaller resonances, such as Tau (triplets at 3.25 and 3.42ppm) and sIns (3.34ppm). These concentrations are

referenced to the concentration of water in the voxel; which removes the need to generate ratios between metabolites.

Some MR spectral features overlap significantly at 1.5T, and for these a combined signal was used. This was applied to the following list of metabolites:

1. glutamate and glutamine (Glx),
2. N-Acetyl Aspartate and N-Acetyl-Aspartyl-Glutamate (tNAA), and
3. phosphocholine and glycerophosphocholine (tCho)

Generally, the Cramer-Rao bounds for the individual components of these metabolites are high, thus removing them from analysis.

3.3 STATISTICAL METHODS FOR THE INTERPRETATION OF RESULTS

The following accounts for a general overview of the statistical tests used.

T-TEST

The T-test is a statistical test which can be used where the data has a normal distribution and the null hypothesis is true. It is used on small samples, to assess whether there is a real difference between the means of two different groups.

Z-TEST

The Z-test uses normalised data to determine whether differences between either sets of data or between individual members of different groups of data is large enough to be significant.

ANALYSIS OF VARIANCE (ANOVA)

The simplest type of ANOVA of these is a one-way ANOVA, which is used to assess for the significance of differences seen between independent groups, by comparing the means of each group. It is used where there are multiple groups.

RECEIVER OPERATOR CHARACTERISTIC (ROC) CURVES

An ROC curve is a plot of the sensitivity Vs (1-specificity) of a given binary classification scheme. The larger the area under this graph, the more accurate the classification scheme is.

PRINCIPAL COMPONENT ANALYSIS (PCA)

A PCA transforms a list of possibly correlated variables, in the cases presented here this is the list of metabolite and LMM concentrations, into a smaller number of uncorrelated variables. Each of these uncorrelated variables is called a principal component (PC). The first of these PCs usually accounts for most of the variability, with each successive PC accounting for less. A plot of the first 2 PCs usually allows for the visualisation of the variability within groups, and how well groups separate. Along with these, loadings plots can be generated. These are charts showing each of the initial

variables used in generating the PC and how heavily each of these is weighted. This allows for the assessment of which metabolite and LMM regions are contributing most to the separation of the groups.

LINEAR DISCRIMINANT ANALYSIS (LDA)

An LDA uses a linear combination of variables that can best separate two or more groups of data. LDA is closely related to PCA, but an LDA models the difference between classes of data whereas a PCA does not take this into account. It is, therefore, termed a supervised method.

CHAPTER 4: CEREBELLAR TUMOURS

4.1 INTRODUCTION

Approximately 50% of childhood brain tumours occur in the posterior fossa [41], and most of these occur in the cerebellum. There are three major tumour types that occur in the cerebellum: PA, medulloblastoma and ependymoma [41]. These all have very different clinical behaviour [41]. PAs generally show a benign course with a good response to surgery, these tumours rarely disseminate [40, 162-165]. Medulloblastoma and ependymoma both require further treatment beyond resection and they show dissemination [36, 44, 45, 166-172]. More aggressive tumours would benefit from an early, non-invasive diagnosis so as to allow for early treatment planning.

For all tumours of the cerebellum, surgery is primarily the initial therapeutic intervention, meaning that tissue of these tumours has been extensively studied [56, 163, 165, 171, 173]. Since surgery is invariably performed on these tumours, a histopathological diagnosis is always offered, meaning that this patient group is ideal for testing analysis tools and classification schemes.

There has been one published study analysing solely this tumour group [73, 98]. This was performed using a long echo time [73] and used sophisticated pattern recognition techniques, not readily available to clinicians [73, 98]. These studies showed that MRS can be used to distinguish between the 3 main types of cerebellar tumour, with high accuracy.

4.2 A DIAGNOSTIC SCHEME BASED ON MRS PEAK HEIGHTS FROM A RETROSPECTIVE ANALYSIS

INTRODUCTION

Successful studies utilising MRS commonly employ sophisticated data analysis techniques, including computerised pattern recognition [28]. This is not readily available to radiologists, meaning that interpretation of spectroscopy performed at diagnosis is often delayed. The difficulty of analysing MRS data remains a barrier to the widespread implementation of MRS in clinical practice.

If this delay in interpretation of spectroscopic data could be reduced or removed then this may be used in conjunction with conventional MRI to aid in obtaining an accurate pre-surgical diagnosis. While we are reliant on sophisticated methods for data analysis this is not logistically feasible. This problem led to the development of a method for simple interpretation of spectroscopy at diagnosis for a well-investigated disease group, using only the software available on the scanner. This chapter develops an algorithm for paediatric brain tumour diagnosis using only the processing software currently available on conventional MR systems.

A study by Wang et al [73] in 1995 used long echo time MRS (135/270ms) to assess the viability of distinguishing between tumours arising from this location using MRS, with promising results. This study successfully employed sophisticated discriminant analysis in order to differentiate the 3 main tumour

groups and is not easily implemented at diagnosis. The longer echo time used also limited the amount of metabolite information extractable from the spectra

A diagnostic tool was developed using data from BCH, processed by the Siemens' NUM4 software, for use at the time of diagnostic imaging. This was tested using a dataset accrued from MR scanners at three CCLG sites: BCH; QMC and RMH. This included data from Siemens', GE and Phillips MR scanners.

4.2.1 A DIAGNOSTIC SCHEME BASED ON MRS PEAK HEIGHTS FROM RETROSPECTIVE ANALYSIS

METHODS

The initial development of this scheme was performed using short echo time (TE=30ms; TR=1500ms) spectra solely from a Siemens' Symphony at BCH, using NUM4 scanner software.

Diagnosis was determined by standard histopathology of tumour specimens obtained at operation, this was verified by the local multidisciplinary team. Ethical approval was obtained for the study from the Local Research Ethics Committee and parental consent was obtained. All scans were pre-operative and performed before chemotherapy or radiotherapy was administered. The voxel had to be placed entirely within the tumour, maximally over the solid tumour component. The placement of the voxel was confirmed by storing MR images with the voxel location recorded (Figure 9). Spectra were assessed using the quality control criteria outlined in chapter 3.2.3.

Peak height ratios were generated between tCho, Cr, tNAA and mIns using the method outlined in chapter 3.2.3 giving six ratios. Two-tailed t-tests were performed between tumour groups, those ratios showing no significance ($P>0.05$) were removed form further analysis. ROC curves were then produced for each of the remaining metabolite ratios for each tumour type, by plotting the sensitivity against the specificity. The area under the ROC curve (AUC) was taken to be the best measure of the accuracy of the test performed, these were calculated using matlab. An area of greater than 0.9 was used to specify the metabolite ratios best able to discriminate between the tumour types. Scatter plots were created of the metabolite ratios that showed best discrimination, to check the distributions visually. Optimal cut-off values for each of the chosen metabolite ratios were taken to be the points at which the sensitivity plus specificity was at a maximum. From this data a simple decision tree classification scheme was built, using the cut-off values for the ratios that offered the best discrimination between groups.

To explore the practical use of this method, and to assess user variability associated with measuring peak heights by hand, 20 spectra selected at random from the dataset were analysed by 2 radiologists and 2 scientists, blinded to the tumour type. These results were then compared against those calculated while designing this scheme.

RESULTS

MRI and short-echo-time MRS (TE=30ms) were performed on 31 children with cerebellar lesions, at the time of their initial diagnostic imaging, between 1 January 2003 and 1 August 2006. A summary of patient details is given in table 1.

Tumour Type	No. Patients	No. Patients Used*	Mean Age	No. Girls	No. Boys
PA	11	7	8.2	3	4
Ependymoma	4	4	2.03	2	2
Medulloblastoma	16	16	7.5	5	11

number of patients whose spectra was of satisfactory quality to be used

Table 1: Patient information for retrospective study of scanner produced spectra of cerebellar tumours

Each patient had a PA (N=11), an ependymoma (N=4) or a medulloblastoma (N=16). Of the 30 MRS investigations performed, data from two of the PA cases were excluded as the tumour size was smaller than that of a 1.5 cm sided cubic voxel leading to a significant level of contamination of the spectrum by uninvolved adjacent brain. Another spectrum, again of a PA, was excluded due to poor line width and poor SNR. In general, the MRS of PAs displayed a lower SNR than the other 2 tumour types.

The only ratio to not show significance between any tumour groups was mIns/Cr; this was removed form further analysis. ROC curves were generated for all remaining metabolite ratios, and the AUCs are given in table 2.

	Area Under ROC Curve (AUC)			
Ratio	**PA vs. all others**	**Ependymoma vs. all others**	**Medulloblastoma vs. all others**	**Ependymoma vs. Medulloblastoma**
Cr/Cho	0.785	**0.924**	0.636	**0.890**
NAA/Cho	**0.889**	0.527	0.761	0.688
Ins/Cho	0.618	**0.935**	0.503	**0.906**
NAA/Cr	**0.964**	0.810	0.594	0.789
Ins/Cr				
Ins/NAA	0.850	**0.946**	0.676	**0.923**

Table 2: AUC values for retrospective study of scanner produced spectra of cerebellar tumours.
Values highlighted in red show those ratios offering good discrimination between specified disease type and other (AUC>0.85)

NAA/Cr appeared to be the strongest discriminator between PA and other tumours other ratios offer moderate distinction on both P-values and AUCs. Cr/Cho, mIns/Cho and mIns/NAA all act as strong discriminators between ependymoma and other tumours. From this table it can be seen that there is no single ratio that can successfully separate all 3 groups. However, using a combination of ratios in a 2-stage classifier proved to be more successful.

NAA/Cr can be used to determine whether a tumour is a PA or not, therefore this ratio can be used as stage 1. PAs are then removed from the second stage, which is to distinguish medulloblastoma spectra from ependymoma spectra. A combination of P-values and AUCs indicated that this is best achieved using Cr/Cho and mIns/NAA. Plots of both stages of this classifier can be seen in Figure 12.

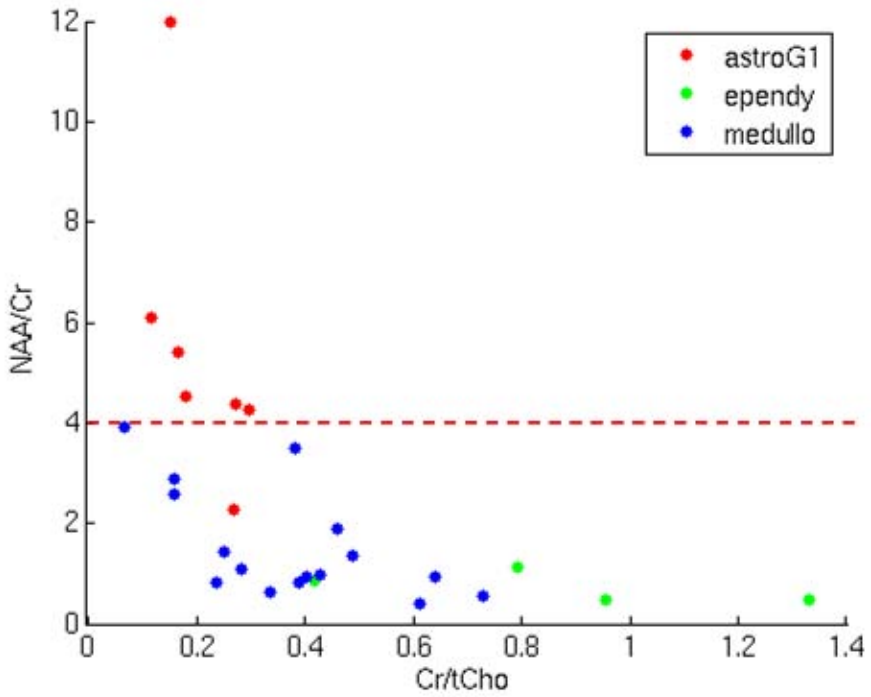

(a) *NAA/Cr Vs Cr/tCho: all 3 cerebellar tumour types plotted*
Red circles – PA; green circles – ependymoma; blue circles – medulloblastoma

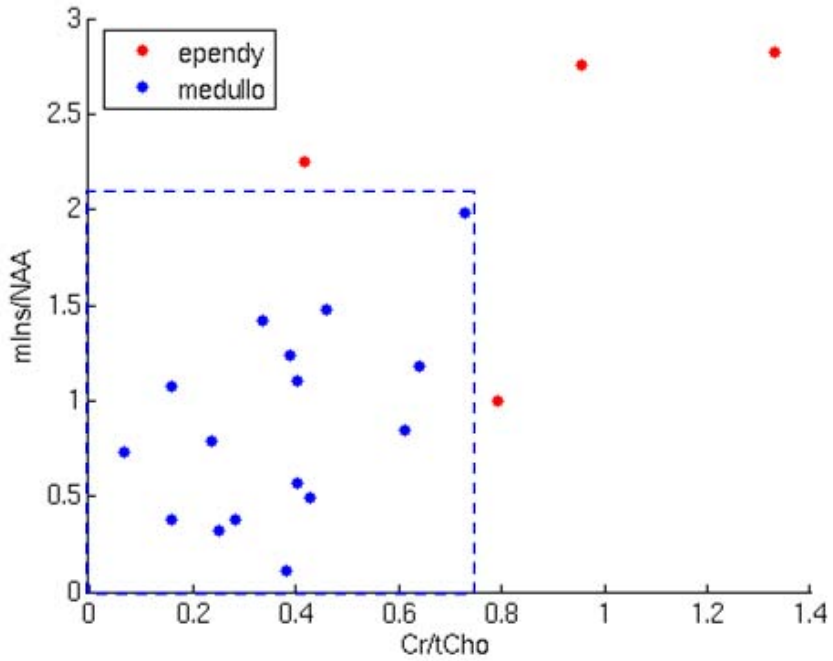

(b) *mIns/NAA Vs Cr/tCho: ependymoma and medulloblastoma*
Red circles – ependymoma; blue circles – medulloblastoma

Figure 12: 2 step classification scheme for cerebellar tumours based on peak height ratio measurement

Figure 12b indicates that a combination of both low Cr/tCho and low mIns/NAA is necessary to classify a spectrum as belonging to a

medulloblastoma. Using this combination of ratios more comprehensively defines the boundaries for medulloblastoma, which is appropriate, as there is most data for this tumour type. In summary, the diagnostic tool consists of in two stages; high NAA/Cr is used to give the diagnosis of PA, and a low Cr/Cho and low mIns/NAA is used to classify medulloblastoma from the remaining ependymoma.

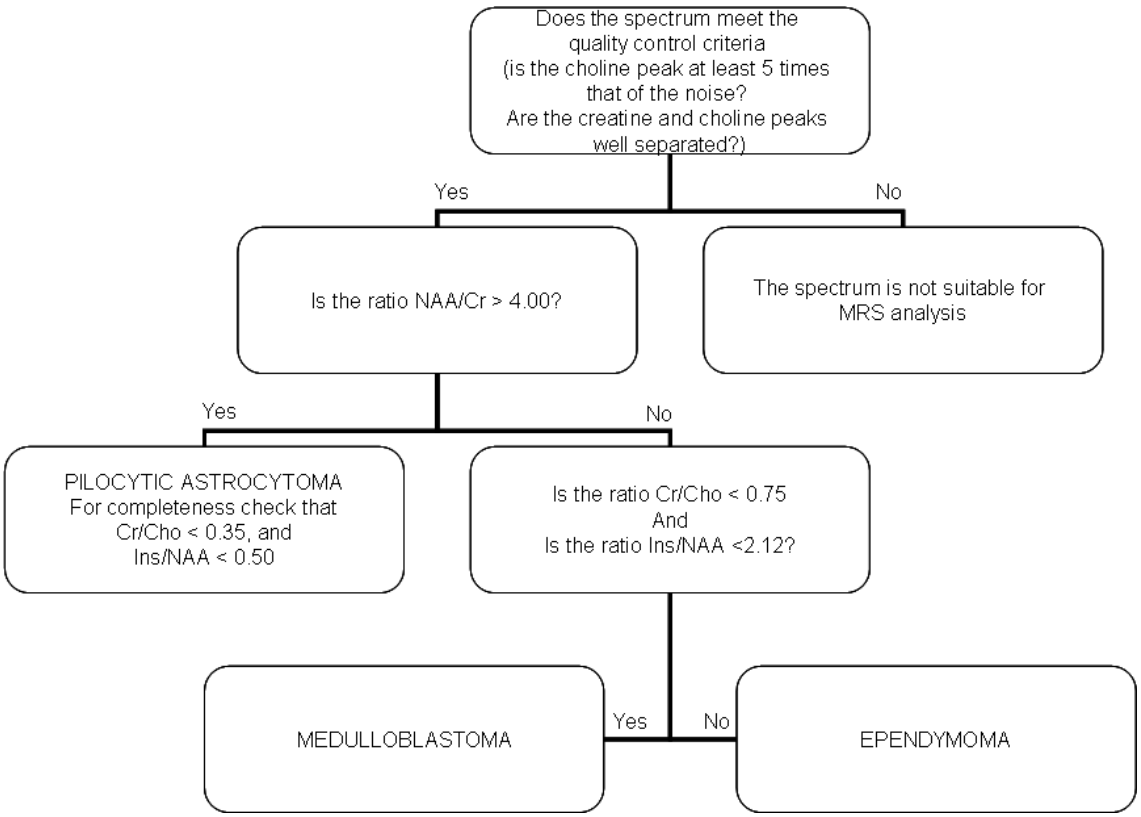

Figure 13: Peak height classification scheme (version 1), based on data taken from the 3 main tumour types of the cerebellum on the Siemens' scanner at BCH.

Based on this scheme, a new tumour may be assigned to one of the three tumour groups. However, in practise, it is useful to have additional checks in place, using other metabolite ratios also known to be good discriminators. Adding these checks leads to the complete classification scheme, shown as a decision chart in Figure 13.

In the test of user variability there was a 92.5% agreement between the results from the group of testers and the researcher. Since the method incorrectly classifies one spectrum from the peak heights determined by myself, the expected accuracy is 89.1%.

DISCUSSION

The peak height classifier described correctly classifies 26 out of the 27 tumours, using short echo time single voxel MRS. The method was designed to aid the ongoing integration of MRS into routine clinical use. This is a simple and effective method which can be easily implemented by radiologists, at the time of the diagnostic imaging. One of the main advantages to this scheme is it's ability to be used as a guide for radiologists who are looking to gain experience in interpreting MRS. The scheme has a solid foundation of robust statistics and, therefore, a firm foundation for further data to be added and the scheme extended.

Previous classification schemes have predominantly used long echo time MRS. The study by Wang et al [73] used peak area ratio's, obtained by long echo time MRS, to classify childhood cerebellar tumours. They achieved a classification accuracy of 85%, using a linear discriminant analysis of NAA/Cho and Cr/Cho. The general finding of high NAA/Cho in astrocytomas and high Cr/Cho in ependymomas corresponds with results presented here. Myo-inositol was found to be an important feature in characterizing ependymomas and, in particular, discriminating ependymomas from medulloblastomas.

The results of the current study show general agreement with findings of other studies. The high NAA/Cr in PAs, low Cr/Cho in medulloblastomas and high mIns/NAA in ependymoma agree with the findings by Panigrapy et al [71]. The high NAA/Cr in PAs agrees with many studies in adults which show a high value for this ratio in low grade, good prognosis tumours [67, 84, 97, 105]. NAA/Cr has also been reported as being a good discriminator between high and low grade tumours in children [105]. The low Cr/Cho values in medulloblastoma is in agreement with studies that have associated this quantity with highly malignant tumours [66-68, 84, 97, 105]. The similar finding in PAs agrees with other studies of this tumour group [71, 73, 105]. This is surprising given the benign nature of these tumours, but this may be explained by a more detailed analysis of the specific choline metabolites which contribute to the total choline MRS signal [86, 98, 103].

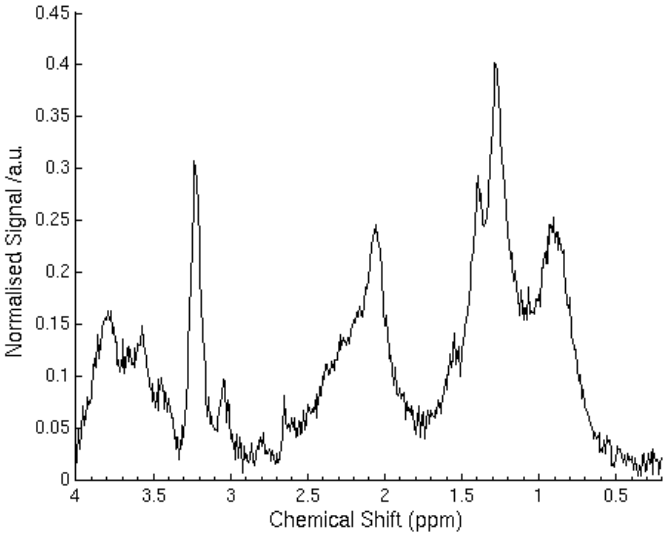

(a) PA

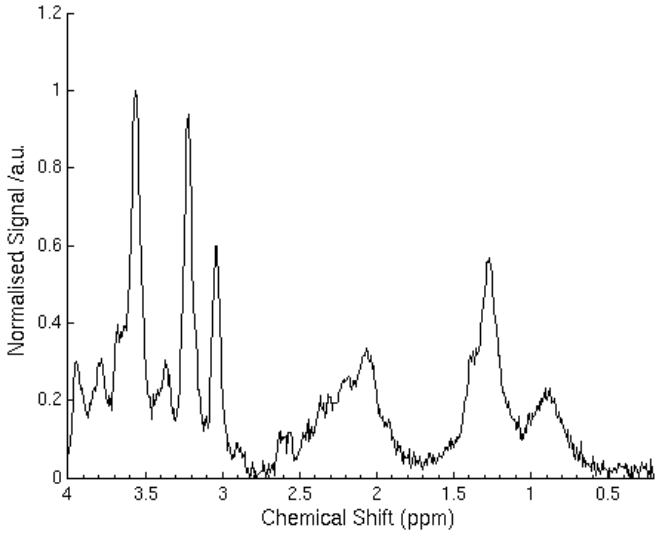

(b) Ependymoma

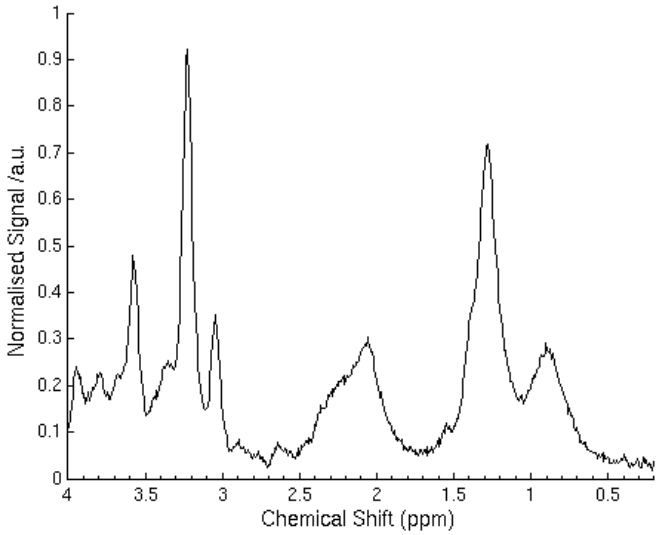

(c) Medulloblastoma

Figure 14: Average spectra for the three main cerebellar tumours

A key feature to note in PA spectra is the presence of sharp NAA peak at 2.0ppm (Figure 14a), along with a small or non-existent Cr peak at 3.03ppm. Both ependymoma (Figure 14b) and medulloblastoma (Figure 14c) spectra do not show a sharp peak at 2.0ppm, but rather show a broad peak between 2.0 and 2.5ppm. Ependymoma show a particularly high peak for mIns at 3.6ppm, not seen in medulloblastoma. Tau is often seen in medulloblastoma spectra at

3.35ppm, although this is not easily assigned visually due to it's proximity to the tCho peak.

With the advancement of technological processes, it is theoretically viable that it shall become possible to quantify increasing numbers of metabolites using MRS. This study supports the view that expansion of the metabolite profile improves its ability to characterize tumours. The method described in this section presents a scheme whereby information regarding additional useful metabolites can be incorporated into the algorithm in a consistent manner. One particular example is the peak at 3.35ppm due to taurine. This peak is commonly present in medulloblastomas [71, 96, 98, 100] and may aid the identification of these tumours.

PAs showed the lowest SNRs of the tumours studied; this may be due to their low cellularity compared with other tumours [36]. This characteristic may be a useful discriminator for these tumours and demonstrates that spectra, which do not meet standard quality control criteria, may still possess useful information.

An important advantage of this approach is that the same process may be used to incorporate further spectra into the model and hence further refine and improve the scheme presented. This is important, given that the current algorithm has been constructed using a relatively small number of cases, all of which were collected using a single scanner.

CONCLUSIONS

A simple peak height ratio classifier was developed as a diagnostic aid for the classification of childhood cerebellar tumours, with a high success rate determined using a retrospective analysis. This scheme was developed using a small dataset, all collected from a single centre. In order for this scheme to be of clinical use it needs to be robust to the addition of new data coming from various sources. The next stage in the development of this classification tool is to test it prospectively and extend it using a larger dataset, including data from more than one centre.

4.2.2 PROSPECTIVE EVALUATION OF PEAK HEIGHT CLASSIFIER

INTRODUCTION

Despite the increase in studies utilizing functional imaging in the diagnosis of brain tumours, few of these studies have published prospective studies associated with the schemes described within. These are vital for evaluation, if the techniques are to be incorporated into regular clinical practice. Single centre studies are subject to bias; these are usually based on data collected on a single MR scanner and often by the same operator. By prospectively testing these schemes on, preferably, a multicentre dataset we can fully evaluate the method, assess how robust it is to a change of data type and reduce the chance that the results presented are biased. We can also expand the scheme to include a larger dataset, this allows for refinement and expansion of scheme.

The peak height classifier, presented previously, was highly successful on single centre data analysed retrospectively, correctly classifying 26 of 27 spectra and having an agreement of 92.5% when using 4 blinded testers. However, this was restricted to a single centre (BCH) dataset acquired on a single scanner. This study was expanded to include a more diverse dataset taken on both GE and Phillips systems, and other Siemens' systems, at 3 centres: BCH, Queen's Medical Centre (QMC) and the Royal Marsden Hospital (RMH). This data was collected and analysed prospectively.

The peak height classifier for classifying cerebellar was published in September 2007; the final cut-off for inclusion of patient data was 01/08/06. Following this cut off date, data was accrued for further patients presenting on BCH, allowing a prospective analysis. In addition to this all data accrued at QMC and RMH was collated and incorporated into the analysis.

METHODS

Spectra were obtained for new patients with cerebellar tumours at the time of diagnostic imaging at BCH, QMC or RMH using 1.5T MR scanners. Ethical approval was obtained for the study from the Multicentre Research Ethics Committee and parental consent was obtained.

Data was all collected using the same parameters to assure that data from different centres could be reasonably compared. The only exception to this was some slight variation of echo time between centres (TE=28-35ms), but this was marginal and did not lead to any significant differences between

spectra acquired. This allowed for a direct comparison using data collected of various scanners, by different operators, in different centres. Whereas the Siemens' NUM4 software produced a flat baseline centred on the ppm axis, not all of the spectra from other software had a flat baseline due to variation in water suppression between scanners. In cases where the baseline was flat, the peak heights were all measured from the baseline to the apex of each peak. For those cases where the baseline was not flat, the peak height was taken to be the base of the individual peak to the apex.

One new spectrum, acquired at QMC on a Phillips system, had very poor water suppression and in addition to this the screen capture had removed the lower part of the screen. It was removed from statistical analysis as peak heights could not be accurately determined, although it was included in classification to assess whether problematic data could still be reasonable classified.

Those new cases, that passed QC, were separated into 1 of 4 groups: PA, ependymoma, medulloblastoma and other. These were assigned by histopathological diagnosis.

Those tumours in the first 3 groups, i.e. the 3 tumour classes used in the initial scheme, were assessed using the classification scheme developed from the retrospective analysis presented in the previous section (Figure 13). From this, classification rates were determined for the additional data.

RESULTS

MRI and short-echo-time MRS were performed on 36 children with cerebellar lesions between 16/02/05 and 01/07/08 at all 3 centres. All of these patients underwent biopsy, leading to a diagnosis of 13 PA, 4 ependymoma, 14 medulloblastoma, 2 atypical teratoid/rhyabdoid tumours (ATRT), 1 ganglioglioma, 1 diffuse low grade astrocytoma (DA) and 1 high grade lesion of undetermined nature (HGT). Of these 4 PA scanned on the Siemens' Symphony at BCH failed to pass quality control, leaving a group of 9 PA for further consideration. In addition, 1 of the medulloblastoma cases at RMH had to be removed due to incomplete data, leaving a total of 13 medulloblastoma for further analysis. Of the 31 cases that passed quality control, 26 were of one of the 3 original disease types, leaving 6 of new disease types not included in the original scheme.

The new data, from tumours of one of the three original tumour types are plotted on the classification axes in Figure 15.

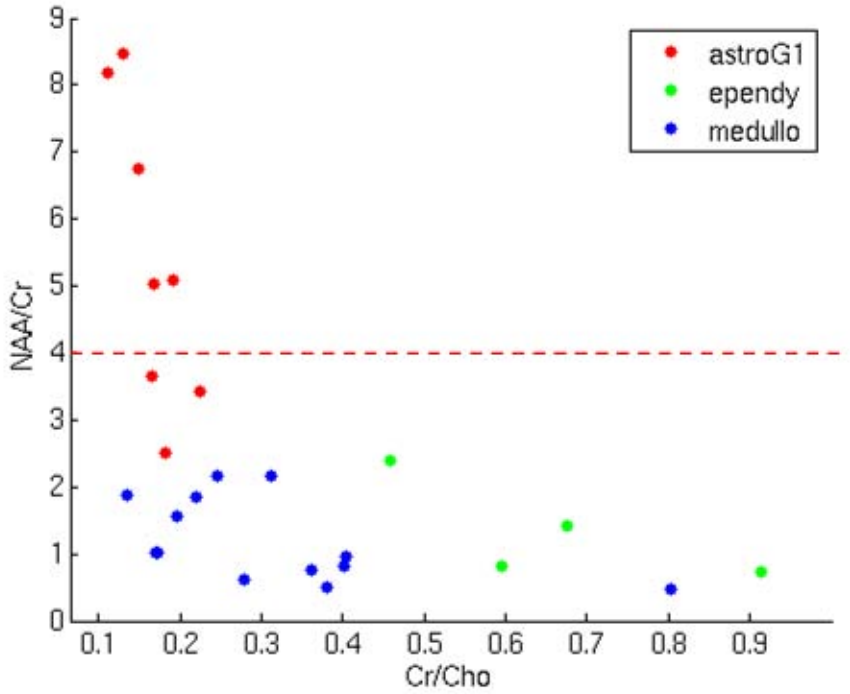

(a) *New cases plotted on the axes NAA/Cr Vs Cr/Cho: Red circles – pilocytic astrocytoma; green circles – ependymoma; blue circles – medulloblastoma*

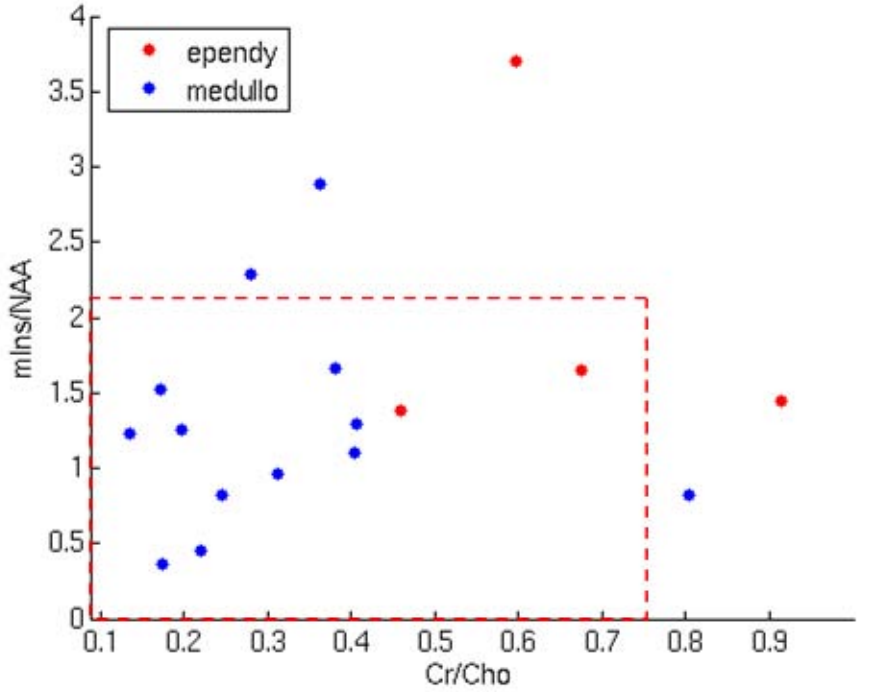

(b) *New ependymoma and medulloblastoma cases plotted on axes mIns/NAA Vs Cr/tCho: Red circles – ependymoma; blue circles – medulloblastoma*

Figure 15: New cases on the original classification axes for the peak height classification scheme

Classification rates are summarised in table 3.

			Classification		
Diagnosis	**No. Patients**	**Correct Classification (%)**	**PA**	**Ependymoma**	**Medulloblastoma**
PA	9	60	5	1	3
ependymoma	4	50	0	2	2
medulloblastoma	13	80	3	0	10

Table 3: Classification Rates for prospective evaluation of classification scheme for cerebellar tumours, based on peak height measurement from spectra produced by MR scanner software

In summary, the original peak height classifier had a correct classification rate 65.4% on the new data, classifying 5 of the 9 PAs correctly, 2 of the 4 ependymomas correctly and 10 of the 13 medulloblastomas correctly.

DISCUSSION

This study was performed to evaluate that the peak height classifier developed using peak height ratios of scanner produced spectra would be robust to new data of a variety of types. Using the initial cut-off values and the original ratios (Figure 13) gave a moderate 65.4% classification rate of the new tumours. It classified 10 of the 12 medulloblastoma spectra correctly, 5 of the 9 PAs (1 of those misclassified was the PA from QMC with poor water suppression) and 2 of the 5 ependymoma spectra.

One of the largest challenges in prospectively evaluating the peak height classifier was the inclusion of spectra produced by other scanners. Different scanners offer a different amount of baseline correction and water suppression. This can lead to a challenge in measuring peak heights accurately. This may offer an explanation as to the relatively poor performance of the peak height classification scheme. This is an inherent problem of measuring peak heights. This is difficult to correct for in the

scheme, although careful measurements made several times and averaged would assist in this.

An additional issue with the scheme is the small number of cases in the initial development. Paediatric brain tumours are relatively rare and constitute a wide variety of tumour types. This leads to a small number of cases in individual groups, making the development of accurate classifiers complicated. This was especially the issue with the ependymoma group, which only had 4 cases in the development of the classifier. This was reflected in the mis-classification of 3 of the 5 new ependymoma cases. One of the original ependymoma cases was also thought to be grade 3 rather than the standard grade 2 and did have a spectrum that appeared marginally different from the other 3 cases, which may have affected the cut-off values for this group. More data is needed in each group to establish optimal ratios and cut-off values. As more data is accrued it will be possible to distinguish between poor accuracy resulting from insufficient data and the issue surrounding the accurate measurement of peak heights on multicentre data.

Individual centres do not receive many cases of individual tumour types, which shows the benefit of using a multicentre study. The next stage of the development of this classifier for cerebellar was to combine the original single centre data with the newer cases from all centres to build a new classifier using the same methods that were used in the development of the original classification scheme.

CONCLUSIONS

The peak height classifier performed with a moderate accuracy on a more diverse data set acquired from a range of scanners at 3 centres. The next stage in the development of a robust classification scheme was to combine single centre data with new multicentre data to build an updated classifier.

4.2.3 UPDATING AND EXTENDING THE PEAK HEIGHT CLASSIFIER

INTRODUCTION

The original peak height classifier was developed using a comparatively small dataset. This was especially true in the group of ependymomas, which had just 4 patients in.

The classifier performed relatively poorly prospectively, when used to classify a dataset acquired from scanners at 3 centres. This was especially true in the classification of ependymomas. To assess whether this was due to the lack of data, a new version of the peak height classification scheme was developed. The data used in the initial development of the classifier was combined with the new multicentre data. This larger dataset of 58 spectra, including both old and new data, was then analysed retrospectively, using the same techniques as for the initial classifier, to create a new scheme.

Previously, the classifier has only been used in the assessment of the 3 most common cerebellar tumours. However, other tumours can occur here in addition to these. In the analysis of this new scheme, these tumours have

been analysed alongside the more common tumours to assess of key features present in MRS of these rarer tumours.

METHODS

Data was accrued on 1.5T clinical MR systems from Siemens', GE and Phillips and processed using the inbuilt software on each scanner. A simple flow diagram is depicted in figure 16 to show how the data goes from being acquired at the hospital of diagnosis through quality control and onto analysis.

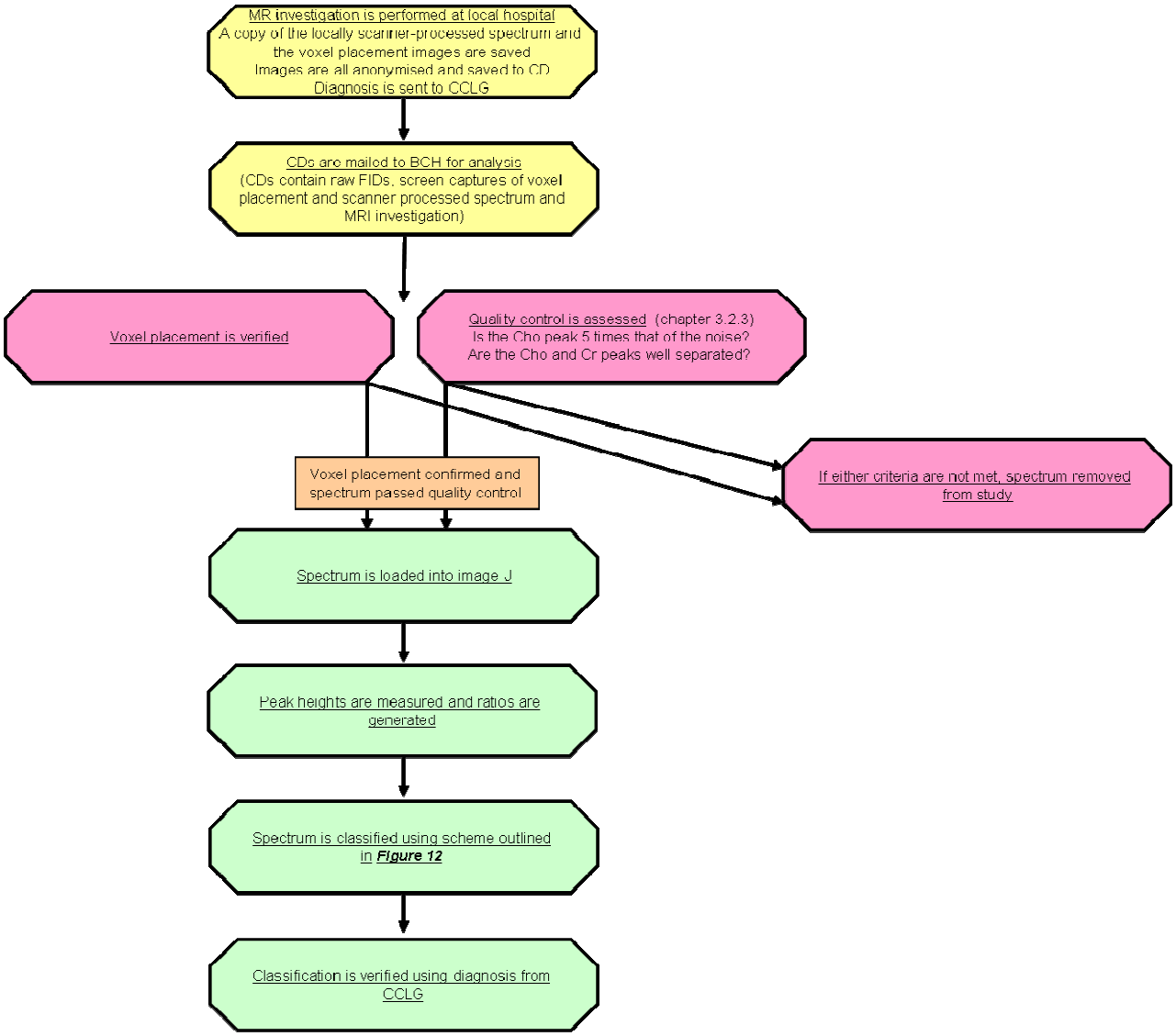

Figure 16: A flow diagram showing the path of data, from acquisition to analysis

All the new spectra were subjected to the same quality control criteria as used previously (section 4.2.1), including the removal of the QMC spectrum with poor water suppression and an incomplete screen capture from statistical analysis.

The complete dataset was retrospectively analysed in the same way as for the original classifier, to determine which ratios offered the best discrimination between groups. This was done by using two-tailed t-tests to detect the ratios which offered the most significant difference between groups. In addition to metabolites used previously, peaks associated with LMM resonances were measured at 1.3ppm and 0.9ppm (LMM1.3 and LMM0.9 respectively). Ratios between these and tCho were generated and used in the ANOVA and further analysis. Metabolite ratios offering the highest significant difference were used to plot ROC curves and the AUC values calculated. Ratios offering the highest AUC values were used to build an updated classifier, with optimal cut-off values being calculated as being the value where sensitivity plus specificity was at a maximum.

Tumours that fell into the ‘other’ category were assessed for their main spectral characteristics. Ratios between peaks were calculated for these tumours and these results were analysed using the updated classifier. This allowed for an assessment as to similarities and differences with the 3 main tumour types, and to predict which tumour these rare cases would have been assigned using this scheme.

RESULTS

Of the 31 cases that passed quality control, 26 were of one of the 3 original disease types, leaving 5 of new disease types not included in the original scheme. These 5 tumours consisted of 2 atypical teratoid/rhabdoid tumours (ATRTs), 1 ganglioglioma, 1 diffuse grade 2 astrocytoma (DA2) and 1 high grade tumour of undefined type (HGT). These 31 new cases were then added to the original 27 spectra giving a total of 58 spectra, of which 53 were of the three groups originally classified.

Results of the two-tailed t-tests between PA Vs ependymoma+medulloblastoma and ependymoma Vs medulloblastoma can be seen in table 4.

	P-Value	
Ratio	**PA Vs Other**	**Medulloblastoma Vs Ependymoma**
Cr/Cho	0.785	0.005
NAA/Cho	<0.001	0.019
Ins/Cho	0.272	<0.001
NAA/Cr	<0.001	0.212
Ins/Cr	0.330	0.075
Ins/NAA	<0.001	0.013
LMM0.9/Cho	0.015	0.184
LMM1.3/Cho	0.436	0.296
LMM0.9/LMM1.3	0.044	0.621

Table 4: T-Test results for re-optimising the classification scheme for cerebellar tumours based on spectra from the scanner software

The ratios with the highest significance difference between PAs and the other 2 tumour types were: NAA/Cho; NAA/Cr and mIns/NAA. All of these had P-values less than 0.001. The ratios offering the highest significant difference between ependymoma and medulloblastoma spectra were Cr/Cho (P=0.005) and mIns/Cho (P<0.001).

	Area Under ROC Curve (AUC)			
Ratio	**PA vs. all**	**Ependymoma vs. all**	**Medulloblastoma vs. all**	**Ependymoma vs. Medulloblastoma**
Cr/Cho	**0.849**	**0.944**	0.562	**0.918**
NAA/Cho	**0.882**	0.659	**0.872**	**0.830**
mIns/Cho	0.677	**0.985**	0.608	**0.978**
NAA/Cr	**0.998**	0.749	**0.818**	0.610
mIns/Cr	0.624	0.696	0.716	**0.862**
mIns/NAA	**0.912**	**0.894**	0.615	**0.840**
LMM09/Cho	**0.834**	0.560	0.795	0.670
LMM13/Cho	0.690	0.596	0.635	0.661
LMM09/LMM13	0.739	0.640	0.639	0.525

Table 5: AUC values for prospective study of scanner produced spectra of the 3 main cerebellar tumour types.
Values highlighted in red show those ratios offering good discrimination between specified disease type and other (AUC>0.85)

AUCs for PA against ependymoma+medulloblastoma (table 5) showed very high AUC values for NAA/Cr and mIns/NAA. In addition to these ratios, Cr/Cho, NAA/Cho and LMM0.9/Cho also showed high AUC values. AUCs for ependymoma against medulloblastoma (table 5) showed a very high AUC for mIns/Cho. Cr/Cho and NAA/Cho both exhibit high AUC values as well. Stage 2 was attempted using mIns/Cho alone, with Cr/Cho and NAA/Cho as checks for verification of class assignment. These ratios were used to develop a 2-step classification scheme, as for the original scheme.

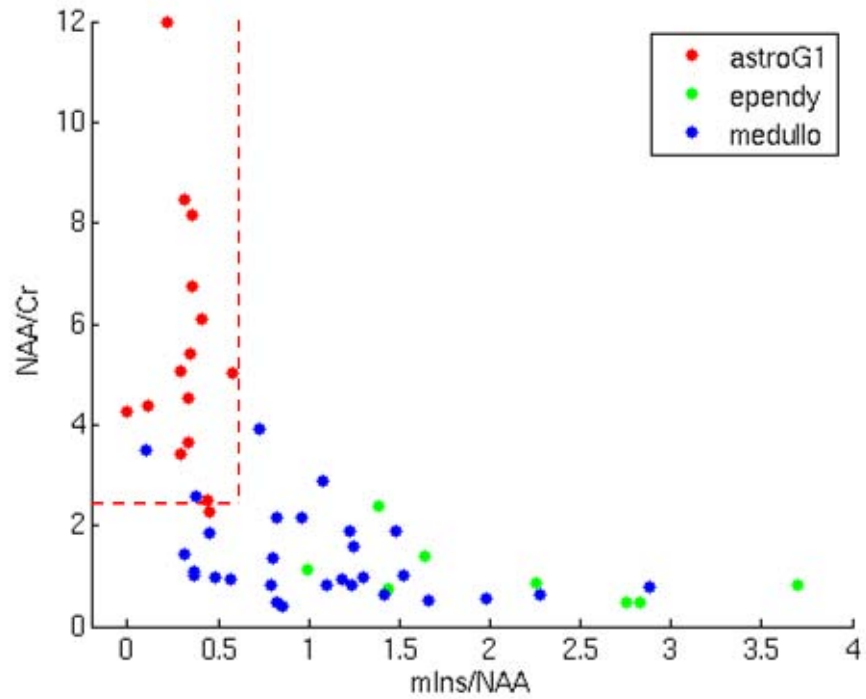

(a) *Step 1: NAA/Cr Vs mIns/NAA. Red circles – pilocytic astrocytoma; green circles – ependymoma; blue circles medulloblastoma*

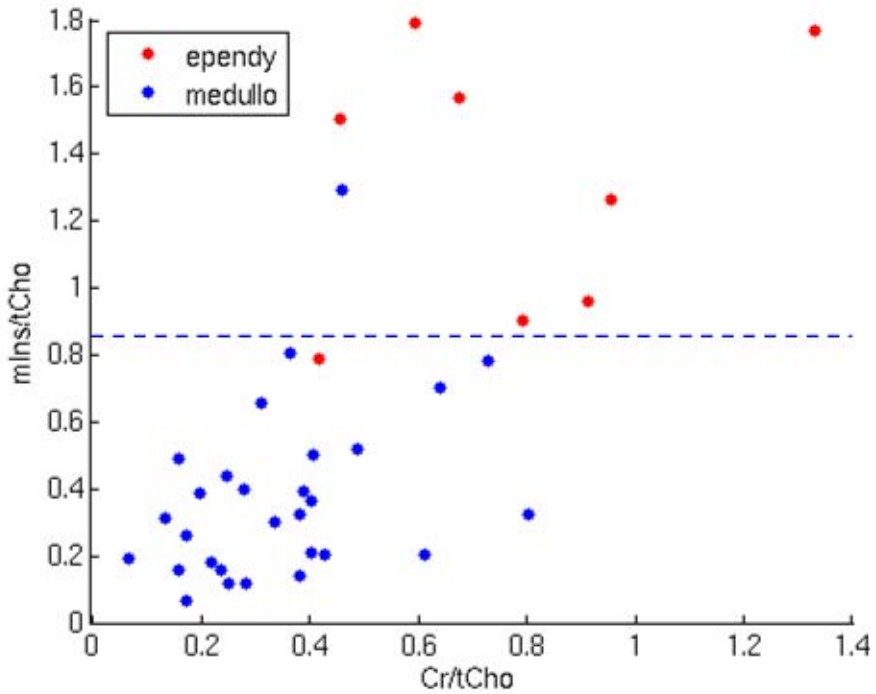

(b) *Step 2: mIns/tCho Vs Cr/tCho. Red circles – ependymoma; blue circles – medulloblastoma*

Figure 17: All data, both from original classification scheme and additional new multicentre data, plotted on classification axes.

Cut-off values were determined for all of these ratios giving the following classification scheme (Figure 18):

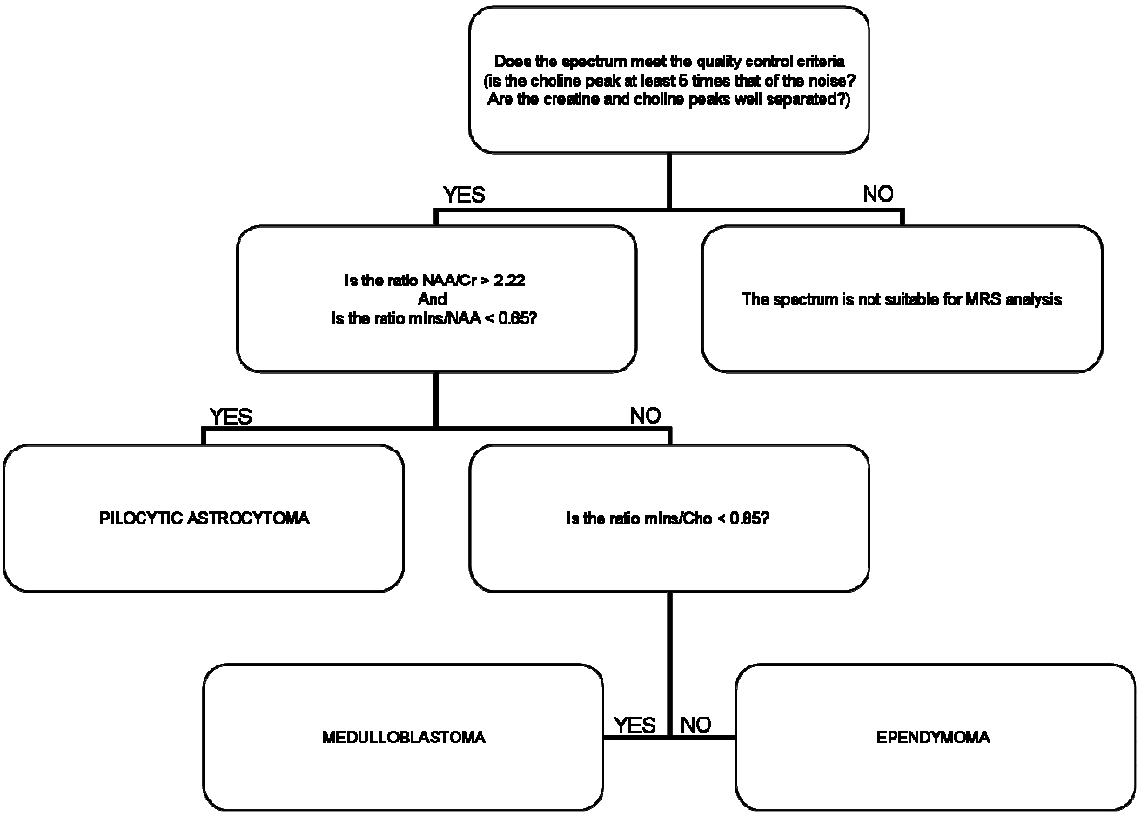

Figure 18: Version 2 of the peak height classifier, based on data taken from the 3 main tumour types of the cerebellum on various scanners at BCH, RMH and QMC.

This updated peak height classifier offered a correct classification rate of 90.6%, correctly classifying 48 of the 53 spectra (table 6).

			Classification		
Diagnosis	**No Patients**	**Correct Classification**	**PA**	**Ependymoma**	**Medulloblastoma**
PA	16	93.8%	15	1	0
Ependymoma	8	87.5%	0	7	1
Medulloblastoma	29	89.7%	2	1	26

Table 6: Classification of cerebellar tumours using a multicentre dataset.

Misclassifications include 1 ependymoma being classified as a medulloblastoma, 2 medulloblastoma being classified as a PA, 1

medulloblastoma being classified as an ependymoma and the outlier PA being classified as an ependymoma.

OTHER TUMOURS OF THE CEREBELLUM

Tumours that did not fall into one of the 3 previously defined groups comprise a diverse group. There were 4 tumour types in the group; each of these had only 1 or 2 cases. Values for each of the ratios are shown in table 7.

	ATRT		DA2	ganglioglioma	HGT
Ratio	***Average***	***StdErr***	**Value**	**Value**	**Value**
Cr/Cho	0.123	0.050	1.245	0.651	0.590
NAA/Cho	0.584	0.299	1.129	1.005	0.967
mIns/Cho	0.386	0.293	1.299	0.499	0.872
NAA/Cr	4.502	0.580	0.907	1.543	1.638
mIns/NAA	0.547	0.222	1.150	0.496	0.903
mIns/Cr	2.593	1.318	1.043	0.766	1.479
LMM0.9/Cho	0.661	0.451	0.152	0.283	0.521
LMM1.3/Cho	0.838	0.515	0.000	0.448	1.902
LMM0.9/LMM1.3	1.799	1.644		0.632	0.274

Table 7: Values for ratios in rare tumours of the cerebellum

Assignments using the scheme outlined in Figure 18 are summarised in table 8.

		Classification		
	No Patients	**PA**	**Ependymoma**	**Medulloblastoma**
ATRT	2	1	0	1
DA2	1	0	1	0
ganglioglioma	1	0	0	1
HGT	1	0	1	0

Table 8: Classification of rare tumours of the cerebellum using revised peak height classifier

There were 2 cases of ATRT in the dataset; each of these had a different profile. This led to relatively large errors in the ratio values for this group. The average NAA/Cr is high for this group, comparable with PA values. This is caused by one of the 2 cases having a very high NAA/Cr value. This would clearly be problematic clinically, since these 2 tumours carry a vastly different

prognosis and require very different treatment strategies. However, for the ATRT case, this is due to a very low Cr peak, and not a high NAA.

The DA2 spectrum exhibits a high mIns peak, and thus shows high values for ratios containing mIns. This tumour would be classified as an ependymoma using the updated peak height classifier. However, these values are still lower that those typically seen in ependymoma spectra. The spectrum of the DA2 also shows very small LMM peaks that could be used to distinguish it from ependymoma.

The HGT has a value for HGT close to the cut-off value for distinguishing between medulloblastoma and ependymoma spectra. Since we do not know the nature of this tumour, no comment can be made with regards the spectrum, other than it appears high grade.

The ganglioglioma is classified as a medulloblastoma on step 2 of the updated peak height classifier. However, NAA/Cho is much higher than would be expected a medulloblastoma and the ratios mIns/NAA and mIns/Cr are lower than in medulloblastoma.

DISCUSSION

This study was performed to update and extend the original peak height classifier, using a larger basis set.

By performing an ANOVA and recalculating AUCs for ROC curves for each class, new ratios were selected to give the best discrimination. This was formulated into a new updated peak height classifier (Figure 18), which now uses 2 ratios in the first stage and 1 in the second. NAA/Cr remained the best discriminator between PAs and other tumour types, but by adding information about mIns/NAA this was improved. However, the cut-ff value is considerably lower than previously. By including information from a second ratio, mIns/NAA, accuracy of classification was improved. Only one ratio, mIns/Cho was now needed for the second stage. This updated peak height classifier offered a classification rate of 90.6%, correctly classifying 48 of the 53 spectra, 1 of those misclassified was the PA from QMC with poor water suppression.

ATRT spectra both showed a strong signal for LMM at 1.3ppm, as did the HGT spectrum. This would be in keeping with these tumours being of a high grade [66, 68, 84, 94]. The DA2 spectrum sits closely with the ependymoma spectra due to the presence of a high mIns peak. The elevation of mIns is in keeping with observations made in diffuse gliomas [112] and grade 2 gliomas [67, 128].

This ATRT group also showed the problems surrounding analysing groups with a small number of cases in, the spectra showed many differences from each other. This group also showed the importance of knowing which metabolite of the ratio is varying. The NAA/Cr ratio of ATRT and PAs are

high. However, in PAs this is due to NAA being elevated, whereas in ATRT this is due to Cr being decreased.

Classification of small numbers of many types of different tumours is a challenge for any classification scheme; this is particularly difficult in a simple rule based classifier. However, the rarer tumours of the cerebellum have all shown some significant differences in their spectra from the tumours they would be misclassified as. These differences are consistent with their known biological characteristics which is encouraging. This again points to the need for the scheme to be extended with more data for a further prospective evaluation.

4.2.4 CONCLUSIONS: DIAGNOSTIC SCHEME BASED ON MRS PEAK HEIGHTS

There are highly significant differences between the mean metabolite profiles, and metabolite ratios, of the major tumour types of the cerebellum of children. However, there is considerable variability in the MRS profiles within each tumour type. This means that there is no one metabolite ratio that can completely distinguish between these tumours. However, a combination of metabolite ratios can be used to distinguish between childhood cerebellar tumours with a high accuracy.

The prospective evaluation performed of the original peak height classifier, gave moderate classification accuracy of 65.4%. To assess the factors was influencing the poor classification rate, a dataset combining the original and

multicentre data was assembled and, from this, a new classifier was constructed.

This new version of the peak height classifier correctly classified 48 of the 53 cases in the combined dataset. One PA with a very poor baseline and partial screen capture was misclassified as an ependymoma, thus highlighting the importance of quality control. Of the other tumours, three medulloblastoma cases and one ependymoma case were misclassified. This gave a high classification accuracy of 90.6%. The high classification accuracy on the larger dataset implies that the inaccuracy of the original classifier on the prospective data was largely due to the small dataset involved rather than variability introduced by multiscanner data or an inherent weakness of the approach. However this needs to be verified by further prospective study and the addition of further on data to the scheme, as it is accrued, will refine the cut-off values further.

Another benefit from a larger cohort is the inclusion of data from rarer tumour types. Classification of small numbers of many types of different tumours is a challenge for any classification scheme; this is particularly difficult in a simple rule based classifier. However, the rarer tumours of the cerebellum have all shown some strong differences in their spectra from the tumours they would be classified as using the straightforward classifier for the 3 major tumour types of the cerebellum. These differences are consistent with their known biological characteristics.

The original scheme has been put into use at BCH since its development, but the radiologists used in the scheme's original testing phase. The ease of use has made this simple to put forward. A simple explanation into its usage and a copy of the peak height classification scheme (figure 13) is all that is required for this to be achieved. An updated version of this will be supplied (figure 18) to replace the outdated scheme.

Up to this point, analysis has been made by visually inspecting screen captures of spectra, as they are processed by MR scanner software. This is a quick and easy method that is simple to implement in a clinical scenario. However, information on more metabolites, and potentially more accurate information on the major metabolites, can be extracted from a spectrum than it is possible to obtain by measuring peak heights if a more sophisticated method of spectral analysis is applied. LCModel™ can be used to obtain a list of concentrations relative to water of a larger list of metabolites than it is possible to assess visually, and can potentially give more accurate concentrations for metabolites, such as NAA, which overlap with other spectral features. More information would also aid in constructing a more complete picture of the metabolites present in the tumours. As such, the next stage in the development of an analysis tool for cerebellar tumours was to construct a classifier based upon these metabolite concentrations, and to compare the classification rate with that of the simple peak height classifier.

4.3 A DIAGNOSTIC SCHEME BASED ON LCMODEL™ METABOLITE CONCENTRATIONS

INTRODUCTION

A comparison of methods was performed to assess whether building a classifier using concentrations generated by software such as LCModel™ [120] is superior to a simple one based on peak height measurement.

To ensure a fair comparison, data from the same patients were used in the development of both classifiers. The same analysis methods were used to decide features offering the best discrimination in both classifiers.

METHODS

MRS was acquired using a PRESS sequence with an echo time of TE 30ms, for all patients used in the development of the original peak height classifier. All raw MRS data was processed using LCModel™, to obtain a table of metabolite and LMM concentrations along with measures for SNR and FWHM.

Quality control was applied using the following measures, as given by LCModel™:

1. SNR had to be greater than 4
2. FWHM had to be less than 0.150ppm

Spectra were also checked visually to ensure phasing was satisfactory, residual water signal was not excessive and the spectra were free of artefacts.

Initially, only the metabolites used in the peak height classifier were used in developing the concentrations-based classifier (mIns, tCho, Cr and tNAA). Ratios were calculated between these values to ensure that a direct comparison was being made between methods. Analysis was performed in the same way as for the peak height classification scheme.

Following this, all metabolites and three LMM (0.9ppm, 1.3ppm and 2.0ppm) concentrations were used to develop this classifier. Ratio were not calculated for the analysis, rather the concentrations relative to water were used for analysis. A PCA was performed using this complete basis set to assess variance across all data. Following this an ANOVA was performed to determine the metabolites that offer the highest significant difference between groups.

To compare the robustness of the simple peak height classifier with the more sophisticated LCModel™ scheme, a prospective analysis was performed using the scheme developed with the absolute values and the complete basis set. The same data were used in studies assessing the peak height classification scheme and the metabolite concentration classification scheme. Tumours falling into one of the original three tumour groups were classified, spectra of rarer cerebellar tumours were assessed for which group they would be classified as, and for key features in their spectra.

4.3.1 AN ENHANCED DIAGNOSTIC SCHEME BASED ON METABOLITE CONCENTRATIONS DETERMINED FROM RETROSPECTIVE ANALYSIS USING ONLY A LIMITED SET OF METABOLITE CONCENTRATIONS

To begin with, a scheme was developed using ratios between four metabolites concentrations: mIns, tCho, Cr and tNAA.

RESULTS

All of the spectra included in the development of the initial peak height classifier passed quality control, using the defined parameters.

Performing an ANOVA removed the ratios mIns/Cr and mIns/tNAA from further analysis (table 9)

		AUC		
Ratio	**P-Value**	**PA Vs Other**	**Ependymoma Vs Other**	**Medulloblastoma Vs Other**
Cr/tCho	<0.001	0.800	**0.929***	0.645
tNAA/tCho	<0.001	**0.932***	0.625	0.795
mIns/tCho	<0.001	0.529	**0.967***	0.591
tNAA/Cr	<0.001	**0.986***	0.614	0.713
mIns/Cr	0.340			
mIns/tNAA	0.710			

Table 9: ANOVA and AUC results for using ratios of LCModel™ derived metabolite concentrations in the classification of cerebellar tumours
**Values highlighted in red show those ratios offering good discrimination between specified disease type and other (AUC>0.85)*

Cr/tCho, tNAA/tCho, mIns/tCho and tNAA/Cr all had P values smaller than 0.05, and were used in ROC curve analysis. Results of this (table 9) showed that the AUCs were lower than for using the peak heights, with only 3 of the 12 curves demonstrating AUCs greater than 0.9.

The strongest discriminator between PAs and other cerebellar tumours was tNAA/Cr, as was found in the original peak height classifier. Cr/tCho and

mIns/tCho both act as strong discriminators between ependymoma and the other 2 tumour groups. By using a combination of tNAA/Cr and mIns/tCho a reasonable separation can be seen between the three groups (Figure 19), using only one stage.

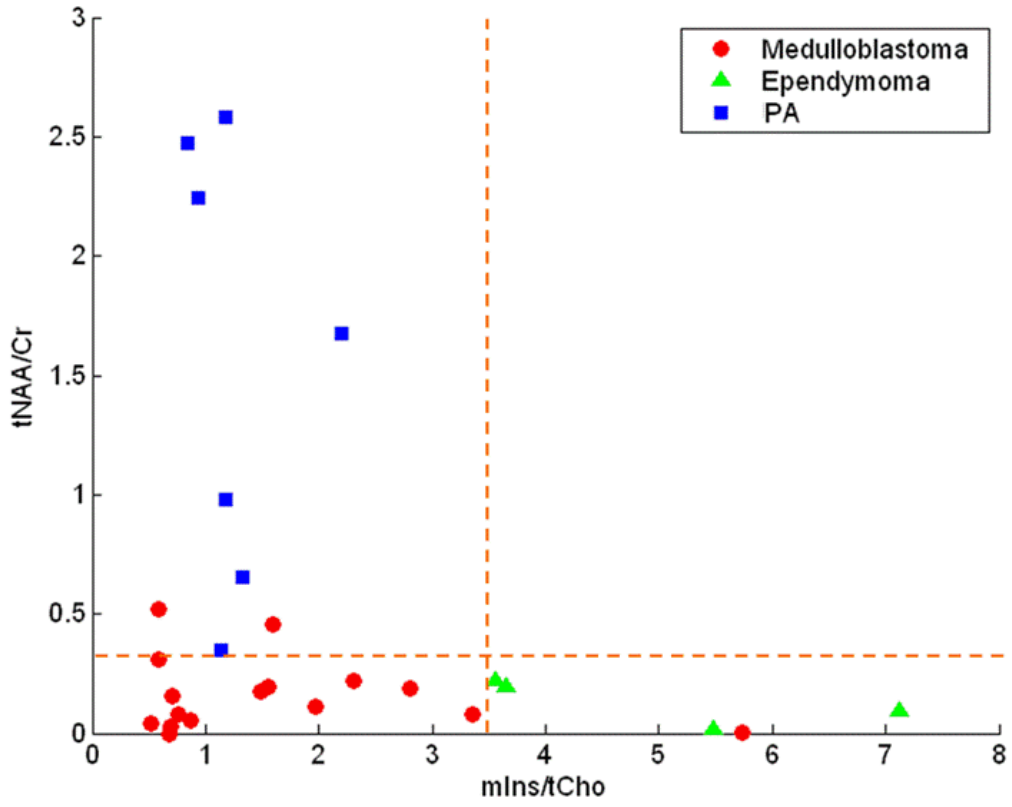

Figure 19: Scatter plot showing cerebellar tumour separation on the axes tNAA/Cr Vs mIns/tCho using LCModel™ generated metabolite concentrations
Blue Squares – PA; Green triangles – ependymoma; red circles medulloblastoma

Cut-off values were determined by maximising sensitivity plus specificity. The cut-off value for NAA/Cr was 0.35; and the value for mIns/tCho was found to be 3.47 (as shown by dashed lines in Figure 19). If a spectrum showed values for tNAA/Cr>0.35 and mIns/tCho<3.47 it was deemed to be that of a PA. For a spectrum to be considered a medulloblastoma, it had to exhibit tNAA/Cr<0.35

and mIns/tCho<3.47. Spectra with values for tNAA/Cr<0.35 and mIns/tCho>3.47 were considered to belong to ependymoma. This results in the misclassification of three medulloblastoma spectra. Two medulloblastoma are classified as PA and one as ependymoma. This error was not reduced by incorporating information from other ratios. This gives a classification rate of 88.9%, in comparison with 89.1% based on peak heights alone.

4.3.2 AN ENHANCED DIAGNOSTIC SCHEME BASED ON METABOLITE CONCENTRATIONS DETERMINED FROM RETROSPECTIVE ANALYSIS USING A FULL SET OF METABOLITE CONCENTRATIONS

To follow on from the scheme based on ratios between metabolite concentrations of mIns, tCho, Cr and tNAA, a more complete data set was used. A total of 19 metabolite and 3 LMM concentrations were used in the following analysis.

RESULTS

The results from the PCA are shown in Figure 20a.

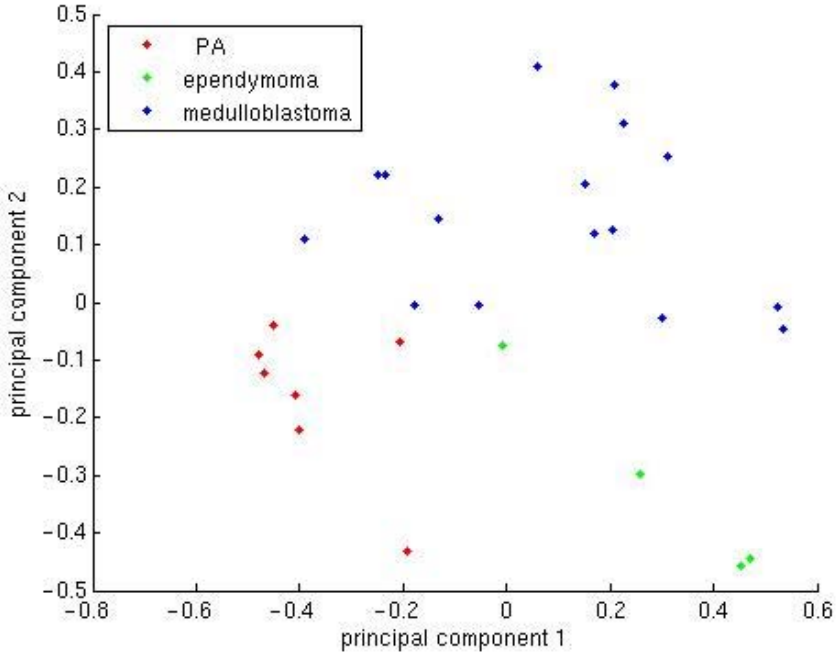

(a) *Principal Component Analysis of LCModel™ produced metabolite and LMM concentrations of the 3 main tumour types of the cerebellum, principal components 1 (x-axes) and 2 (y-axes).*
Red circles – pilocytic astrocytoma; green circles – ependymoma; blue circles – medulloblastoma

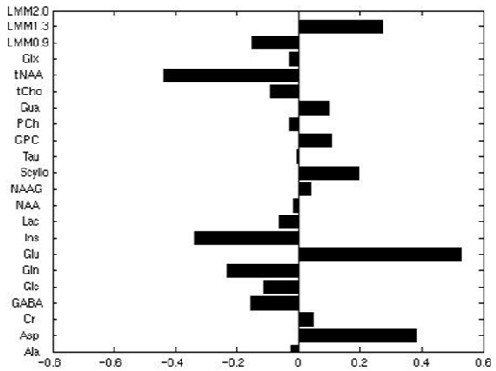

(b) *Loadings plot for PC1*

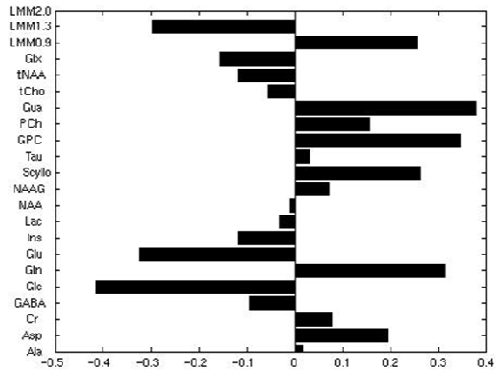

(c) *Loadings plot for PC2*

Figure 20: Principal Component Analysis of metabolite and LMM concentrations for cerebellar tumours

The PCA clearly shows good separation of the three groups, and the loadings plots highlight the key metabolites in achieving this separation of data (Figure 20b and 17c). There does appear to be one ependymoma lying separately from the other three, this was the grade 3 ependymoma.

Results of the ANOVA are shown in table 10:

		PA		Ependymoma		Medulloblastoma	
Metabolite	**P-Value**	**Average**	**StdErr**	**Average**	**StdErr**	**Average**	**StdErr**
Ala	*0.035*	*0.99*	*0.08*	*0.35*	*0.09*	*0.93*	*0.02*
Asp	*0.130*	*0.27*	*0.03*	*0.00*	*0.00*	*0.43*	*0.03*
Cr	0.0002	0.53	0.02	4.76	0.43	3.18	0.10
GABA	*0.001*	*0.10*	*0.01*	*0.55*	*0.12*	*0.71*	*0.02*
Glc	*0.096*	*1.21*	*0.07*	*0.63*	*0.14*	*0.65*	*0.04*
Gln	*0.0001*	*1.90*	*0.13*	*4.41*	*0.46*	*1.28*	*0.07*
Glu	*0.024*	*1.30*	*0.10*	*1.46*	*0.20*	*2.68*	*0.08*
mIns	0.0001	1.38	0.10	11.10	1.02	4.72	0.18
Lac	0.970	2.23	0.07	2.06	0.22	2.26	0.11
NAA	*0.093*	*0.64*	*0.05*	*0.43*	*0.06*	*0.35*	*0.02*
NAAG	*0.032*	*0.15*	*0.02*	*0.09*	*0.01*	*0.06*	*0.00*
sIns	0.048	0.05	0.01	0.39	0.06	0.44	0.02
Tau	0.001	0.07	0.02	0.73	0.21	1.89	0.07
GPC	*0.061*	*0.94*	*0.05*	*2.18*	*0.20*	*1.68*	*0.06*
PCh	*0.001*	*0.12*	*0.04*	*0.20*	*0.10*	*1.76*	*0.07*
Gua	*0.350*	*1.50*	*0.09*	*1.89*	*0.42*	*2.10*	*0.05*
tCho	0.0002	1.06	0.03	2.38	0.28	3.44	0.08
tNAA	0.021	0.79	0.06	0.52	0.08	0.36	0.02
Glx	0.061	3.77	0.11	5.86	0.41	3.97	0.10
LMM0.9	0.150	9.64	0.77	6.99	0.54	11.71	0.27
LMM1.3	0.092	24.78	2.27	18.84	3.51	42.13	1.58
LMM2.0	0.003	8.81	0.42	11.63	0.90	14.80	0.23

Table 10: ANOVA results using a full LCModel™ basis set, and average values for each tumour type. Metabolites in italics represent those that are not always reliably quantitated and have a tendency towards having larger CRLB values. Metabolites in red show those with P < 0.01 (only those with low CRLB)

Three of the four metabolite concentrations offering the highest P-values were used, in both the peak height classifier and the limited basis set LCModel™ analysis: mIns ($p<0.0001$), Cr ($p=0.0002$) and tCho ($p=0.0002$). Of these, mIns was the most significant ($p<0.0001$). Myo-inositol was highest in ependymoma spectra (11.10±1.02), compared with medulloblastoma

(4.72±0.18) and PA (1.38±0.10) spectra. Cr was lowest in PA (0.53±0.02) spectra, and higher in both medulloblastoma (3.18±0.10) and ependymoma (4.76±0.43) spectra. Total Cho was higher in the more malignant tumours, medulloblastoma (3.44±0.08) and ependymoma (2.38±0.28), compared with the PA (1.06±0.03). Other factors of significance were GABA, Gln, Tau, PCh and LMM2.0, all exhibiting p-values < 0.01. Ala, Glu, NAAG, sIns and tNAA also showed some significance, with p-values < 0.05. Metabolites that repeatedly exhibit poor CRLB were excluded from further analysis despite showing significance; these include Gln, Glu, PCh and Ala. Average values for each of these metabolite concentrations for each of the 3 tumour types are listed in table 10. As for the chapter 4.2, ROC curves were calculated (table 11):

	PA vs. all other		Ependymoma vs. Medulloblastoma	
Metabolite	**P-Value**	**AUC**	**P-Value**	**AUC**
Cr	<0.0001	0.986	0.164	0.750
mIns	<0.0001	0.950	0.045	0.891
Lac	0.977	0.607	0.755	0.516
sIns	<0.0001	0.921	0.777	0.547
Tau	<0.0001	0.929	0.062	0.813
tCho	<0.0001	0.993	0.160	0.734
tNAA	0.054	0.793	0.395	0.656
Glx	0.242	0.636	0.099	0.844
LMM0.9	0.632	0.593	0.011	0.844
LMM1.3	0.141	0.671	0.037	0.828
LMM2.0	0.002	0.857	0.182	0.703

Table 11: P-values and AUC values for retrospective study of LCModel processed spectra of cerebellar tumours. For a comparison with the chapter 4.2.1, these have been calculated for firstly comparing Pas with the other two tumour groups and then comparing Ependymomas with Medulloblastomas
Significant values are highlighted in red

A combination of Cr and tCho offered the best separation between PAs and the other two tumour groups (Figure 21a):

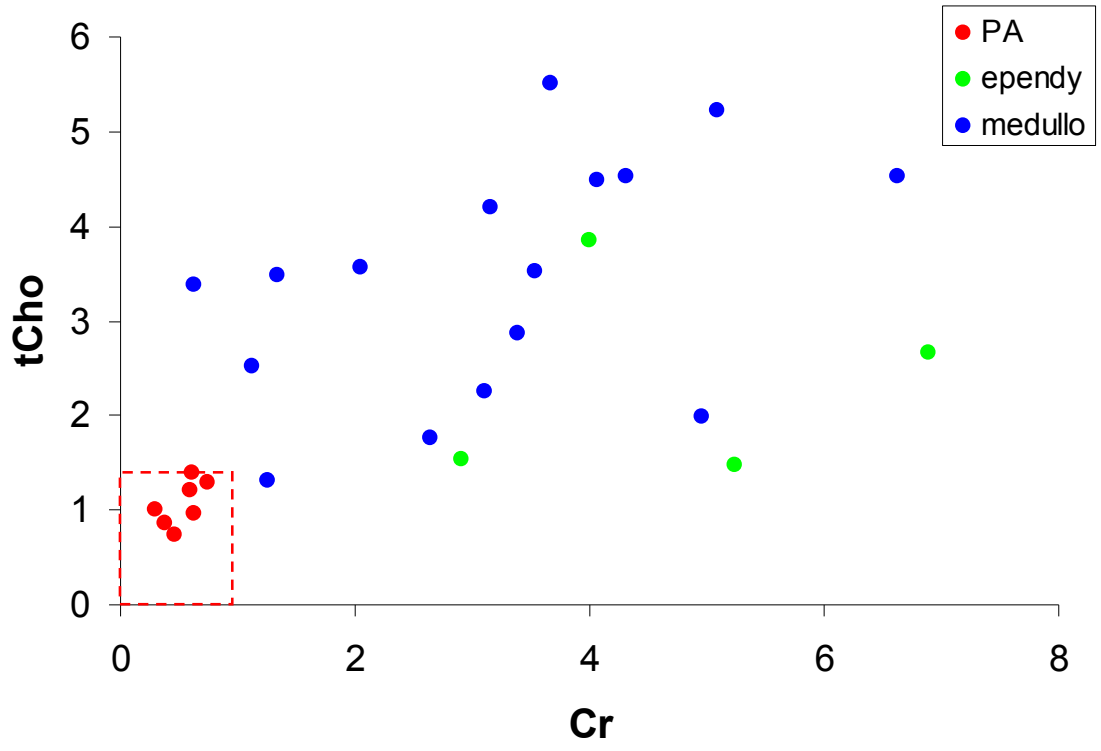

Figure 21a: Scatter plot of tCho Vs Cr
Red – pilocytic astrocytoma; green – ependymoma; blue – medulloblastoma

The cut-off for classification of a PA would be Cr < 0.94 and tCho < 1.40, this gives 100% correct classification of PAs in this group.

Using the same methods as chapter 4.2.1, a 2-step classification scheme can be assessed, using figure 21a to distinguish PAs from the other two tumour types and a further stage to look at distinguishing ependymoma and medulloblastoma. From table 11, it can be seen that only mIns offers a significant difference between these two groups using an AUC > 0.85 for significance. However, LMM0.9 is close to significance on AUC values, and has a P-Value of 0.011 using a two-tailed t-test, plotting these gives (figure 21b).

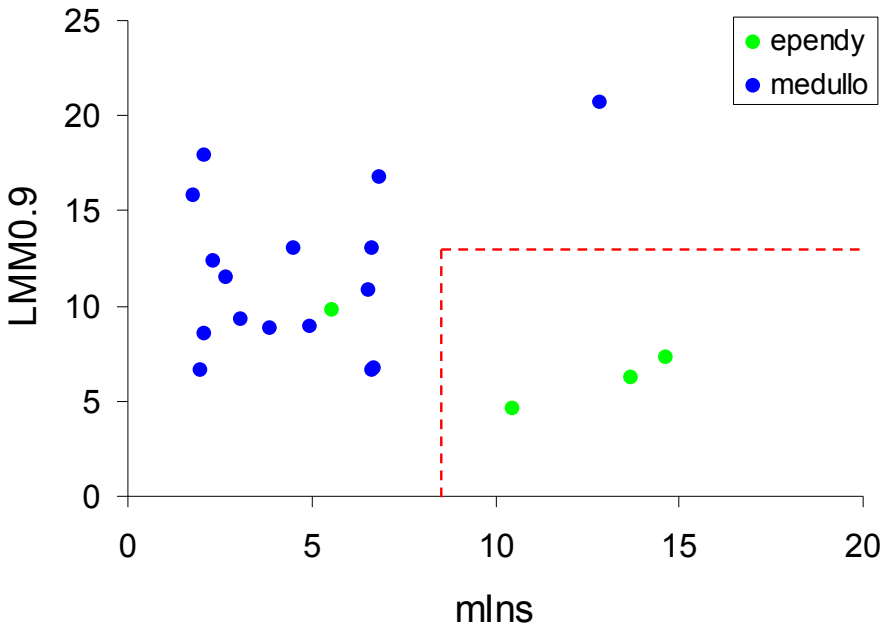

Figure 21b: Scatter plot of LMM0.9 vs. mIns
Green – ependymoma; blue – medulloblastoma

The cut-off for classification of a ependymoma would be mIns > 8.67 and LMM0.9 < 10.29, this misclassifies one ependymoma. The PA spectra all exhibit low concentrations of both tCho and Cr, clustering closely together. PAs are generally characterised by low concentrations of all metabolites. Of the ependymoma spectra, three exhibit very high mIns concentrations, and a low LMM0.9 concentration. The medulloblastoma spectra show lower concentration of mIns than ependymoma spectra, and higher LMM0.9, although this has a larger spread. Using the cut-off values described, only one spectrum would be misclassified. This spectrum is that belonging to the grade 3 ependymoma spectrum, thus highlighting the issues surrounding using small groups with variability within them.

(a)

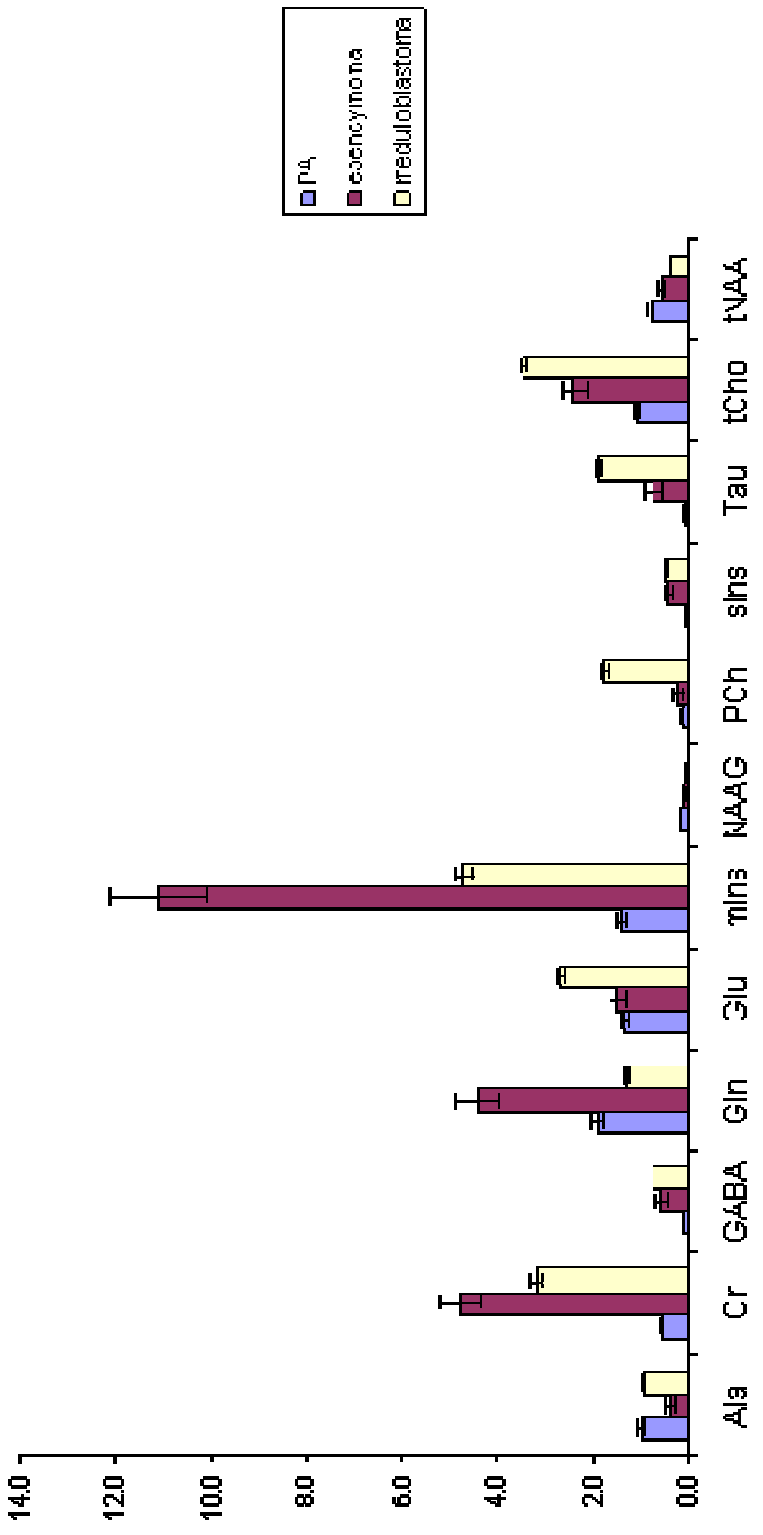
n.a.
ependymoma
medulloblastoma
14.0
12.0
10.0
8.0
6.0
4.0
2.0
0.0
Ala
Cr
GABA
Gln
Glu
mIns
NAAG
PCh
sIns
Tau
tCho
tNAA

(b)

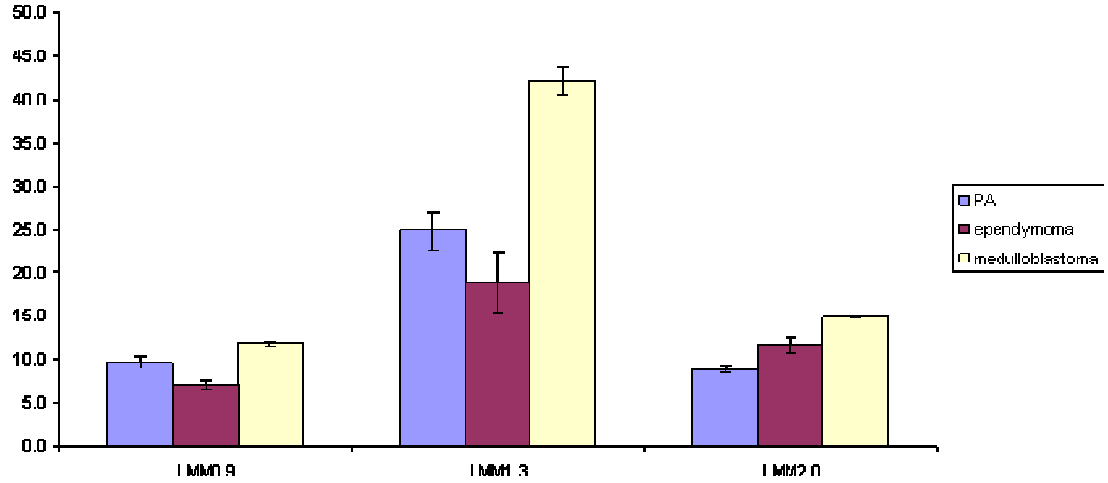

Figure 22: Bar charts showing the average (a) metabolite and (b) LMM concentrations for each of the 3 major tumour types of the cerebellum, as determined from LCModel™

Looking at a bar chart showing the average concentrations for each metabolite and LMM region (Figures 22a and 22b), all differences can be seen. Again, the concentrations of metabolites in PA spectra can be seen across a majority of metabolites. Cr is highest in ependymoma spectra and lowest in PA spectra, with a moderate value for the medulloblastoma spectra. PCh is highly elevated in medulloblastoma spectra compared with the other 2 tumour types. Tau is also elevated in medulloblastoma spectra. The total NAA signal is moderately elevated in the PA spectra compared with the other tumours. Other smaller metabolites also vary between the groups. LMM1.3 is elevated in medulloblastoma, when compared with PA and ependymoma spectra.

DISCUSSION

The most significant metabolite ratios for distinguishing between these groups are still the same as those used in both the peak height classifier and the classifier using a limited LCModel™ basis set: Cr, tCho and mIns. Indicating the largest changes do occur in the metabolites offering the largest signals. However, using the complete basis set allows the assessment of more subtle changes occurring in these tumours in metabolites that are not measureable by hand.

The ratio of mIns/tNAA was highly significant in the peak height classifier, which was not seen when using metabolite concentration ratios. However, two of the medulloblastoma spectra show very low concentrations of tNAA, thus leading to a large variability within the group. This was not seen using peak heights, since there was always a peak present at 2.0ppm, even if this was not wholly due to tNAA. This highlights a flaw in the peak height measurement technique, we cannot determine, without fitting to the spectrum, which metabolite is giving rise to a peak. Thus, it is likely that, at times, we will be assigning and measuring peaks which are not due to the metabolite expected. Maybe it would be more accurate to simply state the chemical shift being measured, and stating that the peak present at this resonance varies between spectra, as opposed to attempting to formally assign them using the peak height measurement technique.

This work compliments and extends work performed by Wang et al [73] in 1995, where ratios between concentrations were used to separate cerebellar

tumours. This was performed by using a combination of NAA/Cho and Cr/Cho, with a diagnostic accuracy of 85%. This accuracy is similar to that seen using the data collected at BCH.

The classifier based on a limited set of metabolite concentration ratios successfully classified 24 out of the 27 cases, in a 1-step classification scheme. It classified all of the ependymoma and PA spectra correctly, but failed to correctly classify 3 of the medulloblastoma spectra. This means that its performance was inferior to the classifier based on peak height measurements, in which only 1 PA spectra was mis-assigned. Although, the expected accuracy of the peak height measurement method is 89.1%, due to this user variability. The method using metabolite concentrations does not suffer from user variability. This would lead to the two schemes being of comparable accuracy.

However, LCModel™ gives much more information than can be visually assessed in a scanner-processed spectrum, including information from smaller peaks not easily quantifiable “by eye”. In addition to this, ratios are not required when using the concentrations. The concentrations given by LCModel™ are already referenced to water concentration. If a comparison is to be made between methods of analysing a spectrum, all these concentrations should be used in building a classifier.

Ependymoma spectra show elevated Cr and mIns signals, which have both been observed previously in these tumours [98, 174]. An interesting finding is

the presence of a decreased mIns signal in the grade 3 ependymoma relative to the grade 2 ependymomas, allowing it to be differentiated. However, only one grade 3 and three grade 2 ependymoma were available in the sample, meaning no conclusions can be drawn from this finding without the assessment of further data from both grades of ependymoma. PA spectra all showed decreased Cho signals, in keeping with these tumours being of a lower grade [67, 72, 74, 93, 97, 175]. Of the three tumour types, medulloblastomas showed the highest tCho, LMM0.9ppm and LMM1.3ppm, in keeping with these being of the highest grade [28, 29, 72, 174, 175].

Changes are also observed in metabolites with smaller signals, such as tau. This has previously been shown to be elevated in medulloblastoma spectra [71, 96, 98, 100], in keeping with observations made here, which could potentially be used as a characteristic of these tumours. One medulloblastoma would be misclassified as an ependymoma in the scheme using only the main metabolites, due to a high concentration of mIns. However tau is elevated in this tumour meaning that misclassification could potentially be avoided. Knowledge of the presence of this metabolite in medulloblastoma spectra may be useful in the correct classification of tumours with some unusual features in the spectrum.

The classification rate of this scheme, using only two metabolites is 96.3%. However, the misclassified ependymoma is thought to be grade 3 rather than grade 2, which is assigned to the other three cases in this study. However, looking at the tau signal can question the misassignment of this as a

medulloblastoma. No Tau is present in this spectrum, which may assist in the correct classification.

4.3.3 PROSPECTIVE EVALUATION – DIAGNOSTIC SCHEME BASED ON METABOLITE CONCENTRATIONS

Data used in prospective testing of the peak height classification scheme was subjected to the same quality control criteria as for the initial development of the initial metabolite concentration classification scheme. Spectra which passed quality control were assessed prospectively.

RESULTS

There were 26 patients in the multicentre dataset, with one of the three original tumour types having LCModel™, which passed the quality control criteria (SNR ≥4; FWHM ≤0.15ppm). The diagnoses of these can be summarised:

- 9 PA (8 from BCH and 1 from QMC)
- 2 ependymoma (1 from BCH and 1 from QMC)
- 15 medulloblastoma (10 from BCH, 3 from QMC and 2 from RMH)

There was a medulloblastoma patient included in this study from RMH which was not used in the peak height classifier testing, due to no screen capture being saved. Some of the patients included in this study failed quality control for the peak height classification scheme, but passed the boundaries placed for this analysis. Tumours outside of the original classification scheme consisted of: two ATRT, one DA2, one ganglioglioma and one HGT.

The scheme based on the metabolite concentrations correctly classified 72.7%. A plot showing the all cases on the original axes is shown in Figure 23:

(a)

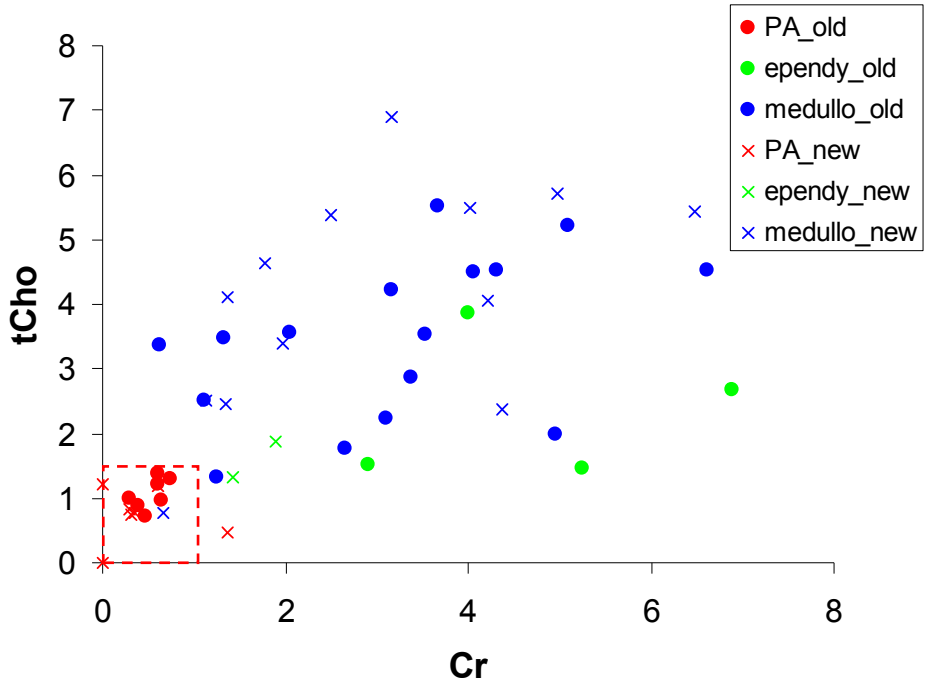

(b)

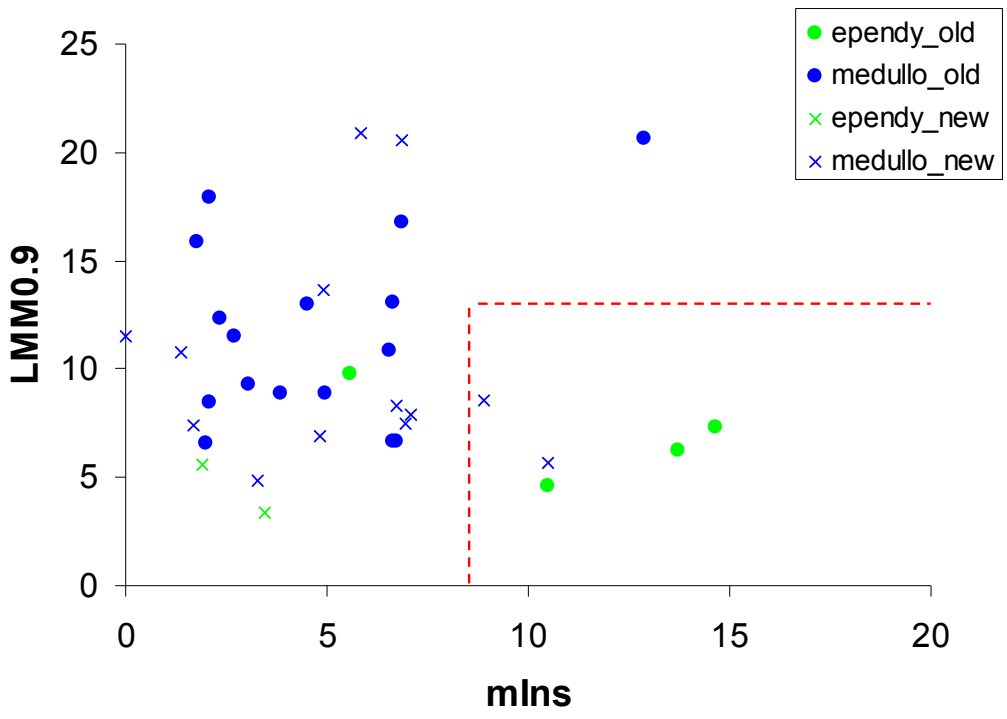

Figure 23: All cases, new and old from all 3 contributing centres
Red circles – old PAs; red crosses – new PAs; green circles – old ependymoma; green crosses – new ependymoma; blue circles – old medulloblastoma; blue crosses – new medulloblastoma

One of the PAs was misclassified, exhibiting slightly elevated Cr compared with the others, although this spectrum did still exhibit a low concentration of tCho compared with the other tumours. Both of the two ependymoma spectra were misclassified as medulloblastoma, with low concentrations of mIns. This was similar to that shown in the grade 3 ependymoma spectrum. Three of the medulloblastoma spectra were misclassified, one of these as a PA and the other two as ependymoma.

In summary, the original scheme had a correct classification rate 72.7% on the new data, which is a moderate improvement on the peak height classifier.

OTHER TUMOUR TYPES OF THE CEREBELLUM

Tumour types not in the original scheme fell into a variety of diagnoses. A series of bar charts showing metabolite and LMM concentrations are shown in Figure 24.

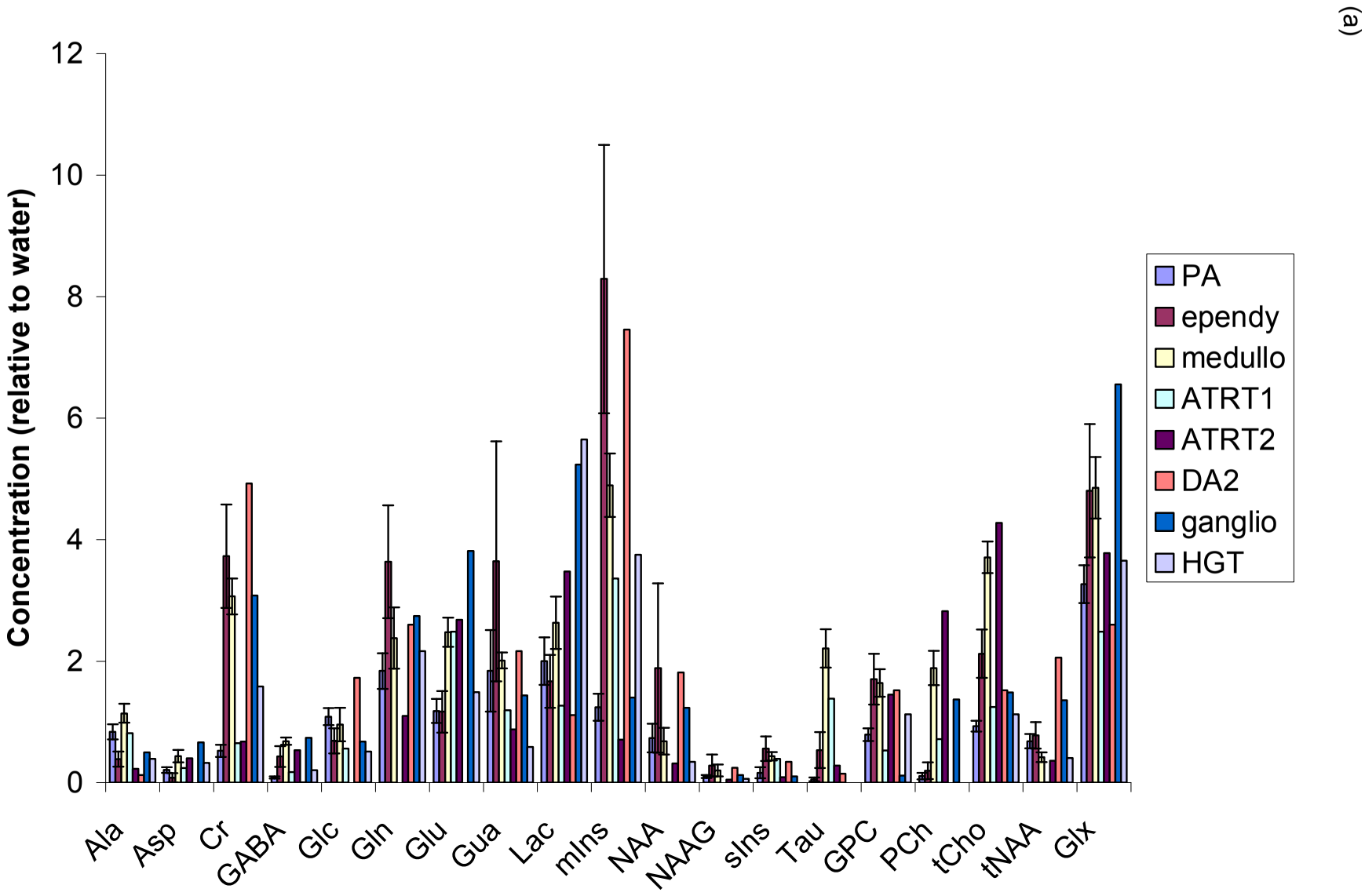
(a)
Concentration (relative to water)
12
10
8
6
4
2
0
PA
ependy
medullo
ATRT1
ATRT2
DA2
ganglio
HGT
Ala
Asp
Cr
GABA
Glc
Gln
Glu
Gua
Lac
mIns
NAA
NAAG
sIns
Tau
GPC
PCh
tCho
tNAA
Glx

(b)

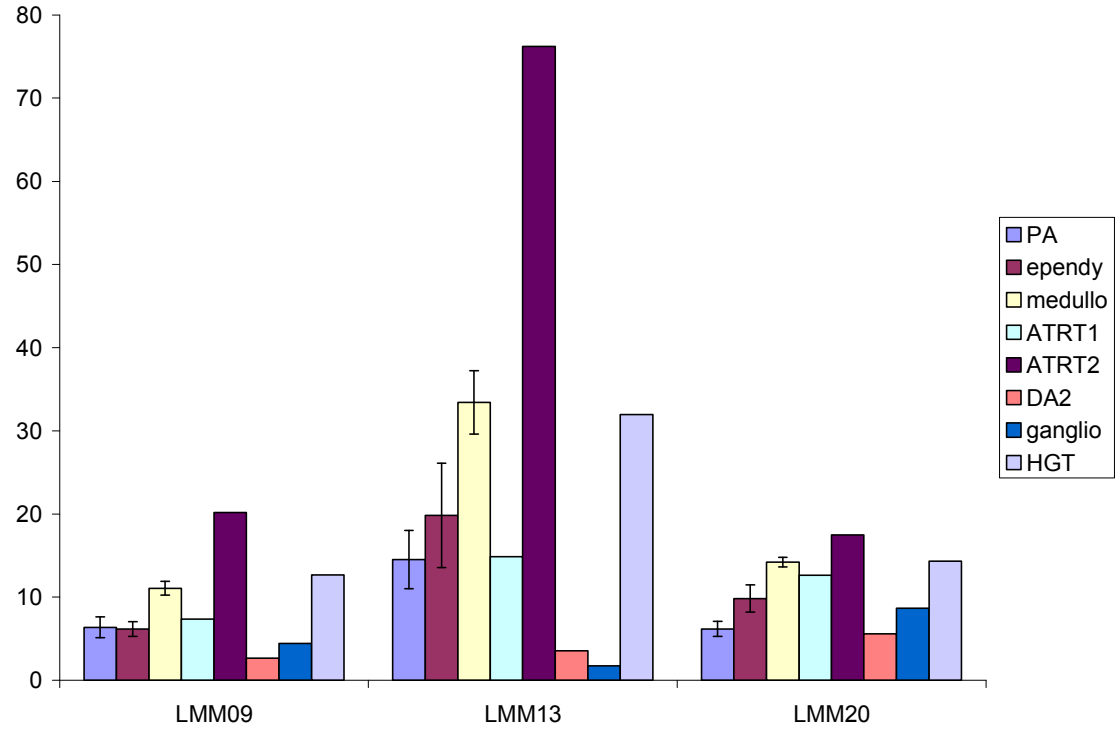

Figure 24: Bar charts showing metabolite (a) and LMM (b) concentrations (relative to water) of rare tumours of the cerebellum compared with those found in the 3 major tumour groups of the cerebellum.

ATRT

There were two ATRT; both had spectra with different features. Both ATRT showed a very low concentration of Cr and low/no NAA. One had relatively low LMM values, while the other ATRT had very high LMM signals.

DA2

The DA2 looked very similar to ependymoma. The spectrum showed high signals for Cr and mIns, which are both seen in ependymoma spectra. However, there was also a high signal for NAA and low LMM signals, which are not seen in ependymoma spectra.

Ganglioglioma

This showed similar concentrations to PA spectra for many metabolites, including mIns, tCho and LMM. However, it had higher tNAA and Glx, which may be used to differentiate it.

HGT

This tumour has not been fully classified histopathologically, but it is known to be of an aggressive nature. It showed high LMM signals and low NAA, but also a relatively low tCho signal.

DISCUSSION

Of the 26 cases tested using the scheme, six were misclassified, this is an improvement on the peak height classification scheme. Amongst these were the two new ependymoma cases, both of which exhibit lower mIns concentrations, in keeping with the grade 3 ependymoma. This highlights the issues surrounding using small groups, as it is uncertain which mIns concentration is more realistic for the ependymoma spectra, and if the grade does have an effect on this. Both of the new ependymoma were labelled as being grade 2 ependymoma, but grading of ependymomas not always definite [44, 45, 47].

The misclassified PA, while being misclassified outside the cut-off box, still sat close to this region and refinement of the cut-offs may correct for this.
Two of the misclassified medulloblastoma were classified as being ependymoma and one as a PA. Both of those classified as ependymoma

show high values for tCho, but also show high mIns concentrations. One of these two cases also shows very high tau levels and this would have questioned an assignment of ependymoma. The medulloblastoma spectrum classified as a PA showed low tCho compared with the other cases, this spectrum also had broad lines and was close to the quality control limits.

Looking a plot on the original axes with all data, old and new (Figure 23), clustering is still apparent with the three tumour types. The PA spectra all cluster with low values for each of the two metabolites and the medulloblastoma spectra still have the highest tCho. The ependymoma spectra appear to cluster in two groups, both with intermediate values for tCho but one cluster having much higher mIns concentrations than the other. This may be to do with grading ependymoma, but this is not histologically confirmed.

The cut-offs for these tumours groups using these two metabolites do need to be reoptimised and more data needs to be accrued, Using other metabolite signals, such as the presence of tau in medulloblastomas, should always be assessed in the assigning of disease type.

One of the main benefits of using a method such as determining concentrations using LCModel™ is allowing for a more complete picture of the biochemical profile of the tumour to be assessed. This is of particular benefit in the assessment of the tumour types not included in the original scheme. There were 5 patients with tumours outside of the original classification

scheme. These would not be classified in the original scheme, which would lead to misdiagnoses. However, the spectra of these tumour types do have characteristics which would make this mis-assignment less likely. These have been highlighted in two bar charts showing metabolite and LMM concentrations (Figure 24).

ATRT

These two cases of apparently the same tumour are highly different. There is little literature on this tumour type, but it is known to be highly aggressive [56]. One of the tumours had a spectrum that appeared to be highly aggressive with high LMM and tCho values. This would fit with the diagnosis, but without a larger series no conclusions can be made.

DA2

The spectrum of the DA2 was very similar to that on an ependymoma in several respects, but differed in both NAA and LMM concentrations. The spectrum was very similar to other diffuse astrocytomas. These have characteristic high mIns and low LMMs [72, 102, 128], and this would be in keeping with the given diagnosis.

Ganglioglioma

These tumours behave similarly to a PA and they are both low grade gliomas [176]. The spectra appear to be similar in many respects except for resonances in the region 2-2.6ppm.

HGT

The spectrum does appear to be of a high grade tumour. In cases like this, where no formal diagnosis is obtained, the extra information could be vital for treatment planning. There are high LMM signals, which are present in high grade tumours [66, 72, 74, 75, 94, 113], there is also a low NAA signal which is usually low or absent in higher grade lesions [66, 72, 96, 97, 107, 114].

CONCLUSIONS

Although the metabolites selected as having the largest significant differences between groups are the same as those used in both the peak height classifier and the limited metabolite basis classifier, a more detailed picture regarding the metabolite profiles of cerebellar tumours can be constructed using a full LCModel™ basis set. Many of the weaker signals offer significant differences between groups. As more data is accrued, a more complete metabolite profile can be constructed for each of the three tumour types, allowing for a better characterisation and classification of the tumours.

4.4 CONCLUSIONS

A simple method involving peak height measurement and the subsequent calculation of ratios between these peak heights was presented. This had a high classification rate and was proven to be usable by both clinicians and scientists in blinded testing. Moving to a more sophisticated method involving determination of metabolite concentrations using a spectral processing tool, in this case LCModel™, offered a reasonable improvement upon this classification rate. In addition, this allowed for the assessment of many more metabolites, including those with weaker signals. This information is potentially vital in the better understanding of these tumours and can help in the assessment of the rarer tumours, such as ATRT, and unusual entities, such as the uncategorised high grade lesion.

Both of these schemes have comparable success rates in classification rates of tumours of the cerebellum using a retrospective study group, however the classification scheme based upon metabolite concentrations appears to be more robust to the addition of new data (table 12).

		LCModel™	
Classification Accuracy	**Peak Height**	**Limited metabolite set**	**Full metabolite and LMM set**
Retrospective Data	89.10%	88.90%	96.3%
Prospective Data	65.40%	61.90%	76.9%

Table 12: Comparison of classification rates of the different schemes for classifying cerebellar tumours

Both of these schemes have benefits in the characterisation of cerebellar tumours, and have their uses in different areas. For a fast, simple diagnosis of tumour types the simple peak height classifier presented is preferable.

However, for more information about a tumour and to obtain a better understanding of tumour biology a more sophisticated method involving metabolite and LMM concentrations would be preferable.

The work performed using the data from cerebellar tumours showed that using a full data set form LCModel™ offered a good means of characterisation. Although the classification rates are comparable between simple schemes of peak height ratios, using limited basis sets and using complete basis sets in the retrospective study, the scheme using the full basis set was more robust to the addition of new data and allows a fuller characterisation. When we can link this to the underlying metabolic pathways; we will gain better understanding of tumour biology. Metabolites such as tau offer the potential for extra confidence in diagnosis.

The major benefit of using a more complete basis set was in the analysis of rarer tumours of the cerebellum. It allowed a more in depth analysis of these tumours, which could be used to either avoid misdiagnosis or aid in the better understanding of these rare tumours. LCModel™ gives values for a larger number of metabolites, and while these are not of huge benefit in a simple classification scheme, they do allow for a more in depth assessment of the spectrum. This also allows more sophisticated pattern recognition methods to be used, which may give better classifiers.

A prospective evaluation of both schemes showed them to be moderately robust to the addition of new data. By adding more data over time, these

schemes can be improved further and the cut-off values described further refined. Both peak height and metabolite based classifiers were shown to be robust to data taken on multiple sites. However, it should be noted that the prospective evaluation showed poor discrimination of ependymomas. This class had very few cases in the original classifier, and the inclusion of more data should improve the accuracy of the classifier for this group. This highlights the importance of both multicentre studies and prospective evaluation of schemes, especially those designed for rarer tumour types.

The main challenge and limitation of the schemes presented is the classification of rare tumours. In groups where there are many cases the cut-off values can be determined and refined to allow for future cases to be assessed and compared in a robust manner. For tumour types that occur less frequently this is more of a challenge, and these will often be misclassified as one of the more common tumour types. These tumours have been shown to have characteristic features in their spectra, but without more cases to compare with no formal conclusions can be drawn. This highlights a problem of using small datasets. A larger multicentre study over a longer period may assist in this problem with more of these rarer cases being assessed.

The classification accuracy compares favourably with those found using a more sophisticated discriminant analysis [73, 98]. One study [73], using long echo-time MRS, quoted a correct classification rate of 85%. A second study, performed at BCH on a similar group of spectra to those used in the original

schemes [98], showed a predictive ability of 93-95% and an accuracy of 80% using the first two principal components alone. It should be noted that neither of these schemes were tested prospectively, so the replication of these results on further data has not been established.

Henceforth, analysis will be performed using LCModel™ concentrations. Multivariate pattern recognition techniques would allow for an analysis based on the complete list of variables, i.e. all metabolites and LMM concentrations, between groups. However, this method was not used for several reasons. Firstly, when performing the analysis on cerebellar tumours using LCModel™ concentrations the classification accuracy was not significantly improved by adding additional criteria beyond the two metabolite cut-off values used in the scheme presented. In addition to this, the scheme using two cut-off values compared favourably with scheme using multivariate analysis [73, 98]. Sophisticated pattern recognition tools are not favourable in a clinical tool, as there is not always the availability of tools such at matlab, required for the application of such methods. Pattern recognition methods have only been proved to be reliable using large data sets, with large numbers in each of the groups for comparison. This is rarely possible in studies performed into childhood brain tumours. These tumours are rare in children and, thus, small numbers are present in each group and as such multivariate pattern recognition may not offer the best means of analysis.

Presented here is a series of clinical studies, using the techniques developed above in a series of important clinical situations. Cerebellar tumours are

usually fully excised as part of their initial treatment and, so, nearly always have a histopathological diagnosis. This means that this group is an ideal test-bed for the development of new classifiers. Other tumours are located in areas of the brain where surgery is more of a challenge, or at times not possible. In these incidences, it would be better to have a means of non-invasive diagnosis. One of these areas is the pineal gland and surrounding area.

CHAPTER 5: PINEAL REGION TUMOURS

5.1 INTRODUCTION

Pineal tumours only account for approximately 5% of childhood brain tumours. Despite this low incidence, they pose significant challenges in both diagnosis and treatment. The majority of tumours occurring in this region fall into 2 groups: germ cell tumours (GCTs) and pineal parenchymal tumours (PPTs). Each of these groups is composed of a highly diverse set of tumour types, both in histological appearance and clinical course. Effective management requires an accurate diagnosis, but surgery to this region of the brain caries significant risks and not all tumours require a resection as part of their curative treatment. Non-invasive methods for diagnosing pineal tumours are particularly attractive and a combination of MR imaging and blood markers is already used to diagnose non-germinomatous secreting GCTs (SGCT). However, the majority of pineal tumours still require a biopsy for diagnosis, and new non-invasive methods for diagnosis would be a significant advance. Biopsies of pineal lesions commonly yield small amounts of tissue, limiting in vitro investigation and hampering the molecular studies required to improve our understanding of these tumours. Non-invasive methods which can provide molecular information to improve our understanding of these tumours would be of additional benefit.

Tumours of many different histopathologies can occur in the pineal gland, making non-invasive diagnosis challenging. GCTs are the most common, accounting for 50-70% of pineal tumours in childhood [9]. For clinical purposes, there are three main sub-categories of GCT [9, 41, 52]:

germinomas; SGCTs; and teratomas. Germinomas constitute approximately 65% of GCTs, are highly malignant and commonly secrete human placental lactogen (HPL). SGCTs constitute approximately 25% of GCTs, are malignant and secrete beta-subunit human chorionic gonadotrophin (BHCG) and/or alpha-fetoprotein (AFP). Teratomas constitute approximately 10% of GCTs, may be either mature with no-malignant elements or immature containing malignant elements. Approximately 20% of pineal tumours arise from pinealocytes and are collectively termed PPTs [53, 80, 85, 177-179]. Pineoblastomas (grade IV) are highly malignant embryonal tumours with a propensity for dissemination in young patients. Pineal parenchymal tumours of intermediate differentiation (PPTID) and the papillary tumour of the pineal region are very rare intermediate grade tumours with a variable clinical course [177, 178]. Pineocytomas (grade II) are slow growing tumours, with mature cells [80]. Astrocytomas may also occur in this region and these can be of any grade.

Characteristic clinical and radiological features, together with raised AFP or B-HCG in cerebrospinal fluid or blood, are sufficient for the diagnosis of SGCTs, without the need for biopsy. Histopathology is required for the diagnosis of all other pineal tumours. The pineal region is a challenging region in which to operate and there is an associated risk of morbidity and mortality [41]. Surgical resection does not form part of the curative treatment strategy for a number of pineal tumours and surgery could potentially be avoided altogether in many if a non-invasive diagnosis could be made. For example, once the diagnosis is made on biopsy, germinomas are commonly treated with

chemotherapy and/or radiotherapy without resective surgery [36, 41] to give long term survival rates of over 90% [53, 85, 179]. They would therefore be ideal candidates for non-invasive diagnosis. For other tumours, such as pineoblastoma, surgical resection is a key component of the treatment [85] and identifying such cases pre-operatively would aid in surgical planning.

Some differences are visible between all tumour groups using conventional MRI, but these are quite subtle and not always consistent. One example would be that teratomas appear to be more heterogeneous than the most other pineal region tumours [180]. These tumours can also have lipid present in them [54]. However, MRI for germinoma, pineocytoma and pineoblastoma are very similar, they are all reasonably homogeneous and appear bright on T2. These tumours are all very different and require completely different management, so additional information would be highly beneficial.

A number of MRS studies have been performed which have included limited numbers of pineal tumours. One study of MRS in childhood brain tumours showed pineal germinomas to have high lipids and macromolecules levels compared with a range of tumours outside the pineal gland [71]. Another study of childhood brain tumours found differences in a number of metabolite ratios between germinomas and a series of other tumours in a range of locations [72]. In a case study of a comparison of a germinoma spectrum with that of normal appearing white matter, the germinoma spectrum was shown to have elevated LMMs [115].

The study presented here extends the findings in these reports by concentrating on MRS of the major pineal tumours and investigates the potential use of MRS profiles to aid their diagnosis and improve tumour characterisation.

5.2 METHODS

Raw data was processed using LCModel™ and Cramer-Rao bounds were used to remove metabolites that were poorly determined. Quality control was applied using the following measures:

3. SNR had to be greater than 3 for analysis of LMM levels and greater than 4 for metabolite levels
4. FWHM had to be less than 0.200ppm for analysis of LMM levels and less than 0.150ppm for analysis of metabolite levels.

LMM peaks are inherently broader than metabolite peaks allowing less stringent quality control criteria.

For analysis, data was combined into 2 groups: GCTs and PPTs. Two-tailed t-tests of significance were performed between the groups to assess for distinguishing features. The group of GCTs was further analysed using z-tests to determine whether teratomas and SGCTs can be shown to have significant differences from germinomas. Z-tests were used to assess whether the differences seen in individual members of different groups are large enough to be statistically significant.

5.3 RESULTS

MRI and short-echo-time MRS were performed on 15 children with tumours of the pineal region between 01/09/03 and 31/12/07. In addition, two children with germinomas in other locations of the brain, one suprasellar and one frontal were included in the study. A comparison was performed with the pineal germinomas. Visual inspection showed all germinoma spectra appear similar and additional z-tests showed pineal germinoma spectra to be indistinguishable from the other germinoma. Thus, these cases were included in this study. All MRS were performed prior to surgery and adjuvant treatment with chemotherapy or radiotherapy. There was one exception, where the MRS was acquired after a small biopsy, where a large fraction of the tumour remained. Sixteen patients proceeded to surgery, providing histological diagnoses of 9 germ cell tumours (7 germinomas and 2 teratomas), 5 pineoblastomas, 1 pineocytoma and 1 PPTID. One patient had a SGCT diagnosed on radiological appearances and serum markers. The average age at diagnosis of children with GCTs was 12.0 years (germinoma 13.0 years; teratoma 9.1 years; SGCT 10.9 years) and for those with PPTs was 6.1 years (pineoblastoma 6.6 years; pineocytoma 7.1 years; PPTID 2.7 years).

Of the 17 MRS studies, 2 did not meet quality control criteria required for quantitative analysis of metabolite concentrations; these cases had a broad FWHM (1 pineoblastoma and 1 germinoma). Both of these cases met the quality control criteria for inclusion in the LMM analysis. However, the germinoma also had considerable residual water in the spectrum, and needed to be removed from the study.

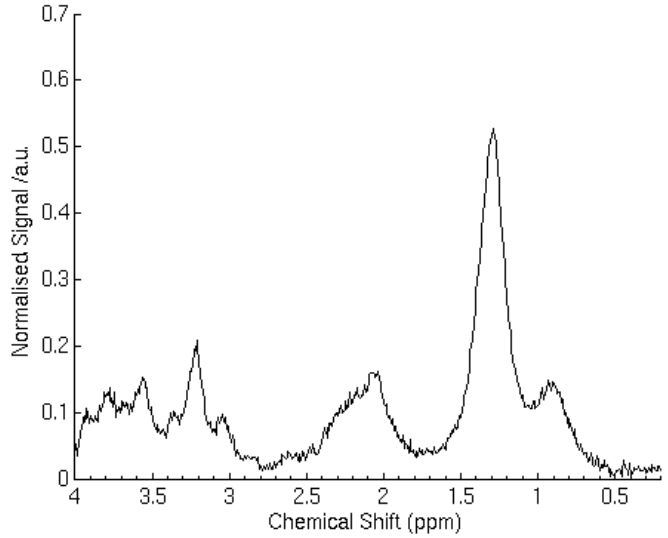
Normalised Signal /a.u.
0.7
0.6
0.5
0.4
0.3
0.2
0.1
0
4
3.5
3
2.5
2
1.5
1
0.5
Chemical Shift (ppm)

(a)

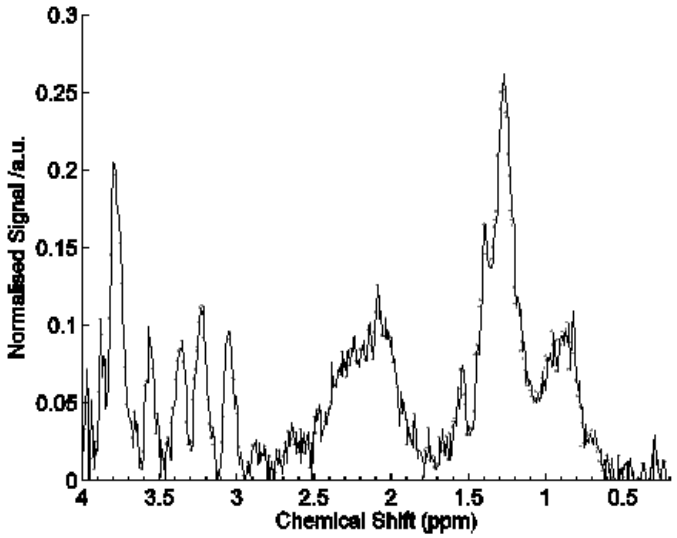
Normalised Signal /a.u.
0.3
0.25
0.2
0.15
0.1
0.05
0
4
3.5
3
2.5
2
1.5
1
0.5
Chemical Shift (ppm)

(b)

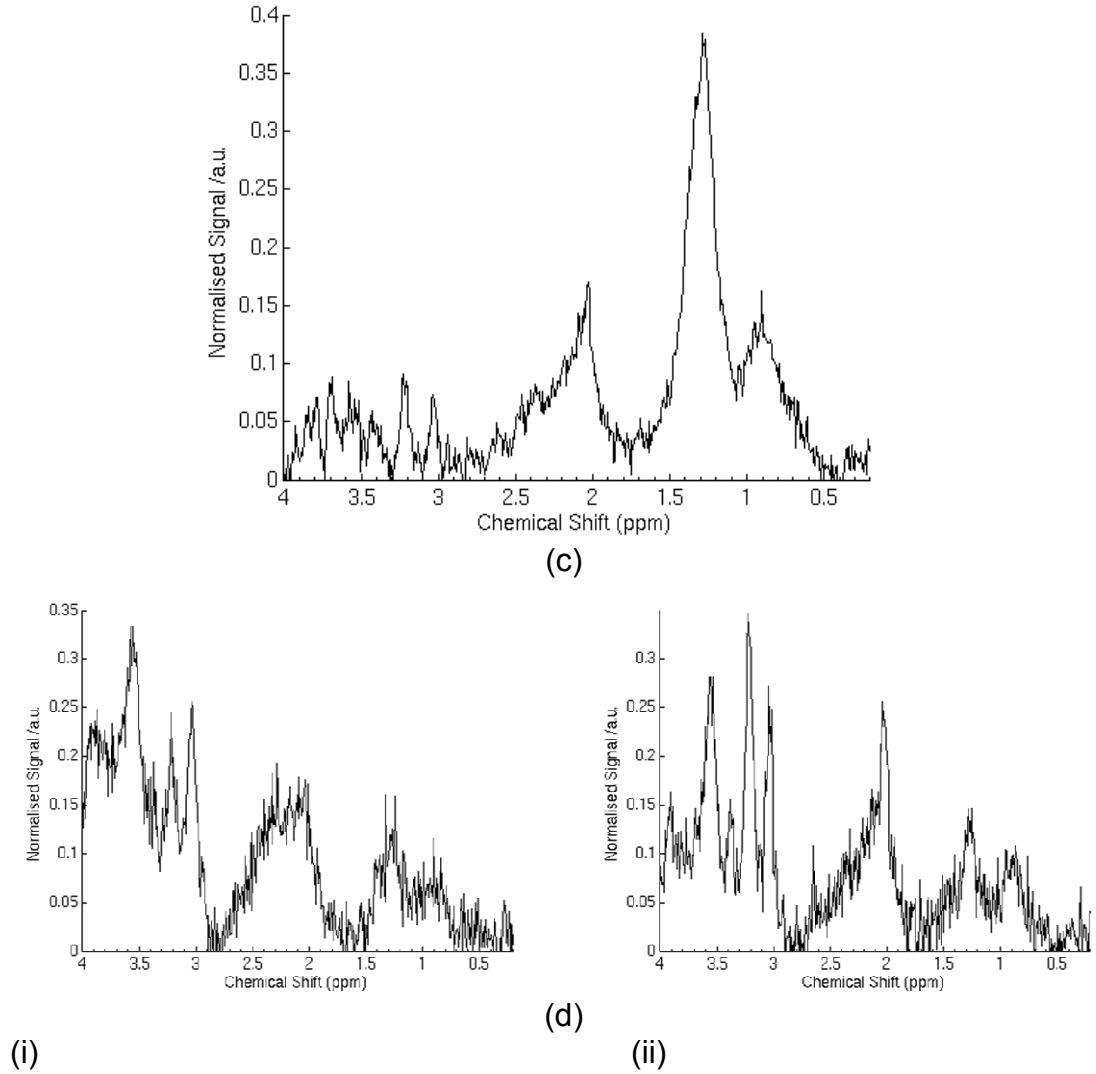

Figure 25: Average Spectra for (a) germinoma, (b) pineoblastoma, (c) teratoma and (d) example spectra for (i) PPTID and (ii) pineocytoma

Mean spectra for germinoma, pineoblastoma and teratoma are shown in Figure 25 with the two cases not meeting quality control criteria excluded. Figure 25d shows the spectra for the only PPTID and pineocytoma, in the study group. Prominent differences can be seen between these spectra, particularly in the LMM regions at 0.9ppm and 1.3ppm. The MRS in GCTs is dominated to such an extent by LMM that the relative values of small metabolites, giving rise to peaks between 3.0ppm and 4.0ppm, are difficult to discern by visual inspection. However, a small peak is seen at 3.35ppm in the germinomas and is attributed to taurine. In PPTs, lipids are particularly low in

the low and intermediate grade lesions (pineocytoma and PPTID). The pineoblastoma spectrum shows a high LMM peak, but the metabolite signals are still clearly visible. In the PPTID, the total choline peak (3.2ppm) is low compared with the creatine peak (3.0ppm). Taurine is prominent in the pineoblastomas. LCModel™ analysis was used to quantify the metabolite and LMM components of the individual spectra.

Mean values of metabolites for each tumour type, relative to water, are given in table 13.

	Germinoma		SGCT	Teratoma		Pineoblastoma		PPTID	Pineocytoma
Metabolite	**Average**	**StdErr**		**Average**	**StdErr**	**Average**	**StdErr**		
Cr	1.63	0.08	1.49	0.35	0.25	1.68	0.30	5.39	
Glc	0.85	0.14	0.76	0.46	0.16	0.74	0.23	2.55	
Gua	1.71	0.16	1.64	0.59	0.42	1.59	0.34	2.74	
mIns	3.17	0.47	1.74	1.40	0.49	1.61	0.35	7.60	
sIns	0.26	0.03	0.17	0.04	0.00	0.20	0.05	0.32	
Tau	0.79	0.13	0.99	0.18	0.01	0.47	0.14	0.33	
tCho	1.44	0.10	0.73	0.31	0.01	0.79	0.17	1.24	
tNAA	1.13	0.18	1.17	0.84	0.13	0.61	0.14	1.31	
Glx	4.82	0.32	5.82	3.96	0.33	4.65	0.91	9.08	
LMM0.9	11.92	1.32	9.91	7.80	2.17	5.28	0.37	3.36	4.93
LMM1.3	51.71	8.68	48.43	29.58	1.89	14.34	0.51	6.75	9.83
LMM2.0	14.12	1.42	11.16	8.68	0.86	7.73	0.68	4.38	12.69

Table 13: Average metabolite and LMM concentrations for pineal region tumours. Where more than one case presented a standard error has been calculated along with the average concentration, for tumours with only one case in the study only the value for the concentration has been listed.

Since only one case is available for some tumour types, a formal statistical analysis across all groups has not been performed. However, it is worthwhile noting some of the main features. GCTs are confirmed to have high LMM concentrations with germinomas having the highest. Germinomas also have the highest tCho levels and teratoma the lowest. Although taurine was quantitated in all tumour types, it was only identified with high confidence (CRLB < 25%) in a pineoblastoma and a germinoma. Taurine was highest in

the germinomas. Teratomas show the lowest concentrations of Cr, sIns, and taurine. Pineoblastoma spectra show the lowest concentration of tNAA. The PPTID spectrum showed a very high concentration of mIns, Cr, and Glx. It also exhibited elevated tCho, similar to that seen in the germinoma spectra and a low concentration of taurine. The pineocytoma has generally low metabolite concentrations, in keeping with a tumour of low cellularity.

Results of a two-tailed t-test between the GCTs and PPTs are presented in table 14.

		GCT		PPT	
Metabolite	**P-Value**	**Average**	**StdErr**	**Average**	**StdErr**
Cr	0.275	1.29	0.09	2.42	0.39
Glc	0.536	0.74	0.07	1.10	0.23
Gua	0.547	1.42	0.11	1.88	0.25
mIns	0.864	2.55	0.25	2.81	0.59
sIns	0.763	0.19	0.02	0.22	0.03
Tau	0.476	0.66	0.07	0.44	0.10
tCho	0.599	1.07	0.08	0.88	0.12
tNAA	0.400	1.06	0.09	0.75	0.12
Glx	0.662	4.73	0.17	5.54	0.74
LMM0.9	0.033	10.78	0.74	4.96	0.24
LMM1.3	0.044	46.43	4.70	12.61	0.53
LMM2.0	0.120	12.59	0.80	7.96	0.53

Table 14: T-test results for comparison between GCTs of the pineal region and PPTs

These results confirm that the LMM signals at both 0.9ppm and 1.3ppm are significantly higher in GCTs compared with the other tumours. No metabolites were significantly different between the two groups. A scatter plot of the LMM levels at 0.9ppm and 1.3ppm is given in Figure 26.

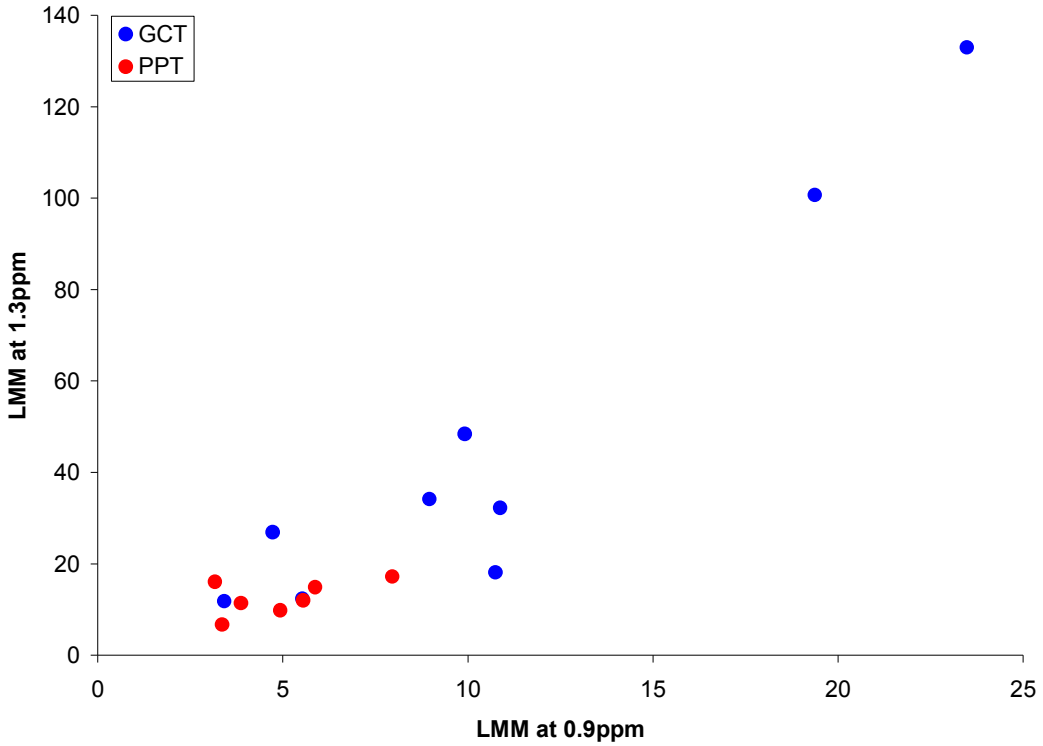

Figure 26: Tumours grouped as either GCT or PPT and plotted on axes for LMM regions around 0.9ppm and 1,3ppm.
red – GCT; blue – PPT

The plot shows the distribution of LMM values across the tumours and shows that there is considerable variability within individual tumour groups. Two germinomas had LMM levels which were as low as the non-GCT cases. One of these was the case where the MRS did not meet quality control criteria for analysis of metabolites. The other had an unusual clinical presentation with a long period of symptoms prior to diagnosis and a strong family history of low stage seminoma. The sub-analysis of the GCT group using a z-test is given in table 15.

Metabolite	secreting GCT	teratoma 1	teratoma 2
Glc	0.390	0.311	0.028
sIns	0.051	<0.001	<0.001
Tau	0.760	0.017	0.014
Gua	0.414	0.062	0.000
Cr	0.203	<0.001	<0.001
mIns	0.089	0.156	0.010
tCho	0.001	<0.001	<0.001
tNAA	0.533	0.395	0.116
Glx	0.918	0.289	0.033
LMM0.9	0.267	0.013	0.373
LMM1.3	0.439	0.122	0.180
LMM2.0	0.198	0.113	0.028

Table 15: P-values for the comparison of germinoma metabolite concentrations with other germ cell tumours of the pineal region

This shows that tCho, Cr, Tau and sIns were all significantly lower in both of the teratomas compared with the germinomas. The SGCT had significantly lower tCho, sIns and mIns than the germinomas. A scatter plot of the most reliably quantitated metabolites, tCho and Cr is given in Figure 27.

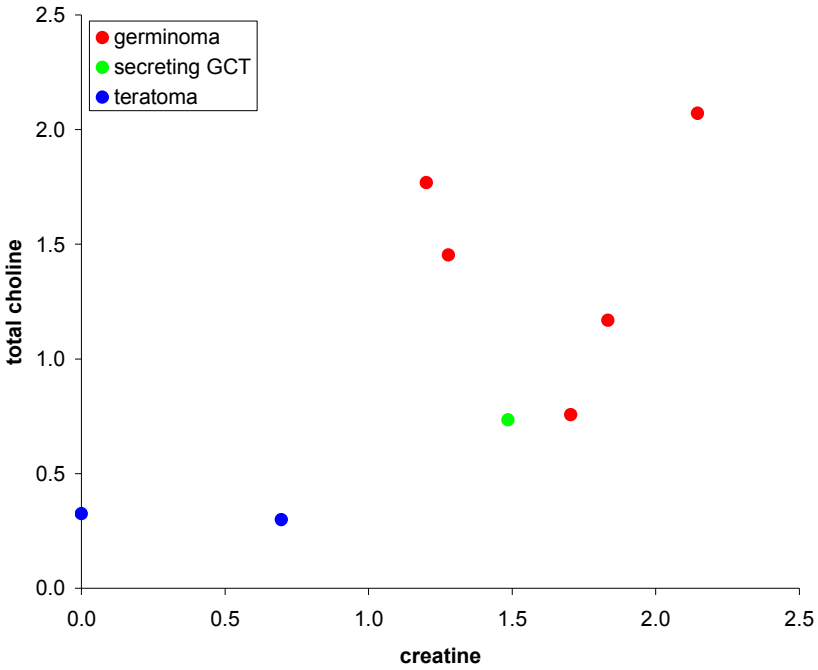

Figure 27: GCTs plotted on axes tCho Vs Cr
Circles – germinoma; empty star – secreting GCT; closed stars – teratoma

The SGCT lies between the teratomas and germinomas. There were no significant differences detected between germinomas arising in the pineal gland and those in other locations. An analysis of the histopathology of the germinomas did not find any correlation between non-germinomatous elements and MRS features.

5.4 DISCUSSION

Short echo-time MRS has been used to investigate pineal tumours occurring in childhood. Key differences have been found between GCTs and PPTs and also between germinomas and teratomas. Pineal region tumours are rare making such studies challenging, but they represent important childhood diseases for which non-invasive biomarkers would be a valuable clinical tool. Whilst the overall numbers in the study are small, they are large compared with previous reports and sufficient to allow statistical analysis. Quality control criteria we relaxed for looking at LMM resonances. This was seen as reasonable, due to the signal strength of these peaks in relation to the noise. This was done to increase the number of cases for analysis, which was seen as important due to the small size of dataset.

The most notable feature found in GCTs was the high levels of LMM. High LMMs in this tumour group have been noted previously both in CNS germinomas [71, 115] and GCTs elsewhere in the body [111]. Raised LMMs are a common feature in many tumours [66, 68, 69, 72-75, 94, 113, 115, 181, 182], and are usually attributed to increased mobile lipid levels rather than changes in the macromolecular component [113]. High mobile lipid levels

have been associated with malignancy in brain tumours [29, 65, 66, 74, 96]. This is consistent with the findings in both germinoma and SGCT spectra, both of these are fast-growing tumours with metastatic potential. Two of the germinoma spectra exhibited lower LMM concentrations. In the case of the patient with a strong family history of low-stage seminoma and long period of symptoms prior to diagnosis, this would be consistent with MRS suggesting a slower growing, less aggressive tumour. The other germinoma with low LMM levels was associated with a spectrum that only just met acceptable quality control; care should be taken in interpreting poor quality spectra even for LMM. Teratomas had lower LMM levels compared with germinomas and SGCT, in keeping with the less aggressive nature of mature teratomas [49, 54, 177]. However, teratomas still have high LMM levels compared with non-GCT tumours indicating that there is an additional source of LMM in these tumours, which is likely to be fat tissue seen on histopathology and conventional MR images in these tumours. The very low LMM concentrations in the pineocytoma and PPTID spectra are in keeping with their low grade [53, 80, 177, 178].

Another metabolite linked with tumour aggressiveness and growth is choline [66, 93, 101, 106, 114]. Within the group of GCTs, germinomas exhibited the highest concentration of tCho with lower concentrations in SGCT and the lowest concentrations in teratomas. This finding is in keeping with the relative growth patterns of these tumours. Given the lack of overlap in the tCho values between the tumour groups (Figure 27) tCho levels may be a useful non-invasive discriminator between these tumours. The pineoblastomas had

higher tCho levels than the teratomas, pineocytoma and SGCT but lower than the germinomas; again in keeping with their known growth pattern. Medulloblastoma have been reported as having very high levels of tCho, these are closely related to pineoblastoma, this very strong tCho signal is not mirrored in the pineoblastoma spectra [71, 98] indicating a different nature of these tumour groups. The PPTID was associated with a spectrum showing a tCho concentration to be lower than the Cr peak whereas the reverse is seen in the pineoblastoma again reflecting the more aggressive nature of pineoblastomas.

Taurine was convincingly identified in germinomas, in addition to pineoblastomas, in keeping with a previous study [71]. Primitive Neuroectodermal Tumours, a group that contains both medulloblastomas and pineoblastomas, have been shown to exhibit higher taurine levels than other tumours and this has been proposed as being of diagnostic value [100]. However, this study shows that taurine levels alone should not be used to discriminate between tumours of the pineal gland. Studies of primitive neuroectodermal tumours are usually dominated by medulloblastomas which are the most common subtype, thus findings are weighted to this group. This would indicate a further difference between the spectra of pineoblastoma and medulloblastoma. The finding of Tau in germinoma would be supported by recent micro-RNA profiling studies that indicate that intracranial germ cell tumours are distinct from their extra cranial counterparts and may arise from endogenous CNS neural progenitor cells rather than primordial germ cells

[183]. However, the role of taurine in brain tumours is not well understood and further studies are required.

5.5 CONCLUSIONS

Key differences have been identified between the spectra of GCTs and other tumours of the pineal region, with GCTs having significantly higher concentrations of LMM at both 0.9ppm and 1.3ppm. Furthermore, within the groups of GCTs, differences have been shown to exist between both teratoma and SGCT spectra and germinoma spectra. All of these findings are preliminary, and further studies with significantly more data would be required to confirm the promising findings presented here.

CHAPTER 6: BRAIN STEM TUMOURS

6.1 INTRODUCTION

Of all brain tumours of childhood, around 10-25% occur in the brain stem [184, 185]. The management of brain stem tumours continues to present a major challenge to paediatric oncology, as it is a particularly difficult area to biopsy [92] and diagnosis is often made on clinical and imaging grounds alone. However, diagnosis of brain stem lesions using imaging alone leads to a misdiagnosis rate of 10-20% [185, 186]. Novel imaging methods offer a means of improving diagnostic accuracy and furthering our understanding of the biology of these important childhood tumours [72, 182].

There are four main types of tumour that occur in the brain stem: tectal plate gliomas (TPGs), diffuse pontine gliomas (DPGs), high grade gliomas (HGGs) and low grade gliomas of the pons and medulla (LGGs). TPGs and LGGs both share a good prognosis and, when biopsied, TPGs are invariably found to be low grade astrocytomas. In contrast to this, DPGs and HGGs have a very poor prognosis; of these tumours DPGs are the most common lesions. DPGs comprise 80% of all brain stem gliomas [182] and 15-20% of all CNS tumours [42] in children. These tumours have a particularly poor prognosis, with median survival of less than a year, and despite their prevalence there has been no improvement in the outcome for 30 years [42].

Long echo time (TE) MRS (TE = 135-144ms) performed on the brain stem has previously been shown to differentiate normal surrounding tissue from tumour tissue [182, 187], and also indolent from aggressive lesions [187].

However, as seen previously, many metabolite and LMM signals will be lost in a long echo time spectrum.

Although brain stem tumours are clinically important, only small numbers present to any one centre each year. This presents major challenges for the use of techniques such as MRS for which there is no universally agreed standardisation of data collection or analysis. This work depicts a multi-centre study using data from the CCLG, using short echo time MRS to characterise childhood brain stem tumours. Issues of protocol selection, quality control, data transfer, data storage and standardised data analysis were addressed within a well-established clinical trails infrastructure.

6.2 METHODS

Raw data was processed using LCModel™ and Cramer-Rao bounds were used to remove metabolites that were poorly determined. Quality control was applied using the following measures:

1. SNR had to be greater than 4
2. FWHM had to be less than 0.150ppm

Where the water unsuppressed spectrum was recorded, metabolite and lipid concentrations could be determined relative to water. In the case of data that did not have paired water unsuppressed and water suppressed MRS, the data was not analysed with the rest of the dataset. However, ratios of metabolite to tCho were generated for all data, and these were compared.

Combined metabolite values were used for tNAA, tCho and Glx. Any signal with consistently high Cramer-Rao lower bounds (>50%) was removed from further analysis, since these would be very poorly determined.

Tissue diagnosis is often not possible in brain stem lesions, in cases where this was the case; diagnosis was made using a centralised radiological review, whereby tumours were grouped into 5 diagnoses:

- focal high grade glioma (HGG),
- focal low grade glioma (LGG)
- tectal plate glioma (TPG),
- diffuse glioma contained fully within the pons (DPG), and
- diffuse glioma centred on the pons but with a component extending outside (DG)

TPGs and LGG were grouped into one group, henceforth known as LGG, this was done as TPGs are assumed to be LGGs and they behave as such. This led to 4 groups being considered: HGG; LGG; DPG and DG.

The variability of MRS metabolite profiles across all cases was determined using a PCA. This was performed using metabolites of appropriate Cramer-Rao lower bounds, normalised to vector length.

An ANOVA was performed between LGGs, HGGs and DPG+DGs to assess for significant difference. In addition to this, two-tailed t-tests were performed between diffuse and focal lesions, and also between focal HGGs and LGGs. .

Finally a comparison between diffuse gliomas confined to the pons and those with components outside the pons was performed, using two-tailed t-tests, to assess whether there were any metabolic differences between these two groups

6.3 RESULTS

MRI and short-echo-time MRS were performed on 32 children (15 from BCH; 5 from GOSH, 4 from QMC and 8 from RMH) with brain stem tumours between 26/09/2003 and 05/10/2007. All MRS were performed prior to surgery and adjuvant treatment with chemotherapy or radiotherapy.

The results of the radiology review can be seen in table 16:

	Total		BCH		QMC		RMH		GOSH	
Diagnosis	**Total**	**In study**	**Total**	**In study**	**Total**	**In study**	**Total**	**In study**	**Total**	**In study**
DPG	14	13	10	10	2	2	2	1	1	1
DG	5	4	1	1	1	1	2	1	1	1
LGG[a]	6	4	2	2	1	1	2	0	1	1
HGG[b]	5	3	3	3	0	0	0	0	2	0
Undecided	2	0	0	NA	0	NA	2	0	0	NA

a: includes 1 biopsied ganglioglioma and 2 biopsied pilocytic astrocytoma
b: includes 1 aggressive tectal plate tumour

Table 16: Diagnosis summary for patients in the brain stem tumour study

In summary, this led to a diagnosis of 6 LGG (including 1 unbiopsied TPG and 1 biopsied ganglioglioma); 5 HGG (3 of these were biopsy proven HGGs, the third was an unbiopsied TPG that appeared to be of aggressive nature on radiological criteria); 14 DPG and 5 DG. There were also two tumours where it was considered that there was insufficient information to make an informed decision; these tumours were removed from further analysis.

Of the remaining 31 spectra, 7 were removed during quality control; these were all due to low SNR. This left a total of 23 spectra, including 13 DPG and 4 DG spectra, in addition to this 3 LGG, 3 HGG and 1 biopsied ganglioglioma were left remaining. Average spectra for the 3 main tumour types are shown in Figure 28.

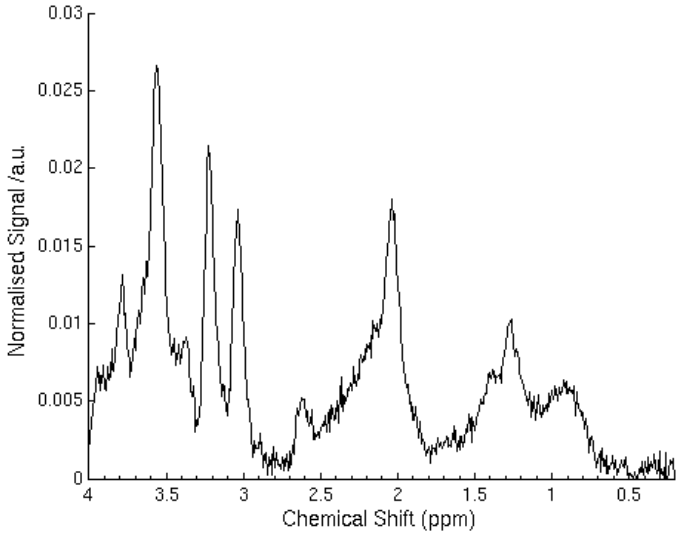

(a)

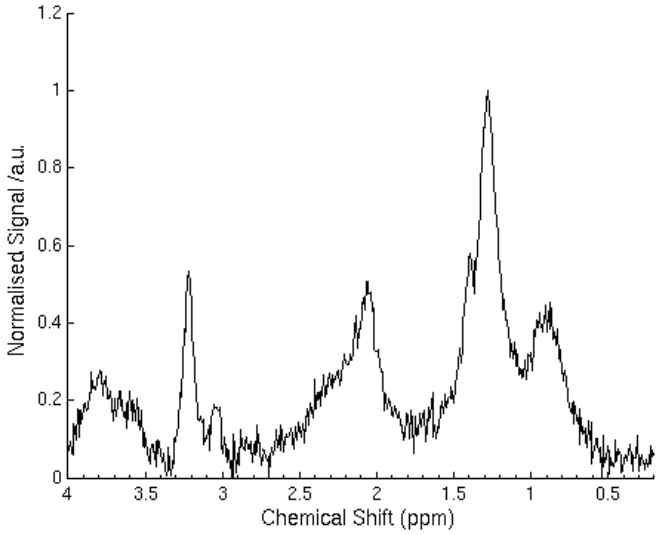

(b)

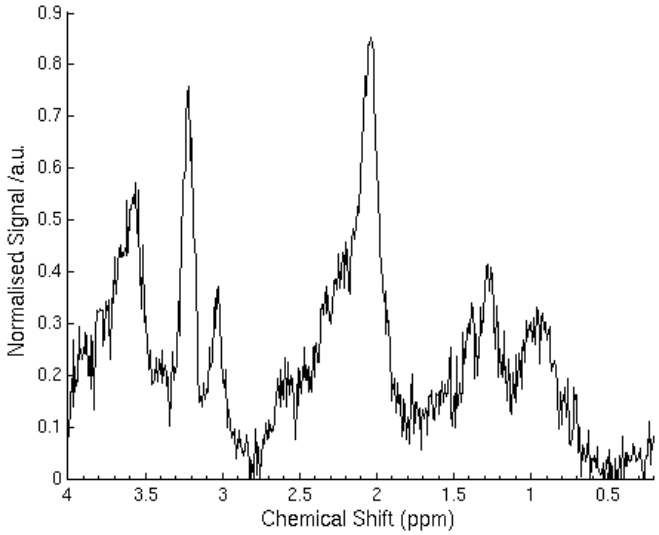

(c)

Figure 28: Average spectra for (a) DPG; (b) HGG and (c) LGG

A PCA was performed using a full list of all metabolite and LMM concentrations, normalised to vector length, on the group separated into three subgroups – diffuse tumours (DPG +DG); DG; LGG; and HGG. Upon producing a PCA for these three groups, it became apparent that five of the DPG+DG spectra were clustering with two HGG separate from the rest of the spectra. A decision was made to separate the DPG and DG into two groups and a PCA was performed with the data separated into four groups: DPG; DG; HGG; and LGG (Figure 29).

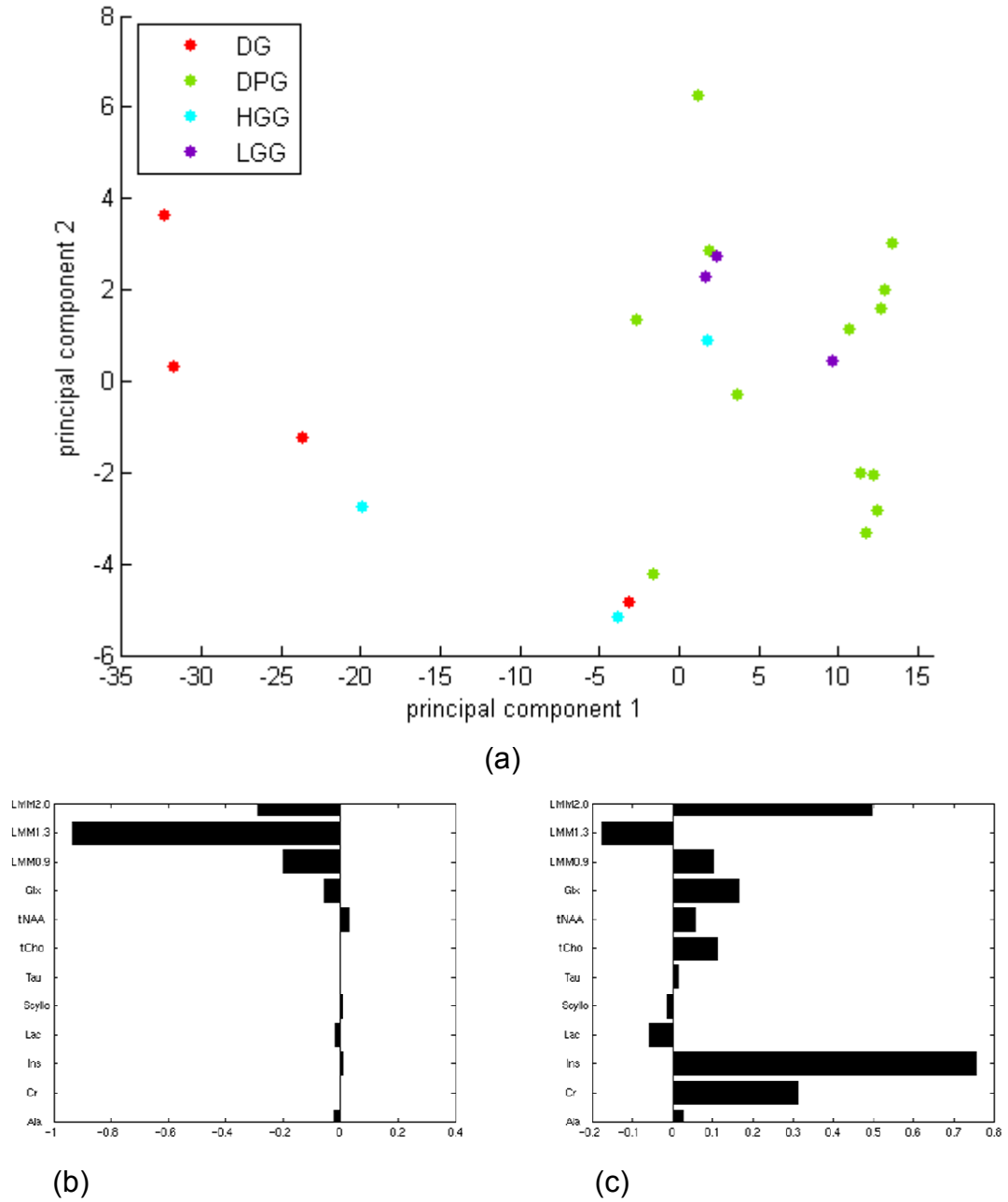

Figure 29: PCA (a) for brain stem tumours collated into 4 groups: HGG – red; LGG – green; DPG – blue; and diffuse gliomas not localised to the pons – purple. Loadings plots are shown for PC1 (b) and PC2 (c)

This highlighted that it was the DG spectra that were clustering with the two HGG spectra. This was primarily using PC1 alone, which was much lower in the DGs and HGG compared with the rest of the spectra. PC1 is largely showing differences seen in the LMM signals (Figure 29b), with a lower value for PC1 relating to stronger LMM resonances. This indicates that LMM

resonances are more pronounced in DGs and HGGs in comparison with LGG and DPGs. These tumours also showed a low PC2 score. A high score of PC2 would be strongly influenced by a strong mIns signal. This is confirmed by the high scores for PC2 in the DPG spectra (Figure 29a); where this peak is one of the main distinguishing features of this tumour.

One of the DPG patients did not have a water unsuppressed file, with which to reference the metabolites concentrations to. Due to the small dataset, ratios to tCho were calculated for metabolites in all spectra, and analysis was performed using these for all data.

Results of two-tailed t-tests performed between different groups are shown in table 17:

	P-Values		
Ratio	**diffuse Vs focal**	**DPG Vs DG**	**HGG Vs LGG***
Cr/tCho	0.003	0.919	0.947
mIns/tCho	0.006	0.678	0.048
tNAA/tCho	0.372	0.096	0.263
Glx/tCho	0.081	0.001	0.483
LMM0.9/tCho	0.451	0.063	0.311
LMM1.3/tCho	0.779	0.028	0.228
LMM2.0tCho	0.515	0.138	0.398

**LGG group without ganglioglioma*

Table 17: P-Values from two-tailed t-tests between groups of brain stem tumours

Table 17 shows only two ratios that differ significantly between the diffuse and focal groups: Cr/tCho (P = 0.003) and mIns/tCho (P = 0.006). Performing an ANOVA (Table 18) between the 3 groups (LGG, HGG and DPG + DG) confirmed that Cr/tCho (P = 0.006) was a discriminating feature between all three groups.

		Averages						
Ratio	**P-value**	**HGG**	**HGTPG**	**ganglioglioma**	**LGG**	**DPG+DG**	**DPG**	**DG**
Cr/tCho	0.006	0.93	1.85	2.44	0.97	2.46	2.44	2.51
mIns/tCho	0.059	1.46	2.12	0.13	3.28	4.38	4.53	3.89
tNAA/tCho	0.210	0.48	0.68	1.75	1.83	1.71	1.90	1.05
Glx/tCho	0.170	4.73	4.87	6.78	3.66	3.13	2.63	4.87
LMM0.9/tCho	0.180	8.40	3.27	5.00	3.79	4.54	3.23	9.13
LMM1.3/tCho	0.450	21.81	7.07	15.27	5.85	12.37	5.61	36.01
LMM2.0tCho	0.720	10.50	5.69	9.86	6.91	7.45	5.16	15.50

Table 18: P-Values for an ANOVA between 3 groups (HGG+HGTPG, LGG+ganglioglioma and DPG+DG)

Although mIns/tCho was not significantly different between all three groups, it was still near significance (P = 0.059). A plot of mIns/tCho Vs Cr/tCho (Figure 30) shows the focal HGGs have very low values for both Cr/tCho (0.93±0.48) and mIns/Cho (1.46±0.45), with the exception of the tectal plate HGG which exhibited a higher value for Cr/tCho (1.85).

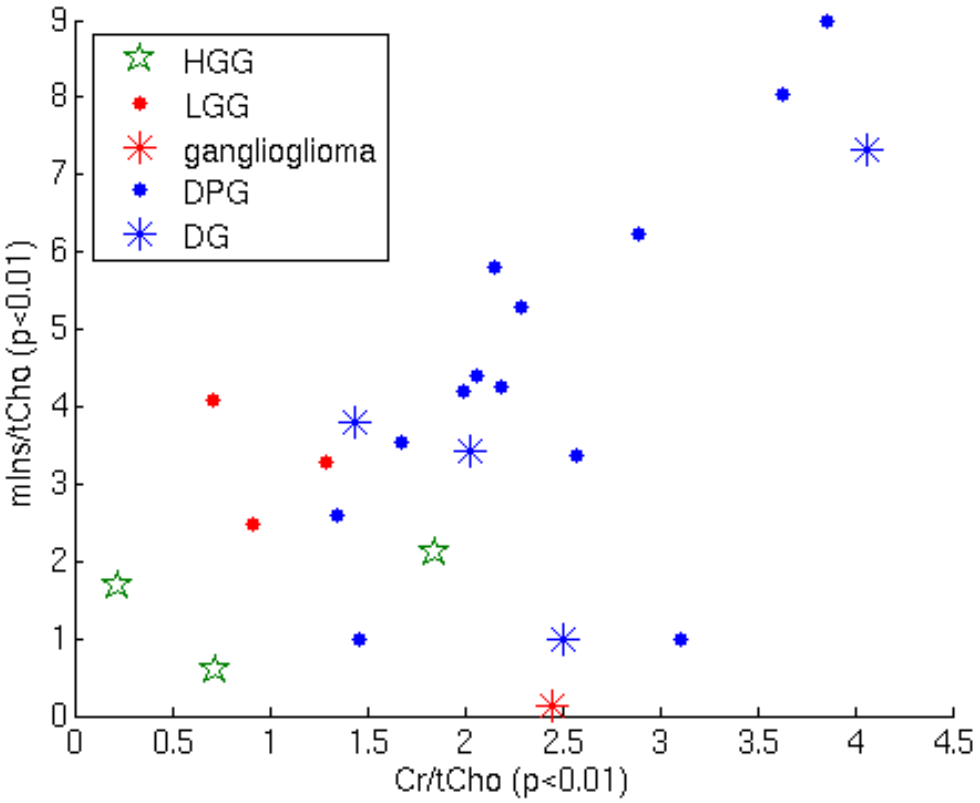

Figure 30: All types of brain stem tumours in the study, from all centres, plotted on axes mIns/tCho Vs Cr/tCho
Green stars – high grade glioma; red circles – low grade glioma; red star – ganglioglioma; blue circles – DPG; blue stars – DG

The focal LGGs showed higher values for mIns/tCho (3.28±0.46) and slightly higher values for Cr/Cho (0.97±0.17) compared with the focal HGGs. The ganglioglioma showed one of the lowest values for mIns/tCho (0.13), in addition to the highest value for Cr/tCho (2.44) of the focal tumours. This indicated that the ganglioglioma may be metabolically different from the other focal tumours. The diffuse tumours showed a large spread in both Cr/tCho and mIns/tCho, but showed consistently higher values for Cr/tCho (2.46±0.19) than the focal tumours. The average values for both Cr/tCho and mIns/tCho are both higher in DPGs (2.44±0.20 and 4.53±0.61 respectively) than DGs (2.51±0.56 and 3.89±1.31 respectively), although this is not significant due to the spread.

Results of two-tailed t-tests (Table 17) between the DPGs and DGs show that LMM1.3/tCho (P = 0.029) is significantly different between these 2 groups. LMM0.9/tCho is also near significance (P = 0.067) (Figure 31).

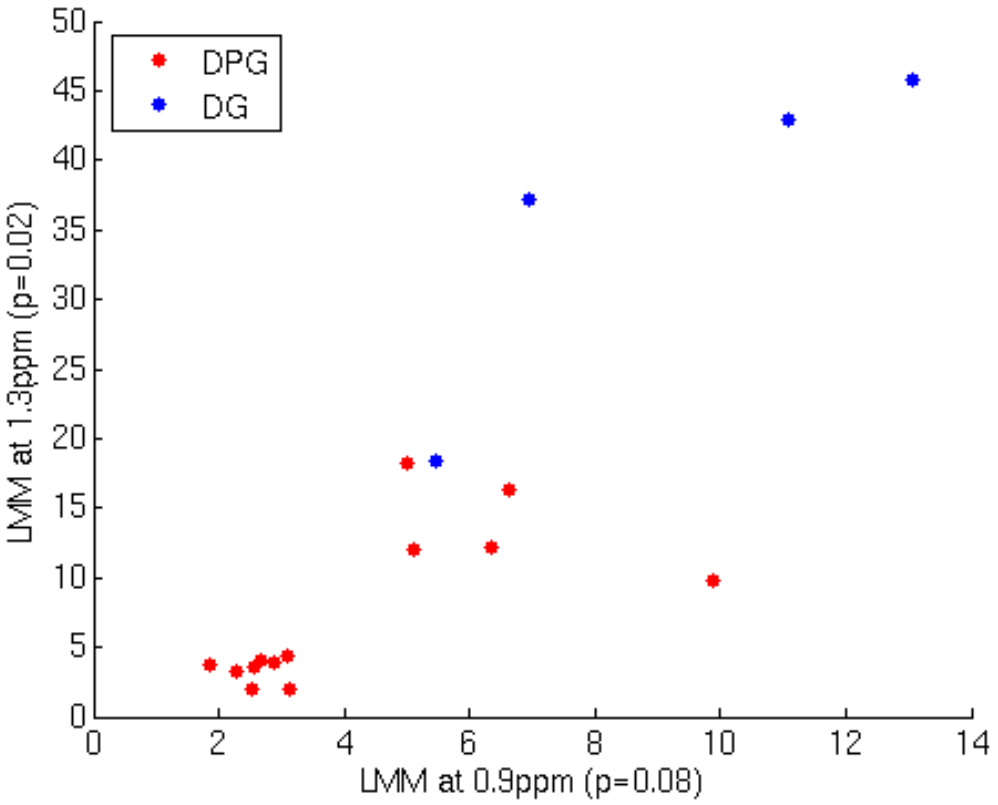

Figure 31: Plot of LMM region concentrations (relative to tCho) at 0.9ppm and 1.3ppm in both diffuse gliomas within and extending beyond the pons
Red circles – DPG; blue circles – DGs

Both of these have higher values in the DGs (36.01±7.76 and 9.13±2.06 respectively) compared with the DPGs (5.61±1.08 and 3.23±0.26 respectively), confirming the observations from the PCA. In addition to these, Glx/tCho (P = 0.0001) is higher in the DGs (4.87±0.33) than the DPGs (2.63±0.37). NAA/tCho is close to significance (P = 0.071), being lower in DGs (1.05±0.33) than DPGs (1.90±0.32).

The final set of two-tailed t-test results are shown in table 17, showing differences between the focal HGGs and LGGs. Only mIns/tCho showed significance (P = 0.048), being higher in LGGs (3.28±0.46) than HGGs (1.46±0.45). Figure 32 shows bar charts of the metabolite/tCho and LMM/tCho in the brain stem tumours.

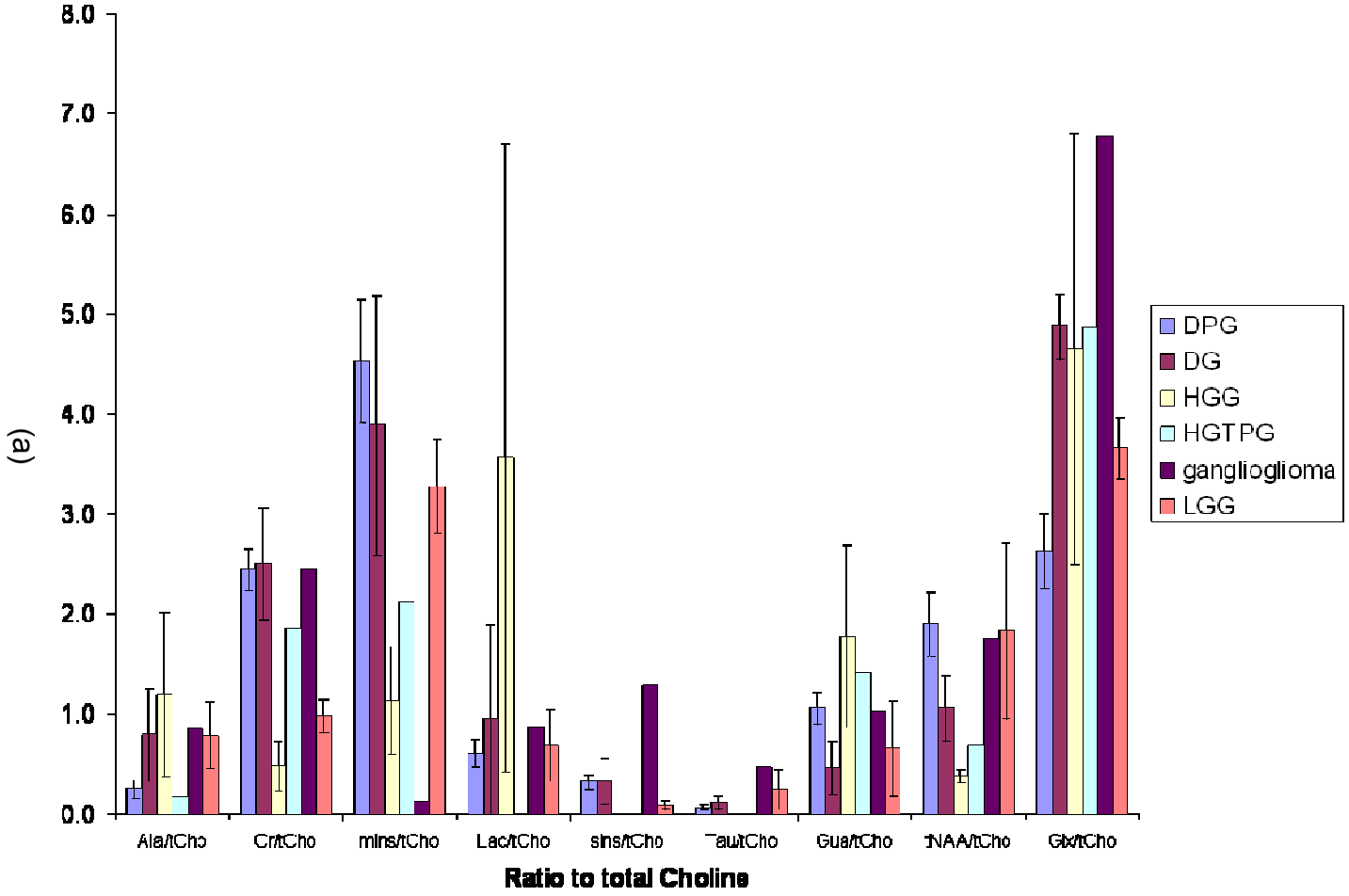
(a)
8.0
7.0
6.0
5.0
4.0
3.0
2.0
1.0
0.0
Ala/tCho
Cr/tCho
mIns/tCho
Lac/tCho
sIns/tCho
Tau/tCho
Gua/tCho
NAA/tCho
Glx/tCho
Ratio to total Choline
DPG
DG
HGG
HGTPG
ganglioglioma
LGG

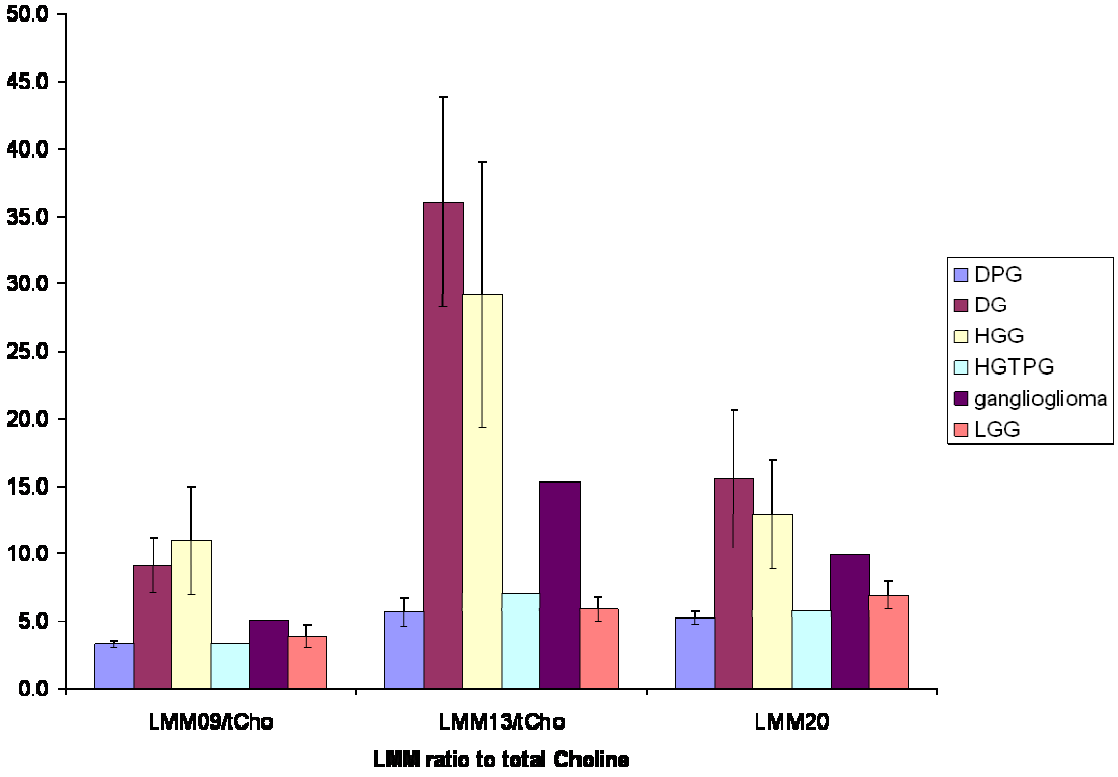

(b)

Figure 32: Bar charts showing (a) metabolite and (b) LMM concentrations (relative to total Cho) for all brain stem tumour types used in the study

For the sake of easy visualisation the high grade TPG is plotted as a separate entity from the other focal HGGs. The plot of LMM/tCho is clearly shows the tendency towards higher ratios in HGGs compared with LGGs.

Analysis was performed to assess whether the ratios mIns/tCho and Cr/tCho varied with sex, this was found to not be the case, this is in agreement with previous studies [184, 185].

In addition to this statistical analysis, visual inspection of the spectra, for unaccounted features, was performed. Looking at the average spectrum of the DPGs and DGs (Figure 28a), it is clear that there is a prominent peak

present at 2.6ppm, that is not assigned by LCModel™. This peak is not seen in any of the other brain stem tumours.

6.4 DISCUSSION

MRS can provide additional information, over and above that of conventional MRI, on the biology of brain stem tumours by providing information on in vivo metabolism.

The PCA results (Figure 29), showed that the main discriminant between HGG and other tumour types being LMM/tCho, especially those at 1.3ppm. This is in keeping with studies on adults and children with brain tumours where grade has been linked to lipid concentration [65, 72]. Despite the aggressive clinical behaviour of DPGs, at diagnosis they can readily be distinguished from HGGs of the brain stem, with the lowest LMM/tCho concentrations of all tumour types assessed (table 18). This finding is of interest as there remains debate as to the true pathological nature of DPGs, with biopsy studies demonstrating a spectrum of histological grades (II to IV) that do not correlate with prognosis [185, 188-190]. Two possible explanations are offered to account for these findings; firstly small size and sampling error of biopsies result in a down grading of heterogeneously high grade tumours or alternatively initial low grade lesions rapidly evolve into more malignant tumours. Autopsy studies tend to find a higher frequency of grade III and IV tumours and along with these MRS findings this may provide support for the idea of malignant transformation [191-193].

On the PCA, the 4 DG cases appeared more closely aligned with the focal HGG than the DPGs. There was a clear separation in the proportion of PC1 in these spectra, the loadings plot of which shows this PC to be dominated by LMM concentrations. In addition to this, these tumours showed consistently higher values for both LMM1.3/tCho and LMM0.9/tCho, and lower values for tNAA/tCho. This would all be in indicative of these being more aggressive tumours than the DPGs in this study. This is not yet substantiated by clinical findings however and needs to be further assessed with a larger study group and follow-up with clinical outcomes and MRS.

From the ANOVA results, mIns/tCho and Cr/tCho offers the best discrimination between all brain stem tumour types. This shows that the DPG+DGs can be classified as having high Cr/tCho and high mIns/tCho, HGGs as having low Cr/tCho and low mIns/tCho and LGGs clustering between these two groups. The exception to this is the high grade TPG, which is more closely aligned with the LGG group than the HGG group on Figure 30. The ganglioglioma spectrum sits separately from both LGGs and HGGs, with a low value for mIns/tCho and a high value for Cr/tCho.

TPGs are usually assumed to be low grade gliomas and are often unbiopsied. In this study there were two unbiopsied TPGs included. Of these cases, one was classified as being typical of a low grade lesion and was included as one of the LGG group. For the other, the radiological review classified it as having appearances of a more aggressive lesion and, due to this; it was included as being one of the HGG group. This tumour was treated with radiotherapy and

the patient is responding to treatment and remaining stable, indicating the tumour may have been of intermediate grade. The metabolite profile (Figure 32) shows that predominantly the ratio values for this tumour are in keeping more with it being a high grade tumour, in particular its low value for NAA/tCho. However, there are some features that would be more in keeping with it being a low grade tumour. It shows a high value for Cr/tCho and also all the LMM/tCho values are low and closer to those seen in the LGG group than those in the HGG group.

Diffuse gliomas (including both DPGs and DGs) exhibit distinct MRS. They all show prominent NAA peaks, a strong signal for mIns and a definite Cr peak. Most astrocytoma spectra, in children, show very little Cr and it would be expected that there would be little NAA present in such an aggressive tumour. It may be possible to explain the presence by the diffuse nature of these tumours. The fact that these tumours are of a diffuse nature means that there will be 'normal' tissue entrapped within them. We cannot separate these 2 tissue types using MRS and, as such, we will be obtaining some signal from this entrapped tissue. It is likely that the signal seen for NAA is coming from this entrapped tissue rather than the tumour tissue itself. The DPG spectra all show very low signals for LMM regions, which may also be partially due to entrapped 'normal' tissue. Finally, all the DPG spectra seen in this study show an unidentified peak at 2.6ppm, which has not been seen in any other astrocytoma spectra of any grade in this study. One study has presented a body of work supporting that this peak could be a resonance of citrate [102, 194].

The metabolite mIns has previously been identified as an important metabolite in the characterisation of paediatric brain tumours [72] and is of particular interest in astrocytomas. In a study of adults, it was found that the mIns levels peaked at grade 2 and were the lowest in grade 4 tumours [67]. This was explained by looking at the change between mIns and phosphatidylinositol. Myo-inositol contributes to the formation of a phosphorylated form of phosphatidylinositol. When this breaks down, diacylglycerol and inositol 1,4,5, triphospate are formed. The resulting diacylglycerol activates protein C kinase, which can activate proteolytic enzymes such as matrix metalloproteases [67]. Matrix metalloprotease-2 (MMP-2) has been shown to partially mediate local aggression in gliomas [195], where it was shown that LGGs had a low expression of MMP-2, as expected for low grade lesions. Both diffuse grade 2 gliomas and focal HGGs showed a high expression of MMP-2 in the tumour borders, but not in the central regions [195]. Since the focal lesions are smaller, the voxel will be more likely to contain some of the tumour border meaning that this characteristic will be more likely to be reflected in the spectroscopy. These would therefore be expected to show a lower concentration of mIns. The diffuse lesions are much larger and the voxel is placed centrally. Voxels in these lesions contain less of the border and would, therefore, be more likely to show a higher value for mIns. This all indicates that an up regulation in phosphatidylinositol can be indicative of a more aggressive tumour. A lower level of mIns would indicate that this may have occurred, and that the pool of mIns has decreased.

There has only been one comparable study looking at high and low grade lesions present in children in the brain stem [187], this was performed at an echo time of 135ms. They found that the Cho/Cr was largely increased in aggressive lesions compared with indolent lesions and control subjects. In addition it was seen that NAA/Cho was decreased in all tumours when compared with normal controls, and this value decreased further when the tumour was more malignant. Looking at Figure 32a it can be seen that this is true for this study in the focal lesions, but not for DPGs. The study does not document whether lesions are diffuse or focal, it simply states size. No comparison of mIns is available and no peak is documented at 2.6ppm.

Previous studies of tumour groups in other locations in the brain commonly document that the Cr/Cho ratio decreases with grade [29, 72, 73, 93, 96, 106]. Previous studies in lesions located in other locations have also shown up mIns as being important in distinguishing between tumour type [71, 72, 129]. Myo-Inositol has been shown to be of particular interest in astrocytomas. It has been linked with aggression and has been used in grading, being highest in grade two tumours and lower in high grade tumours [29, 67, 96, 196]. This is in agreement with the differences seen here between the DPG and HGG groups. The LGG group here was comprised of pilocytic astrocytomas, which are very rare in adults. These do not fit with the trend of lower mIns meaning a higher grade astrocytoma, but mIns has been found to be low in pilocytic astrocytomas in other locations [119]. Interestingly, similar MRS features to those seen in DPGs have previously been noted in gliomatosis [90, 94, 112],

another type of diffuse glioma. This, like DPG, is aggressive despite its appearance of being low grade.

6.5 CONCLUSIONS

Making any firm conclusions on whether it is possible to separate the LGG and the HGG group using MRS alone is not possible due to the small sample sizes of the focal lesion spectra, although this does appear to be hopeful using mIns/Cho. However, it has been shown in this study that diffuse and focal tumours of the brain stem can be well separated. In addition to this, it has been shown that the spectra of diffuse tumours of the brain stem confined to the pons take on a different spectroscopic appearance to those extending beyond the pons. These tumours are not currently recognised as being different biological entities.

CHAPTER 7: PILOCYTIC ASTROCYTOMAS: SPECTRAL VARIATION WITH LOCATION AND PROGRESSION

7.1 INTRODUCTION

Astrocytomas account for 40-55 % of paediatric brain tumours and the majority of these are PAs [38]. PAs occur in various locations of the brain and spine, but are particularly common in both the cerebellum and the optic pathway [41]. The tumours are classified as WHO Grade I and have a low mitotic rate [39-41]. Despite their slow growth, these tumours can present a significant management challenge, particularly when located in areas not readily amenable to surgery. Furthermore, some tumours invade adjacent tissues and occasionally tumours present with multifocal or metastatic disease, behaviour which implies that they are not always as benign as their WHO grading suggests.

The 5-year survival rate for patients with PAs is as high as 95% if a total resection is achieved and 85% if not [197, 198]. Generally a total excision is achieved in PAs in the cerebellum; hence these tumours are usually cured by surgery alone. Tumours arising supratentorially are commonly sited in the optic pathways, hypothalamus or thalamus. These areas are less amenable to surgery, and are usually not fully excised. These tumours have a more diverse clinical course, are more likely to progress after surgery and are commonly treated with adjuvant chemotherapy and/or radiotherapy [10]. It is uncertain whether the difference in prognosis of cerebellar and supratentorial

tumours is due to surgical limitations or whether the tumours are inherently different [10]. For supratentorial tumours, complete response to adjuvant treatment is rare and many patients have a remitting and relapsing course over a period of many years, undergoing several courses of adjuvant treatment [10]. The decision as to whether there is disease progression, that requires further treatment, currently relies upon the combination of clinical findings, changes in visual function, and conventional MR imaging. Clinical findings are often unreliable in younger children; this is particularly an issue for testing that requires a high degree of compliance and concentration, for example testing visual fields or acuity.

New, non-invasive imaging methods for assessing these patients would be particularly beneficial. Given the current difficulties in assessing PAs, non-invasive methods that give reliable repeated measurements throughout the often long course of this condition are needed. Therefore, MRS has the potential to make a particular impact clinically in the management of these tumours.

Previous MRS studies of childhood brain tumours have shown that PAs tend to have low levels of creatine and high levels of NAA when compared with other childhood brain tumours [71, 73]. Furthermore, these features can be used to distinguish cerebellar PAs from other cerebellar tumours [73, 74]. No difference has previously been reported between PAs in the cerebellum and supratentorial tumours.

This study investigates the ability of MRS to characterize PAs in children. The variation in MRS with location is investigated and, for supratentorial PAs, pre-treatment MRS prognostic markers are identified and the changes of metabolite concentrations with treatment developed.

7.2 METHODS

Raw data was processed using LCModel™ and Cramer-Rao bounds were used to remove metabolites that were poorly determined. Quality control was applied using the following measures:

1. SNR had to be greater than 4
2. FWHM had to be less than 0.150ppm

The variability of the pre-treatment MRS metabolite profiles across all cases was determined using a PCA. This was performed using metabolites of appropriate Cramer-Rao lower bounds, normalised to vector length.

Data was initially grouped by location, and two-tailed t-tests of significance were performed between spectra from supratentorial PAs and those in the cerebellum to assess for differences in the spectra.

The patients with supratentorial lesions were grouped into ‘progressors’ and ‘stable disease’. Progressors were defined as those in whom a clinical decision, based on a number of clinical factors and appearances on conventional MRI, had been made to give further treatment due to disease progression. Those with stable disease were taken to be all other patients

provided they had been followed up for more than 6 months at the end of the study. For these two groups, mean metabolite concentrations were calculated and two-tailed t-tests performed on pre-treatment MRS to determine factors associated with progression. In addition to this, patients with follow-up MRS studies, either on-treatment or during observation, were assessed to determine the presence of early metabolite changes with progression, by using paired t-tests.

7.3 RESULTS

MRI and short-echo-time MRS were performed on 27 children with PAs between 01/09/2003 and 01/04/2007, prior to any adjuvant treatment. Twelve patients had cerebellar and 15 supratentorial tumours. Six cases were excluded on quality control grounds: 2 tumours were too small to encompass a 1.5cm sided voxel, 3 had poor SNR and 1 had an inadequate FWHM. All subsequent analysis refers to the reduced cohort of 9 cerebellar and 12 supratentorial cases. A summary of the distribution of PAs, with respect to location in the brain, is shown in Figure 33.

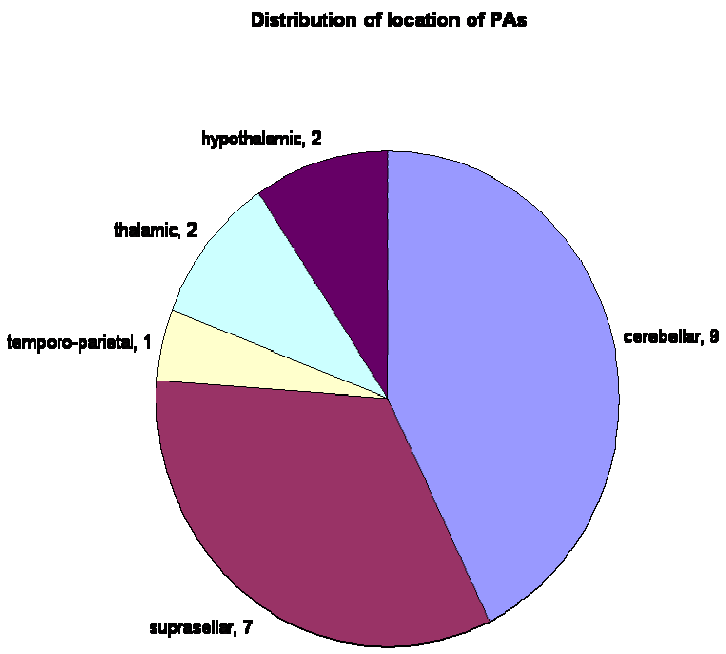

Figure 33: Summary of PA tumour location

All tumours had histopathological diagnoses established except for 4 optic pathway gliomas which were not biopsied, two of which were in children with Neurofibromatosis Type 1 (NF1). Three of the supratentorial cases had NF1. The mean age of the children with cerebellar tumours was 7.9 years and with supratentorial tumours was 4.9 years. Control MRS was recorded from brain distant to the tumour in children with brain tumours who had received no treatment other than surgery.

None of the patients with a cerebellar tumour had a post operative residual lesion of a size amenable to MRS. In the group of patients with supratentorial tumours, 7 of the 8 patients who underwent surgery had significant residual disease. The patient with a cerebral hemisphere tumour had a complete resection. Of the 11 patients with significant residual disease or having had no surgery, 7 proceeded to treatment with chemotherapy and 4 were initially

observed with no adjuvant treatment. No patients had radiotherapy. Five of the patients had progressive disease before the end of the study follow-up period (01/09/2007) leaving 6 patients classified as having stable disease. Two of the patients did not have a follow-up MRS within the study period, leaving 4 “progressors” and 5 with “stable disease” in the study of treatment monitoring.

7.3.1 DIFFERENCES IN MRS METABOLITE PROFILES BETWEEN CEREBELLAR AND SUPRATENTORIAL TUMOURS

Mean MRS for cerebellar and supratentorial tumours are given in Figure 34.

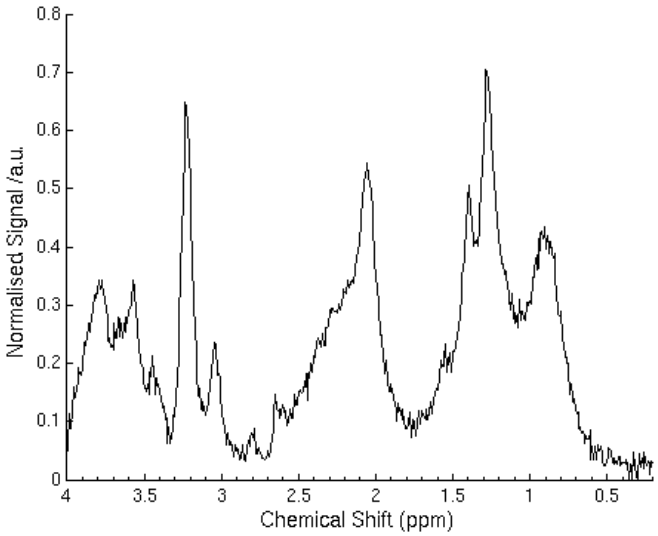

(a)

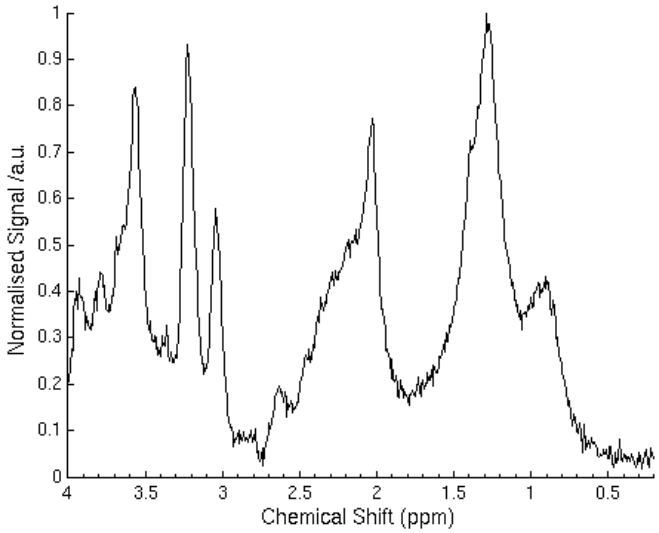

(b)

Figure 34: Mean spectra for PA of the (a) cerebellum and (b) supratentorial locations

The mean supratentorial spectrum shows a more prominent mIns peak at 3.65ppm. The broad component between 2.0ppm and 2.5ppm, attributed to a combination of Glx and LMM, is more also pronounced in the supratentorial compared with the cerebellar spectrum. LCModel™ was used generate metabolite concentrations, relative to water, average values of these are shown in table 19.

		Cerebellar		Supratentorial	
Metabolite	**P-Value**	**Average**	**StdErr**	**Average**	**StdErr**
Ala	0.731	0.95	0.16	0.87	0.15
Cr	0.060	0.50	0.06	1.28	0.37
mIns	0.003	1.26	0.23	3.64	0.63
Lac	0.741	2.13	0.17	1.96	0.46
sIns	0.096	0.04	0.03	0.11	0.03
Tau	0.112	0.07	0.05	0.22	0.08
Gua	0.154	1.48	0.19	1.11	0.16
tCho	0.377	0.99	0.09	1.16	0.17
tNAA	0.164	0.82	0.14	1.22	0.24
Glx	0.017	3.57	0.27	5.95	0.83
LMM0.9	0.446	8.57	1.74	7.03	0.88
LMM1.3	0.675	18.15	3.60	22.78	10.22
LMM2.0	0.181	7.92	1.11	10.11	1.12

Table 19: P-values and averages for comparison between cerebellar and supratentorial PAs

The supratentorial tumours had significantly greater concentrations of both mIns ($p = 0.003$) and Glx ($p= 0.017$) than cerebellar tumours, in agreement with visual differences. No other metabolites were significantly different between the two groups, although the cerebellar tumours tended to have lower creatine ($p=0.06$). The doublet corresponding to lactate appears, visually, different betweent the two locations, but this has a very high P-value. This is due to the large variation seen in lactate between PAs in both locations.

No significant differences were found in the metabolite profiles of supratentorial tumours between patients with and without NF1. A PCA was performed to assess the variability of the metabolite profiles (Figure 35) and shows that cerebellar and supratentorial tumours tend to form separate groups with only one outlier.

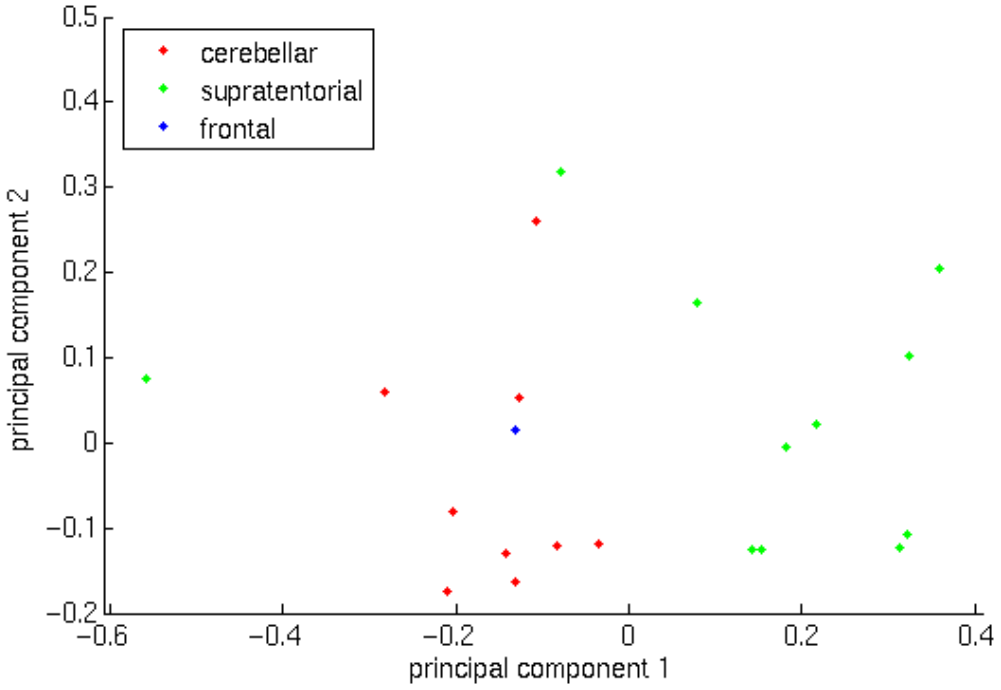

(a)

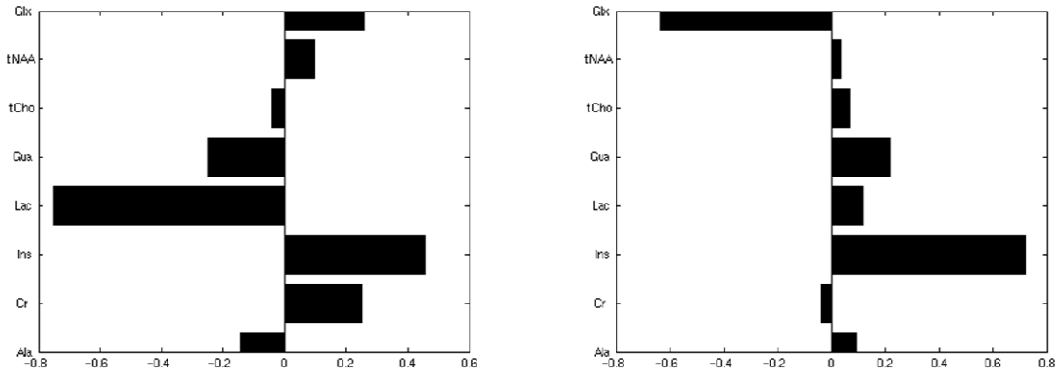

(b) (c)

Figure 35: PCA (a) for PAs by location, cerebellar – red; supratentorial – green; and frontal – blue. Loadings plots are shown in 36b for PC1 and 36c for PC2

Control spectra were used to assess the concentrations of both mIns and in different locations of the brain. The control spectra consisted of a set of spectra taken contralaterally to tumour site, for a group of patients who had only received surgical intervention. This cohort consisted of 11 MRS taken from a variety of regions both infratentorially (7 cases) and supratentorially (4 cases). Glx was significantly higher in the supratentorial regions ($p = 0.02$), but there was no significant difference in mIns levels ($p = 0.60$).

7.3.2 PRE-TREATMENT MRS AS A PROGNOSTIC INDICATOR IN SUPRATENTORIAL TUMOURS

In the cohort of 11 supratentorial tumours with follow up MRS, 5 progressed (mean time to progression 11 months) and 6 had stable disease throughout the study period (mean follow-up time 30 months). The patients who progressed had a significantly lower p-value for mIns ($p=0.04$) on their pre-treatment MRS (table 20).

		Response/Stable		Progression	
Metabolite	**P-Value**	**Average**	**StdErr**	**Average**	**StdErr**
Ala	0.336	1.00	0.25	0.69	0.17
Cr	0.160	2.33	0.74	0.86	0.61
mIns	0.036	5.09	0.86	2.53	0.56
Lac	0.756	1.80	0.56	2.16	0.98
sIns	0.115	0.17	0.06	0.06	0.03
Tau	0.059	0.30	0.12	0.02	0.02
Gua	0.908	1.30	0.28	1.34	0.28
tCho	0.235	1.46	0.20	0.99	0.30
tNAA	0.071	2.09	0.58	0.74	0.23
Glx	0.085	7.46	1.14	4.60	0.94
LMM0.9	0.267	5.29	0.79	7.37	1.51
LMM1.3	0.178	8.53	1.87	17.31	5.29
LMM2.0	0.945	8.91	0.80	8.99	0.77

Table 20: P-Value and averages for determination of progression of supratentorial PAs from pre-treatment MRS

They also tended to have lower Glx (p=0.08) and tNAA (p=0.07).

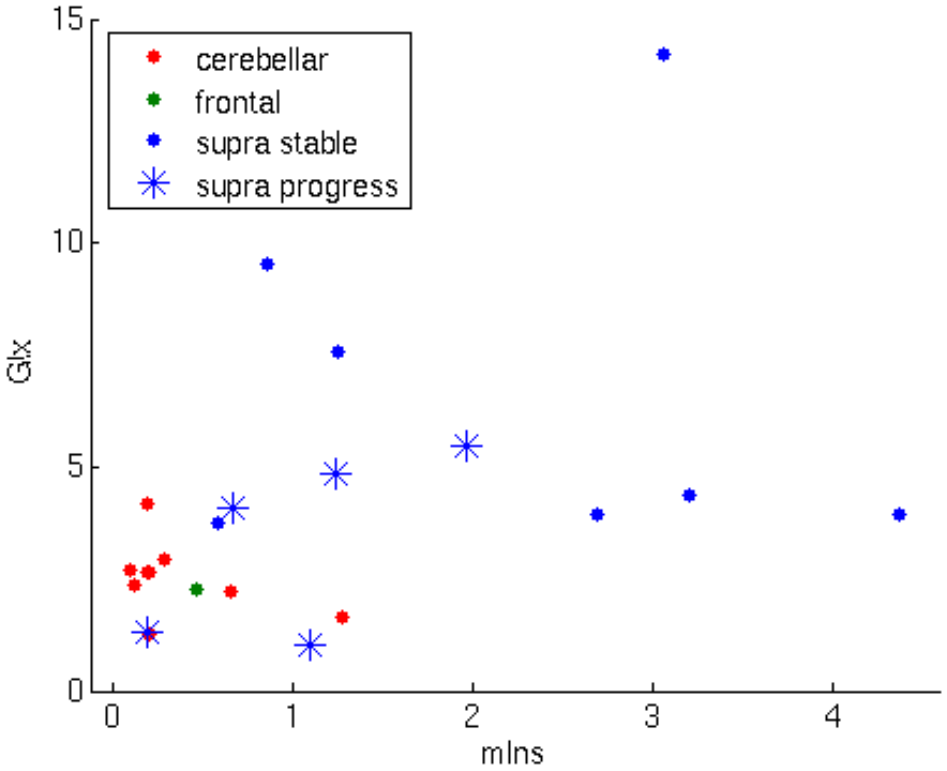

Figure 36: Scatter plot showing both variation in mIns and Glx by location and also by progression in supratentorial PAs.
cerebellar – red circles; temporo-parietal – green circles; stable supratentorial – blue circles; and progressive supratentorial – blue stars.

From the scatter plot of pre-treatment Glx versus mIns Figure 36, it is shown that supratentorial tumours cluster into 2 groups, those with low values of Glx and mIns tend to progress and those with higher values of these metabolites tend to have stable disease. One patient with stable disease had low mIns and Glx. This patient had an optic chiasm tumour treated with surgery followed by chemotherapy (vincristine and carboplatin) for 18 months and was 3 months off treatment at the end of the study period. One patient, with a completely resected temporo-parietal tumour had been followed up for less than 6 months at the end of the study.

7.3.3 SUPRATENTORIAL TUMOURS: TREATMENT MONITORING AND EARLY PREDICTORS OF PROGRESSION

Nine of the 11 patients with supratentorial tumours followed up for at least 6 months had follow-up scans with MRS of acceptable quality. Four of these patients progressed and five had stable disease. Paired t-tests were performed on the metabolite values between the pre-treatment and first on-treatment MRS for each patient to assess any significant changes between the two MRS. No significant changes were found in the metabolite profiles between the two MRS in the patients with stable disease. However, in patients who later progressed, there was a significant decrease in mIns, ($p = 0.03$). The median time between the initial and subsequent MRS was 2.1 months in the progressor group, with a median time to progression of 12.2 months.

7.4 DISCUSSION

Key differences in MR spectra have been identified between PAs arising in supratentorial and cerebellar regions. Moreover, low levels of mIns are significantly associated with adverse clinical behaviour in supratentorial tumours.

Two metabolites, mIns and Glx, are significantly higher in the supratentorial compared to cerebellar tumours. In controls, no significant difference was found in mIns levels in non-involved brain between these two regions, and one previous study actually found mIns to be higher in normal cerebellum than other brain locations [161]. Higher mIns levels in the supratentorial tumours are therefore likely to arise from tumour derived tissue. In controls, Glx levels were higher in supratentorial non-involved brain, than the cerebellum. However, since the tumours studied by MRS were not diffusely infiltrative, it is unlikely that the differences in Glx levels arise from normal tissue entrapped within the tumour. A PCA performed using MRS metabolite profiles showed that the cerebellar and supratentorial tumours form two distinct groups with only one outlier who subsequently progressed. This finding implies that supratentorial tumours are biologically distinct from their cerebellar counterparts. Clear parallels exist here with another glial series tumour, ependymoma, which show key differences in chromosomal abnormalities and gene expression patterns depending on the location [199]. Qualitative review of conventional MR images revealed no difference in major imaging characteristics between the tumours in the different locations including their cystic nature.

All but one of the supratentorial tumours were located in deep structures and, as expected, these patients presented significant management problems. The use of complex treatment strategies involving various combinations of surgery, chemotherapy and active observation was undertaken in this group of patients emphasizing the importance of developing non-invasive prognostic markers to aid clinical decision making. In turn, information from MR spectra could be used in the context of multi-disciplinary review regarding the optimal management of these tumours. In this study significantly lower levels of mIns, and a tendency to lower Glx and tNAA, were found in the group of tumours that progressed. The higher values of mIns in those with stable disease are in keeping with studies on adults with astrocytomas where higher mIns is seen in the lower grade, better prognosis tumours [67, 96]. High levels of NAA have been associated with a good prognosis in a number of studies of brain tumours [107]. The cerebellar tumours had mIns, Glx and NAA values more akin to the supratentorial 'progressors' rather than those with stable disease. Most of the cerebellar cases underwent complete surgical resection leaving minimal residual disease post surgery. None of these tumours recurred, consistent with reports on the outcomes of cerebellar PAs from other studies. This finding implies that extent of surgical resection is a key determinant of prognosis, as supported in the literature [41, 200]. Levels of mIns were also found to decrease significantly between the first and subsequent MRS in the group of supratentorial tumours that progressed. Since the median time between the two scans was only 2 months compared with a time to progression of 12 months, these patients could potentially have had earlier intervention for their disease progression.

Previous studies of MRS in brain tumours have identified tCho as a useful biomarker of tumour aggressiveness across a range of tumour types [74], but this was not shown in the current study of PAs. A potential explanation may be found in the relative proportions of the choline containing metabolites, which give rise to the tCho value. Studies of low grade astrocytomas, in vivo [86, 98] and in tissue [98], have indicated that glycerophosphocholine is the dominant choline containing metabolite in PAs [98], whereas phosphocholine has been demonstrated to be the main biomarker of tumour aggressiveness [201]. Lipid levels have also been demonstrated to be makers of tumour malignancy [74], being a measure of necrosis and apoptosis. However, PAs have lipid levels comparable to those found in higher grade tumours [98]. The origin of MRS detectable lipid in PAs is uncertain and requires further investigation.

Whilst mIns has previously been identified as an important metabolite in the characterisation of brain tumours in both children [71, 72] and adults [67], there has been relatively little work to explain this finding. In the study of Castillo et al [67], variations in mIns levels were explained in terms of the protein kinase C pathway. Myo-Inositol contributes to the formation of a phosphorylated form of phosphatidylinositol which is broken down to form diacylglycerol and inositol 1,4,5, triphospate. The resulting diacylglycerol activates protein kinase C and a cascade of proteolytic enzymes including matrix metalloproteases [67, 202]. Matrix metalloprotease-2 has been shown to mediate local aggression in cerebral gliomas and treatment of a glioma cell line with a metalloprotease inhibitor resulted in a 90% reduction in invasion

[202]. Further work is warranted to establish whether these pathways are upregulated in PAs with low levels of mIns and explore their potential as targets for novel agents.

A previous study has shown differences in genetic profiles of PAs between various locations in the brain [203], Glx was found to be higher in supratentorial regions when compared with cerebellar concentrations . However, tumours from all key brain regions were not included in the study and in particular, of the 10 supratentorial tumours; none were labelled as being in the suprasellar region. This illustrates the difficulty of investigating PAs using tissue since many tumours are not biopsied or have limited tissue taken. Tissue markers of prognosis have also been investigated and a retrospective study found the MIB-1 index to be a predictor of initial tumour progression in PAs [204]. Tissue is rarely available at relapse, limiting the use of tissue based methods in managing the often long clinical course of these patients. Non-invasive methods have the potential to provide both information on the biology of the tumour and be used at multiple time points.

Whilst MRS is a powerful non-invasive method for the characterization of brain tumours, currently there are important limitations on the size of tumour amenable to the technique. In this study, it was necessary to exclude tumours which could not encompass a 1.5cm sided cube. Only two tumours did not meet this criterion at diagnosis, but three other highly cystic tumours had only a small solid component and did not meet the MRS quality control criterion for signal to noise ratio since the signal comes almost entirely from the solid

component. All of these tumours had a favourable outcome. With longer scan times or improved technology such as higher magnetic field strength, smaller tumours could be studied.

7.5 CONCLUSIONS

Key differences have been identified in the MRS metabolite profiles between cerebellar and supratentorial PAs with cerebellar tumours having significantly lower mIns and Glx. Low values of mIns on the initial MRS and decreasing mIns on the subsequent MRS were found to be associated with later disease progression in supratentorial tumours. MRS is a potentially useful additional investigation in assessment of PAs and gives further insight into the diversity of these important childhood tumours.

CHAPTER 8: CONCLUSIONS

Short echo time MRS has been shown to be effective in the characterisation of childhood brain tumours. Metabolites that would be difficult to quantitate in a long echo time spectrum have been proven to be of high importance in the analysis of these tumours. These include mIns in all studies (chapters 4-7), LMM in the analysis of GCTs (chapter 5), Glx in brain stem tumours and PAs (chapters 6 and 7) and tau in medulloblastomas (chapter 4.3). With modern spectral fitting tools such as LCModel™ it is easier to interpret the larger amount of data seen in a short echo time spectrum. If possible, it is still advisable to obtain MRS at both long and short echo time for verification purposes.

This work was started using a well studied and understood data set of cerebellar tumours, all of which have biopsies and thus a histopathological diagnosis. This was done to confirm the best method of analysing these tumours. This was also used as confirmation that short echo time MRS was useful for characterising childhood brain tumours and that metabolites only seen at short echo times, such as mIns, were important in this characterisation. The conclusions from this work were that the method of analysis has to be tailored to the user and the question being posed. For a simple, fast classifier for use by clinicians a simple peak height ratio method with well defined cut-off values is more appropriate to something involving advanced processing and statistical analysis (chapter 4.2). These schemes are also robust to new data of various types as was proven by a prospective

study (chapter 4.2.2). The prospective analysis also highlighted the need for larger data sets to determine and refine cut-off values for classification schemes.

A more sophisticated analysis, using LCModel™ determined concentrations, also remained robust to new data (chapter 4.3.2). The classification rates of both a small single centre data set and a larger multicentre data set were comparable with those seen in the simple scheme using peak heights. However, the larger amount of metabolite information was beneficial in the better understanding of the biology of rarer tumours (chapters 5-7).

Cerebellar tumours have been previously well studied and papers have been published on both the biology and MRS results. This test-bed data set was used to determine the best analysis technique for use in later studies. Although schemes using both peak heights and LCModel™ metabolites concentrations showed comparable accuracy, using both retrospective and prospective data, it was decided that LCModel™ metabolite concentrations offered the best means of characterising these tumours. LCModel™ offered information about more metabolites in a spectrum than is possible to measure using peak height ratios. More metabolite information leads a more complete metabolite profile of the tumour and this is useful in characterising tumours. This is especially useful in the rarer tumour types in areas that are more difficult to access surgically.

Cerebellar tumours are a well studied group, and made for a solid test-bed. However, techniques such as MRS are of greater use in tumours that are less readily amenable to surgical biopsy. Studies were performed on two such groups of tumours: pineal region tumours (chapter 5) and brain stem tumours (chapter 6). In both of these groups it is vital to obtain as much information non-invasively about the nature of the tumour as is possible. The studies on data sets of both pineal region tumours (chapter 5) and brain stem tumours (chapter 6) showed that short echo time MRS could be successfully used to characterise these difficult tumour groups, and with more data could become and important aid to diagnosis. The scheme developed for the diagnosis of brain stem tumours (chapter 6) included information from smaller metabolites, such as mIns. The scheme developed for the differentiation between tumours of the pineal region (chapter 5) included information from Lipid and Macromolecular resonances. Both of these schemes included data not easily interpretable from long echo time MRS, thus highlighting the benefit of performing short echo time MRS for the characterisation of these tumour types.

A further use for short echo time MRS was shown in chapter 7, in the determination of differences between tumours within a disease class that are not visible on conventional histopathology. PAs act differently depending on the location within the brain, yet the histopathology of these tumours does not vary significantly between regions. However, differences were seen using short echo time MRS between PAs arising in the cerebellum and those occurring supratentorially. Supratentorial PAs have a poorer prognosis that

those in the cerebellum. A preliminary study using a small group of supratentorial PAs showed the potential of short echo time MRS was used to predict the prognosis for these tumours. MRS was also used to monitor response to treatment with high success in this small group.

The most important problem found in the studies presented here is the small number of patients within individual study groups. To reduce this, there is a huge need for large multicentre studies, which may introduce the need for an agreed protocol for data collection between centres.

Data quality is a considerable issue with any brain MRS. Location has a large impact on the quality of data, as some areas are more difficult to shim over. This is particularly problematic for lesions close to an air-tissue or bone-tissue interface. Tumours near the skull have addition problems from contamination of signals from outside the voxel from scalp lipid. This problem can be partially overcome by using saturation bands surrounding the voxel. All spectra need to be visually inspected to ensure there are no external contaminates.

Signals from metabolites can be lost in the noise of a spectrum. This problem can either be rectified by obtaining more acquisitions or moving to higher field strength. The former leads to problems of increasing acquisition times, which can often be intolerable. More and more institutions are moving to higher field strength, and while the increases are not those predicted by theory, there are significant improvements seen in spectral quality.

An additional limitation is the lack of availability of sophisticated processing tools and pattern recognition software in the clinical setting. This limits the usability of schemes such as those presented, to those using peak height measurement and ratio comparisons.

In conclusion, short echo time MRS has been shown to be a powerful tool for the characterisation of brain tumours in children. Simple methods, which could be readily applied in a clinical setting have been developed, and in some cases tested, in the areas of diagnosis, prognosis and treatment monitoring. Further multicentre studies are required to improve and evaluate the techniques in clinical use.

REFERENCES

1. Statistics, T.O.f.N. *Mortality Statistics: Cause*. 2008 16/01/2007 [cited 2008 01/06/2008]; Available from: http://www.statistics.gov.uk/statbase/Product.asp?vlnk=618.
2. Childhood Cancer Research Group, U.o.O. *The National Registry of Childhood Tumours*. 2007 [cited 2008 01/07/2008]; Available from: http://www.ccrg.ox.ac.uk/datasets/nrct.htm.
3. Gamble, J.D.B.a.M., *Theory and Practice of Histological Techniques* 6th ed. 2007: Churchill Livingstone. 744.
4. Shibuya, M., et al., *Proliferative potential of brain tumors. Analyses with Ki-67 and anti-DNA polymerase alpha monoclonal antibodies, bromodeoxyuridine labeling, and nuclear organizer region counts.* Cancer, 1993. **71**(1): p. 199-206.
5. Hall, W.A., *The safety and efficacy of stereotactic biopsy for intracranial lesions.* Cancer, 1998. **82**(9): p. 1749-55.
6. Brell, M., et al., *Factors influencing surgical complications of intra-axial brain tumours.* Acta Neurochir (Wien), 2000. **142**(7): p. 739-50.
7. Peretta, P., et al., *Complications and pitfalls of neuroendoscopic surgery in children.* J Neurosurg, 2006. **105**(3 Suppl): p. 187-93.
8. Kersh, C.R., et al., *Primary central nervous system germ cell tumors. Effect of histologic confirmation on radiotherapy.* Cancer, 1988. **61**(11): p. 2148-52.
9. Packer, R.J., B.H. Cohen, and K. Cooney, *Intracranial germ cell tumors.* Oncologist, 2000. **5**(4): p. 312-20.
10. Forsyth, P.A., et al., *Supratentorial pilocytic astrocytomas. A clinicopathologic, prognostic, and flow cytometric study of 51 patients.* Cancer, 1993. **72**(4): p. 1335-42.
11. Walker, D.A., J.A. Punt, and M. Sokal, *Clinical management of brain stem glioma.* Arch Dis Child, 1999. **80**(6): p. 558-64.
12. Brant-Zawadzki, M., et al., *Magnetic resonance of the brain: the optimal screening technique.* Radiology, 1984. **152**(1): p. 71-77.
13. Kent, D.L., et al., *The Clinical Efficacy of Magnetic Resonance Imaging in Neuroimaging.* Ann Intern Med, 1994. **120**(10): p. 856-871.
14. Wilms, G., P. Demaerel, and S. Sunaert, *Intra-axial brain tumours.* Eur Radiol, 2005. **15**(3): p. 468-84.
15. Chang, S.C., et al., *Diffusion-weighted MRI features of brain abscess and cystic or necrotic brain tumors: comparison with conventional MRI.* Clin Imaging, 2002. **26**(4): p. 227-36.
16. Ebisu, T., et al., *Discrimination of brain abscess from necrotic or cystic tumors by diffusion-weighted echo planar imaging.* Magn Reson Imaging, 1996. **14**(9): p. 1113-6.
17. Kim, Y.J., et al., *Brain abscess and necrotic or cystic brain tumor: discrimination with signal intensity on diffusion-weighted MR imaging.* AJR Am J Roentgenol, 1998. **171**(6): p. 1487-90.
18. Gauvain, K.M., et al., *Evaluating pediatric brain tumor cellularity with diffusion-tensor imaging.* AJR Am J Roentgenol, 2001. **177**(2): p. 449-54.

19. Greenberg, G., et al., *Use of diffusion tensor imaging to examine subacute white matter injury progression in moderate to severe traumatic brain injury.* Arch Phys Med Rehabil, 2008. **89**(12 Suppl): p. S45-50.
20. Kashimura, H., et al., *Diffusion tensor imaging for differentiation of recurrent brain tumor and radiation necrosis after radiotherapy--three case reports.* Clin Neurol Neurosurg, 2007. **109**(1): p. 106-10.
21. Levin, H.S., et al., *Diffusion tensor imaging in relation to cognitive and functional outcome of traumatic brain injury in children.* J Head Trauma Rehabil, 2008. **23**(4): p. 197-208.
22. Nimsky, C., et al., *Intraoperative diffusion-tensor MR imaging: shifting of white matter tracts during neurosurgical procedures--initial experience.* Radiology, 2005. **234**(1): p. 218-25.
23. Rutgers, D.R., et al., *Diffusion tensor imaging characteristics of the corpus callosum in mild, moderate, and severe traumatic brain injury.* AJNR Am J Neuroradiol, 2008. **29**(9): p. 1730-5.
24. Sundgren, P.C., et al., *Differentiation of recurrent brain tumor versus radiation injury using diffusion tensor imaging in patients with new contrast-enhancing lesions.* Magn Reson Imaging, 2006. **24**(9): p. 1131-42.
25. Ulmer, J.L., et al., *The role of diffusion tensor imaging in establishing the proximity of tumor borders to functional brain systems: implications for preoperative risk assessments and postoperative outcomes.* Technol Cancer Res Treat, 2004. **3**(6): p. 567-76.
26. Wieshmann, U.C., et al., *Diffusion tensor imaging demonstrates deviation of fibres in normal appearing white matter adjacent to a brain tumour.* J Neurol Neurosurg Psychiatry, 2000. **68**(4): p. 501-3.
27. Hollingworth, W., et al., *A systematic literature review of magnetic resonance spectroscopy for the characterization of brain tumors.* AJNR Am J Neuroradiol, 2006. **27**(7): p. 1404-11.
28. Devos, A., et al., *Classification of brain tumours using short echo time 1H MR spectra.* J Magn Reson, 2004. **170**(1): p. 164-75.
29. Howe, F.A. and K.S. Opstad, *1H MR spectroscopy of brain tumours and masses.* NMR Biomed, 2003. **16**(3): p. 123-31.
30. Maintz, D., et al., *Phosphorus-31 MR spectroscopy of normal adult human brain and brain tumours.* NMR Biomed, 2002. **15**(1): p. 18-27.
31. Kirov, I., et al., *Characterizing 'mild' in traumatic brain injury with proton MR spectroscopy in the thalamus: Initial findings.* Brain Inj, 2007. **21**(11): p. 1147-54.
32. Cohen, B.A., et al., *Proton MR spectroscopy and MRI-volumetry in mild traumatic brain injury.* AJNR Am J Neuroradiol, 2007. **28**(5): p. 907-13.
33. Marino, S., et al., *Acute metabolic brain changes following traumatic brain injury and their relevance to clinical severity and outcome.* J Neurol Neurosurg Psychiatry, 2007. **78**(5): p. 501-7.
34. Babikian, T., et al., *MR spectroscopy: predicting long-term neuropsychological outcome following pediatric TBI.* J Magn Reson Imaging, 2006. **24**(4): p. 801-11.
35. Bonavita, S., F. Di Salle, and G. Tedeschi, *Proton MRS in neurological disorders.* Eur J Radiol, 1999. **30**(2): p. 125-31.

36. Louis, D.N., et al., *The 2007 WHO classification of tumours of the central nervous system.* Acta Neuropathol, 2007. **114**(2): p. 97-109.
37. Butowski, N.A. and S.M. Chang, *Glial tumors: the current state of scientific knowledge.* Clin Neurosurg, 2006. **53**: p. 106-13.
38. Burkhard, T., et al., *Cardiac (31)P-MRS compared to echocardiographic findings in patients with hypertensive heart disease without overt systolic dysfunction-Preliminary results.* Eur J Radiol, 2008.
39. Khalid, H., et al., *Immunohistochemical analysis of progesterone receptor and Ki-67 labeling index in astrocytic tumors.* Cancer, 1997. **80**(11): p. 2133-40.
40. Matsumoto, T., et al., *MIB-1 and p53 immunocytochemistry for differentiating pilocytic astrocytomas and astrocytomas from anaplastic astrocytomas and glioblastomas in children and young adults.* Histopathology, 1998. **33**(5): p. 446-52.
41. Pizzo, P.A.a.P., D.G., *Principles and Practice of Pediatric Oncology*. 5th ed. 2005: Lippincott Williams and Wilkins.
42. Hargrave, D., U. Bartels, and E. Bouffet, *Diffuse brainstem glioma in children: critical review of clinical trials.* Lancet Oncol, 2006. **7**(3): p. 241-8.
43. Warren, K.E. *Ependymomas*. 2008 [cited 2008 01/09/2008].
44. Horn, B., et al., *A multi-institutional retrospective study of intracranial ependymoma in children: identification of risk factors.* J Pediatr Hematol Oncol, 1999. **21**(3): p. 203-11.
45. Reni, M., et al., *Ependymoma.* Crit Rev Oncol Hematol, 2007. **63**(1): p. 81-9.
46. Wolfsberger, S., et al., *Ki-67 immunolabeling index is an accurate predictor of outcome in patients with intracranial ependymoma.* Am J Surg Pathol, 2004. **28**(7): p. 914-20.
47. Paulino, A.C. and E. Melian, *Medulloblastoma and supratentorial primitive neuroectodermal tumors: an institutional experience.* Cancer, 1999. **86**(1): p. 142-8.
48. Russo, C., et al., *Comparative genomic hybridization in patients with supratentorial and infratentorial primitive neuroectodermal tumors.* Cancer, 1999. **86**(2): p. 331-9.
49. Ho, D.M. and H.C. Liu, *Primary intracranial germ cell tumor. Pathologic study of 51 patients.* Cancer, 1992. **70**(6): p. 1577-84.
50. Brodeur, G.M., et al., *Malignant germ cell tumors in 57 children and adolescents.* Cancer, 1981. **48**(8): p. 1890-8.
51. Baranzelli, M.C., et al., *Nonmetastatic intracranial germinoma: the experience of the French Society of Pediatric Oncology.* Cancer, 1997. **80**(9): p. 1792-7.
52. Ogawa, K., et al., *Treatment and prognosis of patients with intracranial nongerminomatous malignant germ cell tumors: a multiinstitutional retrospective analysis of 41 patients.* Cancer, 2003. **98**(2): p. 369-76.
53. Schild, S.E., et al., *Histologically confirmed pineal tumors and other germ cell tumors of the brain.* Cancer, 1996. **78**(12): p. 2564-71.
54. Hiroshima, K., et al., *Apoptosis and proliferative activity in mature and immature teratomas of the mediastinum.* Cancer, 2001. **92**(7): p. 1798-806.

55. American Medical Association, A. *Atlas of the Body: The Brain - Side View* 2009 [cited 2009 06/10/2009]; Available from: http://www.medem.com/.
56. Parwani, A.V., et al., *Atypical teratoid/rhabdoid tumor of the brain: cytopathologic characteristics and differential diagnosis.* Cancer, 2005. **105**(2): p. 65-70.
57. Czyzyk, E., et al., *Optic pathway gliomas in children with and without neurofibromatosis 1.* J Child Neurol, 2003. **18**(7): p. 471-8.
58. Binning, M.J., et al., *Optic pathway gliomas: a review.* Neurosurg Focus, 2007. **23**(5): p. E2.
59. Creange, A., et al., *Neurological complications of neurofibromatosis type 1 in adulthood.* Brain, 1999. **122 (Pt 3)**: p. 473-81.
60. Drouet, A., et al., *Neurofibromatosis 1-associated neuropathies: a reappraisal.* Brain, 2004. **127**(Pt 9): p. 1993-2009.
61. Guillamo, J.S., et al., *Prognostic factors of CNS tumours in Neurofibromatosis 1 (NF1): a retrospective study of 104 patients.* Brain, 2003. **126**(Pt 1): p. 152-60.
62. Janss, A.J., et al., *Optic pathway and hypothalamic/chiasmatic gliomas in children younger than age 5 years with a 6-year follow-up.* Cancer, 1995. **75**(4): p. 1051-9.
63. Listernick, R., et al., *Optic pathway gliomas in children with neurofibromatosis 1: consensus statement from the NF1 Optic Pathway Glioma Task Force.* Ann Neurol, 1997. **41**(2): p. 143-9.
64. McCullough, D.C. and F. Epstein, *Optic pathway tumors. A review with proposals for clinical staging.* Cancer, 1985. **56**(7 Suppl): p. 1789-91.
65. Preul, M.C., et al., *Accurate, noninvasive diagnosis of human brain tumors by using proton magnetic resonance spectroscopy.* Nat Med, 1996. **2**(3): p. 323-5.
66. Calvar, J.A., et al., *Characterization of brain tumors by MRS, DWI and Ki-67 labeling index.* J Neurooncol, 2005. **72**(3): p. 273-80.
67. Castillo, M., J.K. Smith, and L. Kwock, *Correlation of myo-inositol levels and grading of cerebral astrocytomas.* AJNR Am J Neuroradiol, 2000. **21**(9): p. 1645-9.
68. Kim, J.H., et al., *3T 1H-MR spectroscopy in grading of cerebral gliomas: comparison of short and intermediate echo time sequences.* AJNR Am J Neuroradiol, 2006. **27**(7): p. 1412-8.
69. Preul, M.C., et al., *Using proton magnetic resonance spectroscopic imaging to predict in vivo the response of recurrent malignant gliomas to tamoxifen chemotherapy.* Neurosurgery, 2000. **46**(2): p. 306-18.
70. Hall, W.A., et al., *Improving diagnostic yield in brain biopsy: coupling spectroscopic targeting with real-time needle placement.* J Magn Reson Imaging, 2001. **13**(1): p. 12-5.
71. Panigrahy, A., et al., *Quantitative short echo time 1H-MR spectroscopy of untreated pediatric brain tumors: preoperative diagnosis and characterization.* AJNR Am J Neuroradiol, 2006. **27**(3): p. 560-72.
72. Peet, A.C., et al., *Short echo time 1 H magnetic resonance spectroscopy of childhood brain tumours.* Childs Nerv Syst, 2007. **23**(2): p. 163-9.
73. Wang, Z., et al., *Proton MR spectroscopy of pediatric cerebellar tumors.* AJNR Am J Neuroradiol, 1995. **16**(9): p. 1821-33.

74. Astrakas, L.G., et al., *Noninvasive magnetic resonance spectroscopic imaging biomarkers to predict the clinical grade of pediatric brain tumors.* Clin Cancer Res, 2004. **10**(24): p. 8220-8.
75. Marcus, K.J., et al., *Predicting survival of children with CNS tumors using proton magnetic resonance spectroscopic imaging biomarkers.* Int J Oncol, 2007. **30**(3): p. 651-7.
76. Peet, A.C., et al., *The value of magnetic resonance spectroscopy in tumour imaging.* Arch Dis Child, 2008. **93**(9): p. 725-7.
77. Allen, E.D., et al., *The clinical and radiological evaluation of primary brain neoplasms in children, Part II: Radiological evaluation.* J Natl Med Assoc, 1993. **85**(7): p. 546-53.
78. Colosimo, C., et al., *[Magnetic resonance and computerized tomography of posterior cranial fossa tumors in childhood. Differential diagnosis and assessment of lesion extent].* Radiol Med (Torino), 1995. **90**(4): p. 386-95.
79. Deck, M.D., et al., *Computed tomography versus magnetic resonance imaging of the brain. A collaborative interinstitutional study.* Clin Imaging, 1989. **13**(1): p. 2-15.
80. D'Andrea, A.D., et al., *Pineocytomas of childhood. A reappraisal of natural history and response to therapy.* Cancer, 1987. **59**(7): p. 1353-7.
81. Kilgore, D.P., et al., *Pineal germinoma: MR imaging.* Radiology, 1986. **158**(2): p. 435-8.
82. Hargrave, D., N. Chuang, and E. Bouffet, *Conventional MRI cannot predict survival in childhood diffuse intrinsic pontine glioma.* J Neurooncol, 2008. **86**(3): p. 313-9.
83. Henson, J.W., P. Gaviani, and R.G. Gonzalez, *MRI in treatment of adult gliomas.* Lancet Oncol, 2005. **6**(3): p. 167-75.
84. Bendszus, M., et al., *MR spectroscopy in gliomatosis cerebri.* AJNR Am J Neuroradiol, 2000. **21**(2): p. 375-80.
85. Konovalov, A.N. and D.I. Pitskhelauri, *Principles of treatment of the pineal region tumors.* Surg Neurol, 2003. **59**(4): p. 250-68.
86. Albers, M.J., et al., *Proton-decoupled 31P MRS in untreated pediatric brain tumors.* Magn Reson Med, 2005. **53**(1): p. 22-9.
87. Bartha, R., J.F. Megyesi, and C.J. Watling, *Low-grade glioma: correlation of short echo time 1H-MR spectroscopy with 23Na MR imaging.* AJNR Am J Neuroradiol, 2008. **29**(3): p. 464-70.
88. Brockmann, K., et al., *Cerebral proton magnetic resonance spectroscopy in infantile Alexander disease.* J Neurol, 2003. **250**(3): p. 300-6.
89. Chang, K.H., et al., *In vivo single-voxel proton MR spectroscopy in intracranial cystic masses.* AJNR Am J Neuroradiol, 1998. **19**(3): p. 401-5.
90. Galanaud, D., et al., *Use of proton magnetic resonance spectroscopy of the brain to differentiate gliomatosis cerebri from low-grade glioma.* J Neurosurg, 2003. **98**(2): p. 269-76.
91. Imamura, A., et al., *MR imaging and 1H-MR spectroscopy in a case of juvenile Alexander disease.* Brain Dev, 2002. **24**(7): p. 723-6.

92. Lin, A., et al., *Efficacy of proton magnetic resonance spectroscopy in neurological diagnosis and neurotherapeutic decision making.* NeuroRx, 2005. **2**(2): p. 197-214.
93. Meyerand, M.E., et al., *Classification of biopsy-confirmed brain tumors using single-voxel MR spectroscopy.* AJNR Am J Neuroradiol, 1999. **20**(1): p. 117-23.
94. Poptani, H., et al., *Characterization of intracranial mass lesions with in vivo proton MR spectroscopy.* AJNR Am J Neuroradiol, 1995. **16**(8): p. 1593-603.
95. Ross, B. and S. Bluml, *Magnetic resonance spectroscopy of the human brain.* Anat Rec, 2001. **265**(2): p. 54-84.
96. Tong, Z., et al., *In vivo quantification of the metabolites in normal brain and brain tumors by proton MR spectroscopy using water as an internal standard.* Magn Reson Imaging, 2004. **22**(7): p. 1017-24.
97. Yerli, H., et al., *Evaluation of cerebral glioma grade by using normal side creatine as an internal reference in multi-voxel 1H-MR spectroscopy.* Diagn Interv Radiol, 2007. **13**(1): p. 3-9.
98. Davies, N.P., et al., *Identification and characterisation of childhood cerebellar tumours by in vivo proton MRS.* NMR Biomed, 2008.
99. Harris, L.M., et al., *The use of short-echo-time 1H MRS for childhood cerebellar tumours prior to histopathological diagnosis.* Pediatr Radiol, 2007. **37**(11): p. 1101-9.
100. Kovanlikaya, A., et al., *Untreated pediatric primitive neuroectodermal tumor in vivo: quantitation of taurine with MR spectroscopy.* Radiology, 2005. **236**(3): p. 1020-5.
101. Lazareff, J.A., R.K. Gupta, and J. Alger, *Variation of post-treatment H-MRSI choline intensity in pediatric gliomas.* J Neurooncol, 1999. **41**(3): p. 291-8.
102. Panigrahy, A., et al., *Metabolism of diffuse intrinsic brainstem gliomas in children.* Neuro Oncol, 2008. **10**(1): p. 32-44.
103. Sutton, L.N., et al., *Localized 31P magnetic resonance spectroscopy of large pediatric brain tumors.* J Neurosurg, 1990. **72**(1): p. 65-70.
104. Vaidya, S.J., et al., *Potential role of magnetic resonance spectroscopy in assessment of tumour response in childhood cancer.* Eur J Cancer, 2003. **39**(6): p. 728-35.
105. Waldrop, S.M., et al., *Treatment of brain tumors in children is associated with abnormal MR spectroscopic ratios in brain tissue remote from the tumor site.* AJNR Am J Neuroradiol, 1998. **19**(5): p. 963-70.
106. Warren, K.E., *NMR spectroscopy and pediatric brain tumors.* Oncologist, 2004. **9**(3): p. 312-8.
107. Warren, K.E., et al., *Proton magnetic resonance spectroscopic imaging in children with recurrent primary brain tumors.* J Clin Oncol, 2000. **18**(5): p. 1020-6.
108. Lodi, R., et al., *Gliomatosis cerebri: clinical, neurochemical and neuroradiological response to temozolomide administration.* Magn Reson Imaging, 2003. **21**(9): p. 1003-7.
109. Preul, M.C., et al., *Magnetic resonance spectroscopy guided brain tumor resection: differentiation between recurrent glioma and radiation*

change in two diagnostically difficult cases. Can J Neurol Sci, 1998. **25**(1): p. 13-22.
110. Sankar, T., et al., *Prospective serial proton MR spectroscopic assessment of response to tamoxifen for recurrent malignant glioma.* J Neurooncol, 2008.
111. Schwarz, A.J., et al., *Early in vivo detection of metabolic response: a pilot study of 1H MR spectroscopy in extracranial lymphoma and germ cell tumours.* Br J Radiol, 2002. **75**(900): p. 959-66.
112. Saraf-Lavi, E., et al., *Proton MR spectroscopy of gliomatosis cerebri: case report of elevated myoinositol with normal choline levels.* AJNR Am J Neuroradiol, 2003. **24**(5): p. 946-51.
113. Tugnoli, V., et al., *Characterization of lipids from human brain tissues by multinuclear magnetic resonance spectroscopy.* Biopolymers, 2001. **62**(6): p. 297-306.
114. Tzika, A.A., et al., *Spectroscopic and perfusion magnetic resonance imaging predictors of progression in pediatric brain tumors.* Cancer, 2004. **100**(6): p. 1246-56.
115. Kendi, T.K., et al., *Suprasellar germ cell tumor with subarachnoid seeding MRI and MR spectroscopy findings.* Clin Imaging, 2004. **28**(6): p. 404-7.
116. Lindskog, M., et al., *Proton magnetic resonance spectroscopy in neuroblastoma: current status, prospects and limitations.* Cancer Lett, 2005. **228**(1-2): p. 247-55.
117. LM Harris, L.M., TN Arvanitis, D Auer, RG Grundy, D Hargrave, F Howe, T Jaspan, M Leach, P Morgan, K Natarajan, G Payne, D Saunders and AC Peet *Short echo time single voxel 1H Magnetic Resonance Spectroscopy in the diagnosis of pineal region tumours* in *ESPR 2009*. 2008. Edinburgh: Springer Berlin / Heidelberg.
118. LM Harris, S.W., NP Davies, L MacPherson, S Lateef, K Natarajan, M English, TN Arvanitis, RG Grundy and AC Peet. *1H-Magnetic Resonance Spectroscopy as an aid to the Diagnosis of Brainstem Tumours: A Multicentre Study*. in *International Symposium for Pediatric Neuro-Oncology*. 2008. Chicago: Duke University Press.
119. Harris, L.M., et al., *Magnetic resonance spectroscopy in the assessment of pilocytic astrocytomas.* Eur J Cancer, 2008.
120. Provencher, S.W., *Estimation of metabolite concentrations from localized in vivo proton NMR spectra.* Magn Reson Med, 1993. **30**(6): p. 672-9.
121. Bloch, F., *Nuclear Induction.* Physical Review, 1946. **70**(7-8): p. 460.
122. Purcell, E.M., H.C. Torrey, and R.V. Pound, *Resonance Absorption by Nuclear Magnetic Moments in a Solid.* Physical Review, 1946. **69**(1-2): p. 37.
123. de Graaf, R.A., *In Vivo NMR Spectroscopy: Principles and Techniques*. 2nd ed. 2007: John Wiley and Sons, Ltd.
124. Gadian, D.G., *NMR and its Applications to Living Systems*. 2nd ed. 1996, Oxford: Oxford Science Publications.
125. Reynolds, G., et al., *An algorithm for the automated quantitation of metabolites in in vitro NMR signals.* Magn Reson Med, 2006. **56**(6): p. 1211-9.

126. Frahm, J., K.D. Merboldt, and W. Hänicke, *Localized proton spectroscopy using stimulated echoes.* Journal of magnetic resonance 1987. **72**(3): p. 502-508
127. Bottomley, P.A., *Spatial localization in NMR spectroscopy in vivo.* Ann N Y Acad Sci, 1987. **508**: p. 333-48.
128. Londono, A., et al., *Unusual MR spectroscopic imaging pattern of an astrocytoma: lack of elevated choline and high myo-inositol and glycine levels.* AJNR Am J Neuroradiol, 2003. **24**(5): p. 942-5.
129. Clementi, V., et al., *Assessment of glutamate and glutamine contribution to in vivo N-acetylaspartate quantification in human brain by (1)H-magnetic resonance spectroscopy.* Magn Reson Med, 2005. **54**(6): p. 1333-9.
130. Kaiser, L.G., et al., *Scyllo-inositol in normal aging human brain: 1H magnetic resonance spectroscopy study at 4 Tesla.* NMR Biomed, 2005. **18**(1): p. 51-5.
131. Kantarci, K., et al., *Proton MR spectroscopy in mild cognitive impairment and Alzheimer disease: comparison of 1.5 and 3 T.* AJNR Am J Neuroradiol, 2003. **24**(5): p. 843-9.
132. Lien, Y.H., et al., *Scyllo-inositol depletion in hepatic encephalopathy.* Life Sci, 1994. **54**(20): p. 1507-12.
133. Kim, J.H., et al., *Comparison of 1.5T and 3T 1H MR spectroscopy for human brain tumors.* Korean J Radiol, 2006. **7**(3): p. 156-61.
134. Kreis, R., et al., *Brain metabolite composition during early human brain development as measured by quantitative in vivo 1H magnetic resonance spectroscopy.* Magn Reson Med, 2002. **48**(6): p. 949-58.
135. Rigotti, D.J., M. Inglese, and O. Gonen, *Whole-brain N-acetylaspartate as a surrogate marker of neuronal damage in diffuse neurologic disorders.* AJNR Am J Neuroradiol, 2007. **28**(10): p. 1843-9.
136. Li, C.W., et al., *Quantification of choline compounds in human hepatic tumors by proton MR spectroscopy at 3 T.* Magn Reson Med, 2005. **53**(4): p. 770-6.
137. Cirak, B., et al., *Proton magnetic resonance spectroscopic imaging in pediatric pilomyxoid astrocytoma.* Childs Nerv Syst, 2005. **21**(5): p. 404-9.
138. Naressi, A., et al., *Java-based graphical user interface for MRUI, a software package for quantitation of in vivo/medical magnetic resonance spectroscopy signals.* Comput Biol Med, 2001. **31**(4): p. 269-86.
139. Vanhamme, L., A. van den Boogaart, and S. Van Huffel, *Improved method for accurate and efficient quantification of MRS data with use of prior knowledge.* J Magn Reson, 1997. **129**(1): p. 35-43.
140. Jiang, T., et al., *Diagnosis of rejection after liver transplantation: use of phosphorus-31 magnetic resonance spectroscopy ((31)P-MRS).* Abdom Imaging, 2008.
141. Sharma, R., et al., *Investigation of hepatic gluconeogenesis pathway in non-diabetic Asian Indians with non-alcoholic fatty liver disease using in vivo ((31)P) phosphorus magnetic resonance spectroscopy.* Atherosclerosis, 2008.

142. Ratel, S., et al., *Comparative analysis of skeletal muscle oxidative capacity in children and adults: a 31P-MRS study.* Appl Physiol Nutr Metab, 2008. **33**(4): p. 720-7.
143. Beer, M., et al., *Effects of exercise training on myocardial energy metabolism and ventricular function assessed by quantitative phosphorus-31 magnetic resonance spectroscopy and magnetic resonance imaging in dilated cardiomyopathy.* J Am Coll Cardiol, 2008. **51**(19): p. 1883-91.
144. Morimoto, T., et al., *Phosphorous-31 magnetic resonance spectroscopy of cervical cancer using transvaginal surface coil.* Magn Reson Med Sci, 2005. **4**(4): p. 197-201.
145. Hubesch, B., et al., *P-31 MR spectroscopy of normal human brain and brain tumors.* Radiology, 1990. **174**(2): p. 401-9.
146. Karczmar, G.S., et al., *P-31 spectroscopy study of response of superficial human tumors to therapy.* Radiology, 1991. **179**(1): p. 149-53.
147. Naruse, S., et al., *Evaluation of the effects of photoradiation therapy on brain tumors with in vivo P-31 MR spectroscopy.* Radiology, 1986. **160**(3): p. 827-30.
148. Segebarth, C.M., et al., *MR image-guided P-31 MR spectroscopy in the evaluation of brain tumor treatment.* Radiology, 1987. **165**(1): p. 215-9.
149. Ricci, P.E., et al., *Effect of voxel position on single-voxel MR spectroscopy findings.* AJNR Am J Neuroradiol, 2000. **21**(2): p. 367-74.
150. Sankar, T., et al., *Neurosurgical implications of mannitol accumulation within a meningioma and its peritumoral region demonstrated by magnetic resonance spectroscopy: case report.* J Neurosurg, 2008. **108**(5): p. 1010-3.
151. Barker, P.B., D.O. Hearshen, and M.D. Boska, *Single-voxel proton MRS of the human brain at 1.5T and 3.0T.* Magn Reson Med, 2001. **45**(5): p. 765-9.
152. Bartha, R., et al., *Comparison of the quantification precision of human short echo time (1)H spectroscopy at 1.5 and 4.0 Tesla.* Magn Reson Med, 2000. **44**(2): p. 185-92.
153. Di Costanzo, A., et al., *High-field proton MRS of human brain.* Eur J Radiol, 2003. **48**(2): p. 146-53.
154. Edden, R.A., M.G. Pomper, and P.B. Barker, *In vivo differentiation of N-acetyl aspartyl glutamate from N-acetyl aspartate at 3 Tesla.* Magn Reson Med, 2007. **57**(6): p. 977-82.
155. Ethofer, T., et al., *Comparison of longitudinal metabolite relaxation times in different regions of the human brain at 1.5 and 3 Tesla.* Magn Reson Med, 2003. **50**(6): p. 1296-301.
156. Hetherington, H.P., et al., *Biological and clinical MRS at ultra-high field.* NMR Biomed, 1997. **10**(8): p. 360-71.
157. Hurd, R., et al., *Measurement of brain glutamate using TE-averaged PRESS at 3T.* Magn Reson Med, 2004. **51**(3): p. 435-40.
158. Govindaraju, V., K. Young, and A.A. Maudsley, *Proton NMR chemical shifts and coupling constants for brain metabolites.* NMR Biomed, 2000. **13**(3): p. 129-53.

159. Peet, A.C., et al., *1H MRS identifies specific metabolite profiles associated with MYCN-amplified and non-amplified tumour subtypes of neuroblastoma cell lines.* NMR Biomed, 2007. **20**(7): p. 692-700.
160. Grachev, I.D. and A.V. Apkarian, *Chemical heterogeneity of the living human brain: a proton MR spectroscopy study on the effects of sex, age, and brain region.* Neuroimage, 2000. **11**(5 Pt 1): p. 554-63.
161. Pouwels, P.J., et al., *Regional age dependence of human brain metabolites from infancy to adulthood as detected by quantitative localized proton MRS.* Pediatr Res, 1999. **46**(4): p. 474-85.
162. Clark, G.B., J.M. Henry, and P.E. McKeever, *Cerebral pilocytic astrocytoma.* Cancer, 1985. **56**(5): p. 1128-33.
163. Haapasalo, H., et al., *Clinicopathological correlation of cell proliferation, apoptosis and p53 in cerebellar pilocytic astrocytomas.* Neuropathol Appl Neurobiol, 1999. **25**(2): p. 134-42.
164. Kayaselcuk, F., et al., *PCNA and Ki-67 in central nervous system tumors: correlation with the histological type and grade.* J Neurooncol, 2002. **57**(2): p. 115-21.
165. Koeller, K.K. and E.J. Rushing, *From the archives of the AFIP: pilocytic astrocytoma: radiologic-pathologic correlation.* Radiographics, 2004. **24**(6): p. 1693-708.
166. Bellil, S., et al., *Descriptive epidemiology of childhood central nervous system tumours in Tunisia. experience of a single institution over a 15-year period (1990-2004).* Pediatr Neurosurg, 2008. **44**(5): p. 382-7.
167. Gilles, F.H., *Classifications of childhood brain tumors.* Cancer, 1985. **56**(7 Suppl): p. 1850-7.
168. Hargrave, D.R. and S. Zacharoulis, *Pediatric CNS tumors: current treatment and future directions.* Expert Rev Neurother, 2007. **7**(8): p. 1029-42.
169. Holthoff, V.A., et al., *In vivo metabolism of childhood posterior fossa tumors and primitive neuroectodermal tumors before and after treatment.* Cancer, 1993. **72**(4): p. 1394-403.
170. Kurt, E., et al., *Identification of relevant prognostic histopathologic features in 69 intracranial ependymomas, excluding myxopapillary ependymomas and subependymomas.* Cancer, 2006. **106**(2): p. 388-95.
171. Laurent, J.P., C.H. Chang, and M.E. Cohen, *A classification system for primitive neuroectodermal tumors (medulloblastoma) of the posterior fossa.* Cancer, 1985. **56**(7 Suppl): p. 1807-9.
172. Metellus, P., et al., *Multicentric French study on adult intracranial ependymomas: prognostic factors analysis and therapeutic considerations from a cohort of 152 patients.* Brain, 2007. **130**(Pt 5): p. 1338-49.
173. Rorke, L.B., et al., *Revision of the World Health Organization classification of brain tumors for childhood brain tumors.* Cancer, 1985. **56**(7 Suppl): p. 1869-86.
174. Reynolds, G.M., A.C. Peet, and T.N. Arvanitis, *Generating prior probabilities for classifiers of brain tumours using belief networks.* BMC Med Inform Decis Mak, 2007. **7**: p. 27.

175. Payne, G.S. and M.O. Leach, *Applications of magnetic resonance spectroscopy in radiotherapy treatment planning.* Br J Radiol, 2006. **79 Spec No 1**: p. S16-26.
176. Hirose, T., et al., *Ganglioglioma: an ultrastructural and immunohistochemical study.* Cancer, 1997. **79**(5): p. 989-1003.
177. Hirato, J. and Y. Nakazato, *Pathology of pineal region tumors.* J Neurooncol, 2001. **54**(3): p. 239-49.
178. Sasaki, A., K. Horiguchi, and Y. Nakazato, *Pineal parenchymal tumor of intermediate differentiation with cytologic pleomorphism.* Neuropathology, 2006. **26**(3): p. 212-7.
179. Schild, S.E., et al., *Pineal parenchymal tumors. Clinical, pathologic, and therapeutic aspects.* Cancer, 1993. **72**(3): p. 870-80.
180. Barkovich, A.J., K.R. Moore, and E. Grant, *Diagnostic Imaging: Pediatric Neuroradiology*. Third ed. 2007: AMIRSYS.
181. Howe, F.A., et al., *Metabolic profiles of human brain tumors using quantitative in vivo 1H magnetic resonance spectroscopy.* Magn Reson Med, 2003. **49**(2): p. 223-32.
182. Laprie, A., et al., *Longitudinal multivoxel MR spectroscopy study of pediatric diffuse brainstem gliomas treated with radiotherapy.* Int J Radiat Oncol Biol Phys, 2005. **62**(1): p. 20-31.
183. Scotting, P.J., *Are cranial germ cell tumours really tumours of germ cells?* Neuropathology and Applied Neurobiology, 2006. **32**(6): p. 569-574.
184. Carrie, C., et al., *Diffuse medulla oblongata and pontine gliomas in childhood. A review of 37 cases.* Bull Cancer, 2004. **91**(6): p. E167-83.
185. Cartmill, M. and J. Punt, *Diffuse brain stem glioma. A review of stereotactic biopsies.* Childs Nerv Syst, 1999. **15**(5): p. 235-7; discussion 238.
186. Schumacher, M., et al., *Magnetic resonance imaging compared with biopsy in the diagnosis of brainstem diseases of childhood: a multicenter review.* J Neurosurg, 2007. **106**(2 Suppl): p. 111-9.
187. Curless, R.G., et al., *Magnetic resonance spectroscopy in childhood brainstem tumors.* Pediatr Neurol, 2002. **26**(5): p. 374-8.
188. Albright, A.L., R.A. Price, and A.N. Guthkelch, *Brain stem gliomas of children. A clinicopathological study.* Cancer, 1983. **52**(12): p. 2313-9.
189. Berger, M.S., et al., *Pediatric brain stem tumors: radiographic, pathological, and clinical correlations.* Neurosurgery, 1983. **12**(3): p. 298-302.
190. Burger, P.C., *Pathology of brain stem astrocytomas.* Pediatr Neurosurg, 1996. **24**(1): p. 35-40.
191. Badhe, P.B., P.P. Chauhan, and N.K. Mehta, *Brainstem gliomas--a clinicopathological study of 45 cases with p53 immunohistochemistry.* Indian J Cancer, 2004. **41**(4): p. 170-4.
192. Nishio, S., M. Fukui, and J. Tateishi, *Brain stem gliomas: a clinicopathological analysis of 23 histologically proven cases.* J Neurooncol, 1988. **6**(3): p. 245-50.
193. Yoshimura, J., et al., *Clinicopathological study of diffuse type brainstem gliomas: analysis of 40 autopsy cases.* Neurol Med Chir (Tokyo), 2003. **43**(8): p. 375-82; discussion 382.

194. Seymour, Z.A., et al., *Citrate in pediatric CNS tumors?* AJNR Am J Neuroradiol, 2008. **29**(5): p. 1006-11.
195. Guo, P., et al., *Up-regulation of angiopoietin-2, matrix metalloprotease-2, membrane type 1 metalloprotease, and laminin 5 gamma 2 correlates with the invasiveness of human glioma.* Am J Pathol, 2005. **166**(3): p. 877-90.
196. Bowen, B.C., *Glial neoplasms without elevated choline-creatine ratios.* AJNR Am J Neuroradiol, 2003. **24**(5): p. 782-4.
197. Burkhard, C., et al., *A population-based study of the incidence and survival rates in patients with pilocytic astrocytoma.* J Neurosurg, 2003. **98**(6): p. 1170-4.
198. Kayama, T., T. Tominaga, and T. Yoshimoto, *Management of pilocytic astrocytoma.* Neurosurg Rev, 1996. **19**(4): p. 217-20.
199. Taylor, M.D., et al., *Radial glia cells are candidate stem cells of ependymoma.* Cancer Cell, 2005. **8**(4): p. 323-35.
200. Fisher, P.G., et al., *Outcome analysis of childhood low-grade astrocytomas.* Pediatr Blood Cancer, 2008. **51**(2): p. 245-50.
201. Ackerstaff, E., K. Glunde, and Z.M. Bhujwalla, *Choline phospholipid metabolism: a target in cancer cells?* J Cell Biochem, 2003. **90**(3): p. 525-33.
202. Uhm, J.H., et al., *Glioma invasion in vitro: regulation by matrix metalloprotease-2 and protein kinase C.* Clin Exp Metastasis, 1996. **14**(5): p. 421-33.
203. Sharma, M.K., et al., *Distinct genetic signatures among pilocytic astrocytomas relate to their brain region origin.* Cancer Res, 2007. **67**(3): p. 890-900.
204. Bowers, D.C., et al., *Study of the MIB-1 labeling index as a predictor of tumor progression in pilocytic astrocytomas in children and adolescents.* J Clin Oncol, 2003. **21**(15): p. 2968-73.